UNIVERSIDADE DO ALGARVE

Development of Biosensors for Molecular Analysis

João Miguel Encarnação

Doutoramento em Ciências Biotecnológicas

(Especialidade de Biotecnologia Molecular)

Centro de Biomedicina Molecular e Estrutural

Instituto de Biotecnologia e Bioengenharia

2007

UNIVERSIDADE DO ALGARVE

Development of Biosensors for Molecular Analysis

João Miguel Encarnação

Doutoramento em Ciências Biotecnológicas

(Especialidade de Biotecnologia Molecular)

Tese orientada por:

Orientador- Doutor Guilherme Ferreira

Co-Orientador- Doutor Peter Stallinga

2007

Abstract

This thesis deals with the application of piezoelectric sensors, namely quartz crystal microbalances (QCM), for the study of molecular interactions and for biomedical purposes.

Piezoelectric transduction allows the detection of biorecognition events and its operation depends on the mechanical vibration of the crystal whose resonance frequency is sensible to surface mass changes. But in liquid medium these sensors also respond to the properties of solutions and adsorbed films. Thus, a major aspect explored in this thesis is the expansion of the physical understanding of the behavior of these sensors in liquid medium and also how organic or biological layers can affect the results and their interpretation. This was achieved using impedance analysis where the behavior of the piezoelectric sensor is interpreted with the help of equivalent electric RLC circuits. The potential electroacoustic interference of charged species in solution was particularly studied and a new equivalent circuit is proposed in order to detect and quantify these effects with the assistance of impedance analysis.

The efficiency of the key steps taken for the development of our QCM system, was experimentally demonstrated with the qualitative and quantitative analysis of the process of

11-hydroxy-1-undecanothiol SAMs (self-assembled monolayers) formation and the recognition of streptavidin in aqueous medium using biotin modified sensors.

Finally the work was focused on the development of a new detection tool for the HIV1 virus using piezoelectric immunosensors based on recombinant antibodies to detect the Vif molecule (virion infectivity factor). The developed immunosensors selectively detected Vif in aqueous solutions and presented specificity and good sensibility when detecting the target protein in complex samples like mixtures of proteins and cell extracts.

Key words: Biosensor, piezoelectric, QCM, impedance analysis, equivalent circuit, kinetics, SAM, Streptavidin, HIV1-Vif, recombinant antibodies, nanoparticles, DNA.

Resumo

A integração da electrónica e da biologia para a produção de bio-sensores tem-se tornado uma área de enorme potencial. Os sensores biomoleculares têm-se revelado uma ferramenta fundamental para a compreensão dos princípios biofísicos de reconhecimento molecular assim como na detecção da presença de analitos específicos. Os bio-sensores são instrumentos analíticos nos quais biomoléculas (ex. anticorpos, DNA, receptores, enzimas) são associadas a transdutores de sinal físicos ou químicos com o objectivo de reconhecer específica e selectivamente moléculas alvo.

Nesta tese é abordada a aplicação de sensores piezoeléctricos, nomeadamente microbalanças de cristal de quartzo (QCM) com eléctrodos de ouro, para o estudo de interacções moleculares e para o desenvolvimento de sistemas bio-sensores para aplicação biomédica.

A operação de um QCM assenta no efeito piezoeléctrico, no qual um sensor de cristal de quartzo é induzido a vibrar mecânicamente com uma frequência de ressonância específica através da aplicação de um campo eléctrico alternado aos eléctrodos metálicos. A frequência de ressonância do cristal é proporcional à massa deslocada na vibração, e consequentemente à variação de massa na superfície do sensor. Esta pode ser estimada através da equação de

Sauerbrey, $\Delta f_m=[-2nf_0^2/(\rho_q\mu_q)^{½}]\times[\Delta m/A]$, que relaciona a variação de frequência (Δf_m), a frequência de ressonância no modo fundamental (f_0), a harmónica (n), a densidade e o módulo de rigidez ou torção do quartzo (ρ_q e μ_q), a variação de massa (Δm) e a área activa do sensor (A). Desta forma, um QCM gera um sinal que permite caracterizar um evento de reconhecimento molecular na sua superfície. Este modelo assume que a massa depositada na superfície do cristal acompanha a sua vibração e por conseguinte o sensor comporta-se como se fosse simplesmente mais espesso. Assim, a equação de Sauerbrey é apenas válida para filmes finos, rígidos e uniformes. No entanto a resposta do quartzo em meio líquido depende, não só da variação da massa depositada, como também das propriedades reológicas dos tampões, das propriedades viscoelásticas dos biofilmes depositados, da presença de electrólitos e da variação de cargas na superfície do sensor. Estes factores resultam em variações de frequência interferentes que são aditivas e impossíveis de eliminar recorrendo unicamente a sistemas de medição de frequência de ressonância. A quantificação e eliminação das variações destas frequências de ressonância interferentes pode ser conseguida recorrendo a metodologias de análise mais complexas, através da espectroscopia de impedância.

Em espectroscopia de impedância é possível analisar processos interfaciais que ocorrem no sensor de quatzo, interpretando-os sob a forma de um circuito eléctrico equivalente RLC, denominado modelo de Butterworth–Van Dyke. Esta análise permite distinguir e individualizar o contributo de propriedades reológicas de soluções e propriedades de filmes depositados. Na essência e no que diz respeito a filmes, há dois componentes que são estimados em análise de impedância: massa depositada, representada em circuito equivalente, como um indutor (L) e viscoelasticidade da mesma, representada como uma resistência (R).

Assim, um aspecto importante explorado nesta tese é a expansão da compreensão do comportamento físico destes sensores em meio líquido e também como as propriedades de camadas orgânicas ou biológicas podem afectar resultados e sua interpretação.

Neste trabalho são demonstrados os passos críticos necessários ao desenvolvimento instrumental e uso de sensores QCM para análise molecular em meio líquido e a optimização do seu desempenho na monitorização de eventos de reconhecimento molecular em tempo real. Utilizando um circuito oscilador com contador de frequências e um analisador de impedâncias, foram medidas a propriedades dos sensores de cristal de quartzo e sua resposta sistemática ao ar e em líquidos, tanto para a sua frequência de ressonância fundamental como para as suas harmónicas.

A validade e funcionalidade do sistema QCM desenvolvido nesta tese, foram verificados através do modelo de Kanazawa que determina a relação entre frequência de ressonância e a densidade e viscosidade de soluções. Para a validade de medições de impedância em meio líquido, utilizou-se o modelo de Martin que relaciona a variação de frequência de ressonância com variação de resistência em análise de circuito equivalente RLC. Para ambos os modelos o sistema respondeu de acordo com o teóricamente previsto.

No desenvolvimento instrumental do sistema de 5 MHz são focadas questões como a regeneração dos cristais para sua reutilização, o controlo de temperatura, efeitos de pressão, evaporação de líquido e presença de gases dissolvidos.

A reutilização de cristais é determinante, pois tendo em conta que no decorrer de um ensaio ocorre a deposição de massa na superfície, esta terá de ser eficientemente removida de modo a se proceder a novo ensaio utilizando o mesmo sensor QCM. São apresentados dois métodos, em que um consiste na limpeza com um agente químico (solução piranha) e outro de natureza electroquímica que se baseia na aplicação de um potencial específico. Ambas as técnicas

revelaram-se eficientes, no entanto a limpeza electroquímica apresentou ser segura para a integridade física dos sensores, ao contrário da aplicação de solução piranha que é significativamente agressiva para os eléctrodos de ouro.

Foram avaliados os impactos de efeitos interferentes, especialmente no que diz respeito a introdução de ruído ou desvios no sinal de frequência de ressonância. O controlo de temperatura é absolutamente crucial considerando que os sensores utilizados em meio líquido apresentam um coeficiente de variação de aproximadamente 8 Hz/ºC. Efeitos de pressão, evaporação de líquido e presença de gases dissolvidos demonstraram introduzir desvios e ruído que podem mimetizar ou dissimular os sinais esperados em ensaios de adsorção de massa.

Para a devida aplicação de sensores QCM em meio líquido foi desenvolvido um aparelho construído de forma a prevenir ou minimizar os efeitos interferentes estudados, que consiste basicamente num circuito de fluxo com uma célula de fluxo integrada, onde os cristais são montados. Este sistema é assistido por uma bomba peristáltica e é termostatizado (± 0.1ºC) por um termocriostato com controlador PID. Os ensaios são efectuados em fluxo contínuo, utilizando soluções tampão como veículo para o transporte das amostras, injectadas em fluxo, até à célula onde se encontra o sensor de quartzo. Ao sensor estão conectados simultaneamente três sistemas transdutores para análise de frequência de ressonância, análise de impedância e análise electroquímica.

Neste trabalho é demonstrado que a resposta de sensores QCM é afectada pela presença de espécies carregadas em solução, que podem ter um impacto considerável em aplicações de bio-sensores, conduzindo a conclusões erróneas.

Particularmente, a influência de electrólitos presentes em solução, traduz-se pela formação de uma dupla camada difusa eléctrica na interface sólido/líquido do eléctrodo de ouro do sensor.

A influência da dupla camada para regimes de baixa variação de força iónica (I ≤1 mM) manifesta-se como uma camada que localmente aumenta a densidade e viscosidade da solução induzindo uma diminuição da frequência de ressonância. Para elevada variação de força iónica (1 mM ≤ I ≤ 50 mM) predominam efeitos de carga de natureza capacitiva que induzem aumentos da frequência de ressonância.

Face a estes fenómenos, é proposto um circuito equivalente modificado onde se introduz um elemento capacitivo (C), baseado no modelo RLC de Butterworth–Van Dyke. Com base neste circuito modificado é efectuada espectroscopia de impedância e respectiva interpretação dos espectros obtidos de forma a detectar, quantificar e eliminar a influência deste efeitos interferentes utilizando a relação linear 8 Hz/pF.

A aplicação desta relação foi demonstrada na detecção de nanopartículas de ouro revestidas com um oligonucleotiodo complementar de uma cadeia simples de DNA previamente imobilizada na superfície dos sensores de quartzo. A adsorção das nanopartículas funcionalizadas na superfície dos sensores QCM processa-se através da hibridação das cadeias complementares de oligonucleótido. Este processo foi acompanhado em tempo real por análise de frequência e impedância. Verificou-se que a mera análise de variação total de frequência de ressonância produziu um sinal que subestima a massa adsorvida, face aos resultados obtidos em análise de impedância para o desvio do espectro em frequência. A adsorção das nanopartículas provocou uma variação do elemento capacitivo em análise de circuito que representava um efeito interferente traduzido pela subestimação em 40% da massa real adsorvida.

A estimativa da influência de electrólitos ou outras espécies carregadas sobre a resposta dos sensores QCM permite a aquisição de dados mais exactos no que diz respeito à exclusiva

influência de massa, o que é fulcral para a utilização do sistema piezoeléctrico para análise molecular quantitativa suportada pelo modelo de Sauebrey.

A aplicação prática do cicuito equivalente modificado, é demonstrada na medição simultânea de variação da frequência de ressonância e a impedância electroacústica dos sensores, permitindo a análise quantitativa em processos de adsorção de massa orgânica. Deste modo, a partir dos dados adquiridos é possível avaliar modelos cinéticos e estimar constantes cinéticas sem o risco de uma sobre ou subestimação dos valores devido a efeitos não-mássicos.

Esta abordagem foi aplicada ao estudo de camadas orgânicas auto-montadas em ouro (SAM-self assembled monolayer) utilizando a molécula 11-hidroxi-1-undecanotiol e também para estudar a interacção de estreptavidina com biotina imobilizada no sensor.

Para ambos os processos moleculares foi possível acompanhar as curvas cinética de adsorção em tempo real através da variação da frequência de ressonância dos sensores de quartzo. Cada curva obtida foi devidamente analisada por espectroscopia de impedância de forma a detectar possíveis efeitos interferentes. A partir dos transientes de frequência para a adsorção de 11-hidroxi-1-undecanotiol em ouro e também para ligação estreptavidina-biotina, foram estimados parâmetros cinéticos e de equílibrio, isotérmicas de adsorção, análise de Scatchard e análise de Hill. A validade destas estimativas e análises depende fortemente do estabelecimento directo de variação de frequência de ressonância exclusivamente com massa, o que foi conseguido através da análise de impedância.

A resultante análise de dados demonstrou que a formação do SAM de 11-hidroxi-1-undecanotiol é caracterizado por uma cooperatividade positiva, enquanto o processo de ligação de estreptavidina a biotina imobilizada na superfície do sensor, rege-se por uma cooperatividade negativa. Foi também possível estimar com sucesso as constantes cinéticas e de equílibrio para os processos moleculares estudados, utilizando um modelo cinético 1:1.

Em suma, foi demonstrado que a análise de impedância melhora significativamente a análise quantitativa com sensores piezoeléctricos em meio líquido. A abordagem com o circuito equivalente modificado permite o estudo de interacções moleculares observando as propriedades particulares das moléculas envolvidas assim como os fenómenos superficiais que ditam a resposta dos sensores.

Esta metodologia demonstrou a aplicabilidade de QCM em procedimento analíticos quantitativos, o que conduziu ao estudo e desenvolvimento de uma nova ferramenta biomédica para diagnóstico de HIV1. Para atingir este objectivo construíram-se imuno-sensores piezoeléctricos baseados em anticorpos recombinantes para reconhecer a molécula Vif (virion infectivity factor) do HIV1.

A molécula alvo, Vif, é uma proteína fosforilada de aproximadamente 23 kDa localizada no citoplasma de células infectadas por HIV1 e essencial para a replicação e disseminação do vírus em linfócitos, macrófagos e em linhas de células T.

Anticorpos recombinantes 4BL, VH e VHD gerados contra a proteína Vif-HIV1 foram individualmente imobilizados sobre a superfície de sensores de quartzo, gerando assim três tipos diferentes de imuno-sensor.

Análises de frequência assim como de impedância foram aplicadas no estudo de imobilização de cada anticorpo, permitindo a eliminação de efeitos interferentes e consequentemente a correcta quantificação de anticorpos imobilizados.

O reconhecimento molecular da Vif por cada imuno-sensor, foi analisado quantitativamente com o apoio de análise de impedância para estimar as constantes cinéticas e de equílibrio que regem o reconhecimento antigénio-anticorpo. Na análise molecular quantitativa foram detectados e quantificados sinais interferentes gerados por viscoelasticidade das moléculas e

efeitos de carga, permitindo assim a correcção dos transientes de frequência de ressonância de forma a aplicar o modelo de Sauerbrey. Nesta fase, a molécula VHD destacou-se relativamente a 4BL e VH, apresentando um maior valor para a constante de associação à Vif.

A análise de impedância permitiu também compreender alguns aspectos relativamente à orientação superficial de cada molécula e alterações conformacionais tanto no processo de imobilização, como no processo de reconhecimento anticorpo-antigénio.

Qualitativamente, mostrou-se que os três imuno-sensores reconhecem específicamente a molécula Vif em amostras líquidas complexas, tendo os resultados mostrado uma melhor sensibilidade por parte da molécula VHD. Mostrou-se que o sensor baseado nesta molécula apresenta maior eficiência na detecção selectiva de Vif em misturas proteícas e em extractos celulares de células humanas embrionárias de fígado, manipuladas para expressar a Vif.

Os estudos apresentados constituem um valioso contributo para os mecanismos de reconhecimento molecular de Vif, por parte dos anticorpos 4BL, VH e VHD, com impacto na pesquisa que decorre actualmente focada na aplicação destas moléculas para a neutralização funcional da proteína alvo, constítuindo assim uma estratégia terapêutica para a neutralização do poder infeccioso do vírus HIV1.

É demonstrado nesta tese que os sensores piezoeléctricos apresentam um elevado potencial como núcleos de desenvolvimento de biosensores com múltiplas aplicações. Apesar da sua aparente simplicidade, a correcta utilização destes sensores em meio líquido requere o conhecimento e entendimento do seu funcionamento sob ponto de vista físico, particularmente no que diz respeito ao seu comportamento face ao meio que o rodeia, assim como a interacção com massa adsorvida na sua superfície.

A validade dos dados adquiridos com QCM depende da aquisição de um sinal que esteja exclusivamente relacionado com massa adsorvida na sua superfície. Neste trabalho, são apresentadas soluções que permitem isolar os sinais relacionados com a massa, através da eliminação/prevenção da influência de fontes de interferência e também através da detecção e quantificação da influência de interferentes na transdução piezoeléctrica.

Deste modo, sensores QCM podem potencialmente tornar-se plataformas qualitativas e quantitativas, o que acrescido da sua versatilidade, permite o desenvolvimento de biosensores com elevada aplicabilidade e validade analíticas.

Palavras chave: Bio-sensor, piezoeléctrico, QCM, análise de impedância, circuito equivalente, cinéticas, SAM, estreptavidina, HIV1-Vif, anticorpos recombinantes, nanopartículas, DNA.

Acknowledgments

This dissertation represents the end of a long and hard process, but also the very fruitful and fascinating period of my PhD research.

I am grateful to Prof. Guilherme Ferreira, my supervisor, for believing in me and convincing me to quit my job and embracing a fascinant world of knowledge, science and invaluable experience. Our scientific discussions helped planting the seeds of my research, crystallizing ideas and experimental results to a whole and harmonized picture.

I would also like to express my deep gratitude to Prof. Peter Stallinga, my co-supervisor, to whom I owe much of my knowledge in how to be a passionate and credible scientist. Prof. Stallinga has literally raised me into the scientific world, guiding me slowly towards becoming an independent researcher.

Special thanks to Prof. Henrique Gomes and Prof. Paulo Pinheiro with whom I learned a lot in their laboratories and collaborated in part of my work. Their theoretical insight helped clarify some of the underlying physical mechanisms and establish wider perspectives for interpreting my experimental results.

I am grateful to all those who helped me to accomplish this work, like my colleagues Luís Rosa, Raul Baltazar, Luisa Pedro and Rogério Rodrigues, and also Mário Freitas for technical advises and help in constructing part of the experimental setups used in this work.

I would like to acknowledge the Portuguese Science Foundation, an organism of the Portuguese Ministry of Science and Higher Education, for my PhD grant number SFHR/BD/12772/2003 and the funding to the projects POCTI/CTM/37719/2000 and POCI/BIO/61912/2004.

Devoted to my family, specially my parents Jacinto and Suzel, my brother Carlos, my goddaughter Inês and my grandparents Antero and Marieta. They always knew I had the science bug in me.

"O homem não nasceu para trabalhar, mas para criar"

Professor Agostinho da Silva (1906-1996)

Contents

Acronyms and Symbols

$|Z|$ - Impedance magnitude

ϕ - Impedance phase angle

τ- Relaxation time of binding

Δf_C- Frequency variation to charge interference

Δf_L- Frequency variation due viscoelasticity of the liquid

Δf_M- Frequency variation due to mass loading

Δf_T- Total frequency variation due to mass loading

Δf_V- Frequency variation due viscoelasticity of the adsorbed/deposited mass

Δf_{visc}- Frequency change due to viscoelastic effects

$|Y|$- Admittance magnitude

Δf_{FWHM}- Frequency Width at Half Maximum

Δm- surface mass change

ΔR- Change of resistance

ΔX_L- Change of inductive reactance

μ_Q- shear modulus of quartz

4BL- anti-Vif single chain antibody

A- Amplitude of oscillation of shear wave

AC- Alternating current

B- Susceptance

BVD- Butterworth van Dyke model

C- Initial ligand concentration

C_0- Parallel capacitance

C_F- Capacitance due to charge variation upon mass loading

C_L- Capacitance due to charge variation upon liquid loading

C_m- Series capacitor

d- Damper

DDL- Double diffuse layer

DMF- Dimethyl Formamide

DNA- Deoxyribonucleic Acid

DSU- Dithiobis Succinimidyl Undecanoate

F- Force

f- Resonance frequency

f_0- Fundamental resonance frequency

f_A- Antiresonant frequency for phase angle zero and maximum impedance magnitude

FET- Field Effect Transistor

f_P- Frequency at phase angle zero

f_R- Resonance frequency for phase angle zero and minimum impedance magnitude

f_s- Frequency at phase angle zero

f_{Zmax}- Frequency at maximum impedance

f_{Zmin}- Frequency at minimal impedance

G- Conductance

g- Gravitational acceleration

G- Shear complex modulus

G"- shear loss modulus

G'- Shear storage modulus

h- Liquid height

h_f- Thickness of a layer

HIV1- Human Immunodeficiency Virus Type 1

HUT- 11-hidroxy-1-undecanothiol

I- Ionic strength

IEQCM- Impedance assisted electrochemical quartz crystal microbalance

IUPAC- International Union of Pure and Applied Chemistry

k- Spring constant

k_1- Association rate constants

k_{-1}- Dissociation rate constant

K_D- Dissociation constant

L_F- Inductance due to surface mass variation upon mass loading

L_L- Inductance due to viscoelastic variation upon liquid loading

L_m- Series inductor

l_{Q-} thickness of the resonator

m- Mass

MB- Methylene blue

ODN- Oligonucleotide

p- Hydrostatic pressure

PBS- Phosphate buffer solution

Q- Charge

Q- Quality factor

QCM- Quartz Crystal Microbalance

R- Resistance

R_F- Resistance due to viscoelastic variation upon mass loading

R_L- Resistance due to viscoelastic variation upon liquid loading

RLC- Circuit with resistors, capacitors and inductors

R_m- Series resistor

S/N- Signal to noise ratio

SAM- Self Assembled Monolayer

SNP- single nucleotide polymorphism

ssDNA- Single stranded deoxyribonucleic Acid

TSM- Thickness-Shear-Mode Resonator

VH- anti-Vif single domain antibody

VHD- anti-Vif camelized single domain antibody

Vif- Virion infectivity factor

v_s – Velocity of sound

x- Displacement

X- Reactance

X_L- Inductive reactance

Y- Admittance

Z- Impedance

δ- Decay length of shear wave

Δf- Change in resonance frequency

η_{L-} viscosity of liquid

θ - Relative amount of surface coverage

λ- Wavelength

ρ_f- Density of a layer

ρ_L-density of the liquid

ρ_{Q-} density of quartz

ω- Angular frequency

List of Figures

Figure 1.10. Representation of impedance and phase angle spectrums as obtained with a network analyzer, for air (A) and liquid exposure (B) of a QCM. Considering the BVD equivalent circuit, for the case of unloaded sensor ($R_m \rightarrow 0$) there are two marked resonance frequencies: f_R and f_A. For the case of sensor damping ($R_m > 0$) there are four marked resonance frequencies: f_{Zmin}, f_s, f_p, and f_{Zmax}.

Figure 1.11. Modified Butterworth van Dyke model representing a loaded resonator in liquid medium. The original four BVD electrical elements L_m, R_m ,C_m and C_0 are the sum of different contributions, namely the liquid loading and mass adsorption.

Figure 1.12. Factors influencing the response of a QCM coated with a viscoelastic film and/or working in a liquid environment (Lucklum and Hauptmann, 2003).

Figure 2.1. Silver-stained SDS-PAGE of purified 4BL (lane 1), VH (lane 3), VHD (lane 5) and Vif (lane 7) and respective western blot autoradiographs (lanes 2, 4, 6, and 8); M-Molecular weight markers. Adapted from Ferreira *et al.*, 2007.

Figure 2.2. Representation of the formation of a self-assembled monolayer (SAM). Alkanethiol molecules present in solution start to spontaneously adsorb to gold surfaces and self assemble as oriented monolayers.

Figure 2.3. Scheme of the steps taken to detect streptavidin molecules in solution using quartz crystals covered with biotin. The same scheme is applicable for all sensors based on protein molecules.

Figure 2.4. Scheme of the functionalization of the gold electrodes with (A) the thiolated ssDNA probe and finally with (B) the alkanethiol, to form a mixed monolayer.

Figure 2.5. Experimental set-up of the 5 MHz quartz crystal microbalance system. Dark lines represent liquid flow tubes and gray lines are electrical connections.

Figure 3.1. Resonant frequency decrease upon immersion of a 5 MHz quartz crystal in Milli-Q water at 20ºC.

Figure 3.2. A) QCM frequency response to increasing density and viscosity of glycerol solutions at 20ºC and (inset) ethanol aqueous solutions at 20ºC, compared to the

correspondent theoretical Kanazawa curve (□ experimental data; ▬ theoretical data). B) Frequency linear dependency on $(\rho_L \times \eta_L)^{1/2}$, for the glycerol solutions case where the black solid line represents the Kanazawa model and the white triangles represent the experimental results. The slope of the solid line corresponds to the Kanazawa liquid sensitivity factor for a 5 MHz crystal.

Figure 3.3. Home-made 5 MHz QCM system typical admittance spectrum in air (black triangle) and in Milli-Q water (white square), at 20ºC.

Figure 3.4. Admitance spectrum of the quartz crystal in contact with water (the same as in Fig 3.4). The admittance magnitude equation is fitted to the experimental curve to extract the equivalent circuit components.

Figure 3.5. A) Parametric plot of ΔX_L vs. ΔR (□ experimental data; ▬ theoretical data), for increasing percentages of glycerol (from left to right = 0 -80%) in aqueous solution in contact with a quartz crystal. The solid line has a slope of unity and represents the predicted behavior of a QCM system in contact with Newtonian fluids of increasing viscosity and density. Inset: calculated frequency linear dependency on $(\rho_L \times \eta_L)^{1/2}$, for the glycerol solutions case (○ experimental data; ▬ Kanazawa model). The deviation obtained with the experimental results for both plots is only 3%. B) For the system-check using glycerol solutions, the obtained frequency shift with the oscillator is linearly related to the resistance shift obtained with the network analyzer, validating the experimental results obtained simultaneously with both instruments according to Equation 17 (□ experimental data; ▬ theoretical data).

Figure 3.6. Resonant frequency readings noise amplitude obtained after each regeneration cycle procedure to remove a deposited film of 11-hidoxy-1-undecanothiol, using "piranha" solution and a -1.4 V tension (■ electrochemical cleaning; □ piranha solution cleaning).

Figure 3.7. Cyclic voltammograms of 4.0 mM potassium hexacianoferrate (III) (a) on a clean crystal (bare gold electrode) and (b) on a crystal covered with a 11-hidroy-1-undecanothiol SAM in PBS buffer (pH 7.0) at a scan rate of 0.1 V/s.

Figure 3.8. Potassium hexacianoferrate (III) reduction and oxidation peaks (■ reduction peak; □ oxidation peak; --- original peaks) obtained with cyclic voltammograms conducted after each electrochemical cleaning procedure of the crystal covered with the alkanethiol SAM.

Figure 3.9. A) The quartz crystal response in an open support, to contact with air (a) and water (b), showing clearly a very stable frequency signal for the first case but a periodic shift in the second case. B) Quartz crystal response to contact with absolute ethanol (6 mm liquid height) in (a) a closed support and in (b) an open support. Inset: the first 100 minutes of curve b.

Figure 3.10. A) Batch QCM experiment where the crystals were assembled in a 300 µl closed cell. The quartz crystal frequency response was followed with the sensor in contact with degassed (a) and non degassed water (b). B) Batch QCM experiment where the crystals were assembled in a 300 µl closed cell, and only loaded with degassed fluids. The chamber was first loaded with 200 µl of water and then a 100 µl sample (indicated by arrow) of the same fluid was injected. In one crystal the sample was carefully injected with a syringe (a), but for the other a micropipette was used (b) and one single air bubble was introduced inside the chamber.

Figure 3.11. QCM response to hydrostatic pressure drops by diminishing the height of a water column to which the sensor, enclosed in a flow-cell, is connected through tubing. (dashed line is an aid to the eye).

Figure 3.12. QCM response to air pressure. A crystal was assembled in a closed metal chamber, from which air was first pumped out (causing a resonant frequency decrease) and then let in (causing a resonant frequency increase). The pressure differential studied was of approximately 100 kPa.

Figure 3.13. QCM in contact with water at 25ºC in batch (a), afterwards 50 µl of water were injected on top of the crystal (b) and then again in a vessel connected by tubing to the crystal flow cell (c). A peristaltic pump was turned on (d), and the water started flowing by overpressure to the crystal chamber, at 1 ml/min in a 1 mm silicone tube (e). The same flow was then achieved but with a 1 mm tygon tube in overpressure mode (f) and then on underpressure mode (g).

Figure 4.1. QCM resonance frequency response to increasing ionic strength. Experimental result with transient response for successive additions of concentrated NaCl solution (arrows) to the final ionic strengths I- 0.2 mM; II- 1.0 mM; III- 3.4 mM; IV- 9.9 mM; V- 26.5 mM; VI- 52.6 mM.

Figure 4.2. Resonant frequency response in function of the addition of injection of 1 ml of NaCl solutions at different concentrations in a PBS 100 mM (pH 7.0) flow (500 µl/min at 25ºC).

Figure 4.3. QCM resonance frequency response to increasing ionic strength. Average resonance frequency variation (Δf) with increasing ionic strength for (●) NaCl, (■) KCl, (♦) $CaCl_2$ and (▲) $MgCl_2$, resulting from $n = 6$ independent measurements for each salt.

Figure 4.4. Variation of the Butterworth van Dyke model parameters in liquid (subscript L), relatively to the crystal loaded with Milli-Q water, with the ionic strength for (●) NaCl, (■) KCl, (♦) $CaCl_2$ and (▲) $MgCl_2$. (A) inductance; (B) resistance; (C) calculated resonance frequency variation, (D) parallel capacitance and (E) parametric polar impedance plot where the ionic strength increases counter-clockwise, as indicated by the arrow. The figures correspond to the average of impedance analysis data resulting from three independent experiments with each salt.

Figure 4.5. Butterworth van Dyke equivalent circuit model (A) and proposed Butterworth van Dyke equivalent circuit (adding B and C) of QCM sensors. I - unloaded resonator; II - elements added due to liquid medium exposure; and III - elements added due to the adsorption of mass on the surface of the sensor.

Figure 4.6. Scheme representing the strategy used to develop a piezoelectric DNA sensor. The crystals were first functionalized with a thiolated oligonucleotide, forming a ssDNA film, used to target the complementary sequence. The complementary oligonucleotide was detected non-labeled and labeled with 10 nm gold nanoparticles.

Figure 4.7. Crystal sensor response to DNA hybridization. All crystal sensors used were functionalized with HS-Pr1 probe and blocked with 11-hydroxy-1-undecanothiol: (A) resonance frequency recorded for crystal sensors incubated with (I) PBS buffer, (II) 1 µM of Ctr1, (III) 1 µM of Tgt1, (IV) 1.7 nM of Au-SAM nanoparticles, (V) 1.7 nM of Au–HS-Tgt1 nanoparticles; (B) impedance data acquired for crystal sensors incubated with gold nanoparticles modified with 11-hydroxy-1-undecanothiol (Au-SAM) and gold nanoparticles functionalized with complementary target HS-Tgt1 (Au–HS-Tgt1).

Figure 4.8. Relation between measured resonance frequency variation and calculated parallel capacitance in the range of 1 mM $\leq I \leq$ 50mM. Triplicate independent experiments for (●)

NaCl (12 experimental points), (■) KCl (12 experimental points), (♦) $CaCl_2$ (12 experimental points), and (▲) $MgCl_2$ (9 experimental points) were performed; Linear regression of experimental data yielded the correlations $\Delta f = (7.8\pm0.4)\times\Delta C + (-24\pm1)$; r = 0.9862; p < 0.0001, for NaCl; $\Delta f = (8.7\pm0.3)\times\Delta C + (-23.6\pm0.8)$; r = 0.9935; p < 0.0001, for KCl; $\Delta f = (7.8\pm0.5)\times\Delta C + (-31\pm2)$; r = 0.9790; p < 0.0001, for $CaCl_2$; and $\Delta f = (7.7\pm0.9)\times\Delta C + (-28\pm4)$; r = 0.9372; p = 0.0002.

Figure 5.1. (A) Frequency shift response of quartz crystal gold sensors to the exposure to increasing bulk concentrations (a- 10 μM; b- 30 μM; c- 50 μM; d- 100 μM; e- 200 μM; f- 300 μM) of 11-hydroxy-1-undecanothiol. (B) Saturation curve showing the total frequency shift obtained for each concentration of alkanethiol used. The curve represents the non-linear interpolation of the data to the saturation component of the molecular model presented in Equation 22, with accepted goodness for $Chi^2 = 9.14 <$ critical $Chi^2 = 11.07$ ($\alpha = 0.05$, $n = 5$). (C) The residuals data for the interpolation presented in B. (D) Scatchard plot and (E) Hill plot for the data presented in B. (F) Linear dependence of the 1:1 molecular model calculated constant τ (relaxation time of binding), to the lowest bulk alkanethiol concentrations used (10-100 μM). Linear regression of experimental data yielded the correlation: $\tau = (2.1\pm0.4)\times10^{-4}$ $\mu M^{-1} s^{-1} \times C + (1.6\pm0.2)\times10^{-2} s^{-1}$; r = 0.9659; ANOVA analysis accepts linear interpolation for F statistic $p = 0.034 < \alpha = 0.05$. Each presented data is the average result of three independent experiments.

Figure 5.2. (A) Blank assays compared to biotin-streptavidin molecular recognition: (1) crystal with biotin exposed to streptavidin at 3 μg/ml, (2) crystal with biotin exposed to BSA at 50 μg/ml (3) clean crystal exposed to streptavidin at 3 μg/ml, (4) crystal with biotin exposed to PBS and (5) crystal with SAM exposed to streptavidin at 3 μg/ml. (B) Biotin functionalized QCM resonance frequency response, to different streptavidin concentrations (μg/ml): (a) 0.025, (b) 0.05, (c) 0.1, (d) 0.2, (e) 0. 5, (f) 1.0, (g) 2.0 and (h) 3.0. Each presented curve represents the average of three transients obtained experimentally. (C) Saturation curve showing the total frequency shift obtained for each concentration of streptavidin used. The curve represents the non-linear interpolation of the data to the saturation component of the molecular model presented in Equation 22, with accepted goodness for $Chi^2 = 0.79 <$ critical $Chi^2 = 14.07$ ($\alpha = 0.05$, $n = 7$). (D) The residuals data for the interpolation presented in C. (E) Scatchard plot and (F) Hill plot for the data presented in C.

Figure 5.3. Impedance measurements for each streptavidin concentration. The (▲) inductance XL_F , (●), resistance R_F and (◊) parallel capacitance C_F contribution of streptavidin film to the BVD equivalent circuit, for each tested concentration.

Figure 5.4. Linear dependence of the 1:1 molecular model calculated constant τ (relaxation time of binding), to the streptavidin concentrations used (0.5-57 nM). Linear regression of experimental data yielded the correlation: $\tau = (4.6\pm0.3)\times10^5\ M^{-1}s^{-1} \times C + (0.3\pm5)\times10^{-5}\ s^{-1}$; r = 0.9882; ANOVA analysis accepts linear interpolation for F statistic $p < 0.0001 < \alpha = 0.05$. Each presented data is the average result of three independent experiments.

Figure 5.5. Dependence of the calculated streptavidin-biotin association kinetic constant k_1 to increasing flow rates (Q) of carrier buffer used during piezoelectric biosensing experiments.

Figure 6.1. Representation of the antibodies 4BL, VH and VHD produced to develop the piezoimmunosensor. IgG- Immunoglobulin G; HCAb- Humanized Chimeric Antibody. Adapted from Gonçalves *et al.*, 2002 and da-Silva *et al.*, 2004.

Figure 6.2. Immobilization of the recombinant antibodies on the surface of activated sensors. Measured resonance frequency variation during antibody immobilization using solutions of increasing concentration of (A) anti-Vif ScFv 4BL, (B) anti-Vif VH single domain, and (C) anti-Vif VHD camelized single domain; (D) immobilization isotherms of 4BL, VH, and VHD.

Figure 6.3. Variation of BVD parameters during antibody immobilization at 50 µg/ml (◊),75 µg/ml (■),100 µg/ml (Δ), 150 µg/ml (♦), and 200 µg/ml (○).

Figure 6.4. Total variation of the resonator resistance obtained after at the equilibrium for immobilization of (♦) 4BL, (□) VH and (▲) VHD.

Figure 6.5. Binding of HIV1 Vif preparations of increasing concentrations (values next to each curve with units µg/ml) to sensors modified with (A) anti-Vif scFV 4BL, (B) anti-Vif single domain antibody VH, and (C) anti-Vif camelized single domain antibody 4BL; (D) specific equilibrium frequency signal for each antibody concentration (♦) 4BL, (□) VH, (▲) VHD. The data presented correspond to average transients from 6 independent measurements for each Vif concentration. Indicated concentrations refer to total protein quantification in purified HIV1 Vif preparations and not to HIV1 Vif monomeric isoforms. Cytochrom C (▬),

BSA (—), and Ribonuclease A (—), all at a concentration of 100 µg/ml, were used as controls.

Figure 6.6 Figures A (ΔXL), B (ΔR), and C (ΔC) present the variation of the Butterworth van Dyke model parameters, relatively to the response of the three immunosensors (◊) 4BL, (▲) VH and (●) VHD to different concentrations of Vif. Each presented data is the average result of six independent experiments.

Figure 6.7. Corrected frequency transients for the binding of HIV1 Vif to 4BL biofilms.

Figure 6.8. Linear dependence of the 1:1 molecular model calculated constant τ^{-1}, to the bulk Vif concentrations used for each immunosensor: (♦) 4BL, (□) VH and (▲) VHD. Linear regression of experimental data yielded the correlations: $\tau^{-1} = (1.3\pm0.2)\times10^{-5}\times C + (1.1\pm0.1)\times10^{-3}$; $r = 0.9697$; $p = 0.0063$, for 4BL; $\tau^{-1} = (2.5\pm0.2)\times10^{-5}\times C + (0.4\pm0.09)\times10^{-3}$; $r = 0.9963$; $p = 0.0037$, for VH; $\tau^{-1} = (3.6\pm0.3)\times10^{-5}\times C + (1.2\pm0.2)\times10^{-3}$; $r = 0.9885$; $p = 0.0015$, for VHD. Each presented data is the average result of six independent experiments.

Figure 6.9. Detection of HIV1 Vif in complex mixtures with VHD camelized single domain antibody piezoimmunosensors. Arrows indicate the moment of sample application to the sensor. (A) A mixture of 100 µg/ml BSA, Cytochrom C, and Ribonuclease A was added to the crystal and the frequency was monitored for a period of time before spiking with 50 µg/ml HIV1 Vif preparation; (B) sensor response obtained for cell extracts: HEK293 cell extracts from the control cell cultures (cells only expressing CFP) were applied to the sensor (curve I) and spiked with 50 µg/ml HIV1 Vif preparation (curve II); curve III shows the sensor response for cell extracts obtained from HEK293T cell cultures expressing HIV1 Vif.

List of Tables

Chapter 1

Introduction

1.1. What is a Biosensor?

The integration of advanced microfabrication technologies, signal processing systems and biological sensing interfaces to produce biosensors, has emerged in very recent years as a rapidly growing area of enormous potential, aiming specially at the simplification of chemical/biochemical measurements and extending assay reliability outside the confines of a central laboratory (Pearson *et al.*, 2000; Willner and Wilner, 2001). The field of biomolecular sensors is now beginning to materialize as an aid to understand the underlying biophysical principles of molecular recognition as well as to detect the presence of specific analytes.

Currently, biosensors are widely used in clinical diagnosis and biomedicine as diagnostic tools and for drug screening (Sakai *et al.*, 1995; Chang *et al.*, 2000; Aizawa *et al.*, 2004). There are also developed applications for environmental monitoring and pollution control, for military and security tasks like the detection of chemical/ biological weapons and explosives

and for industrial processes (Gomes *et al.*, 1998; Su *et al.*, 2001; Mirmohseni and Alipour, 2002; Skládal, 2003).

The IUPAC (International Union of Pure and Applied Chemistry) definition for a biosensor is: "A biosensor is a self-contained integrated device, which is capable of providing specific quantitative or semi-quantitative analytical information using a biological recognition element (biochemical receptor) which is retained in direct spatial contact with a transduction element. Because of their ability to be repeatedly calibrated, we recommend that a biosensor should be clearly distinguished from a bioanalytical system, which requires additional processing steps, such as reagent addition." (IUPAC, 1999).

A biosensor is basically a molecular sensing element (*e.g.* bioreceptors like antibodies, DNA, enzymes, cells) attached to a transducer (Fig. 1.1).

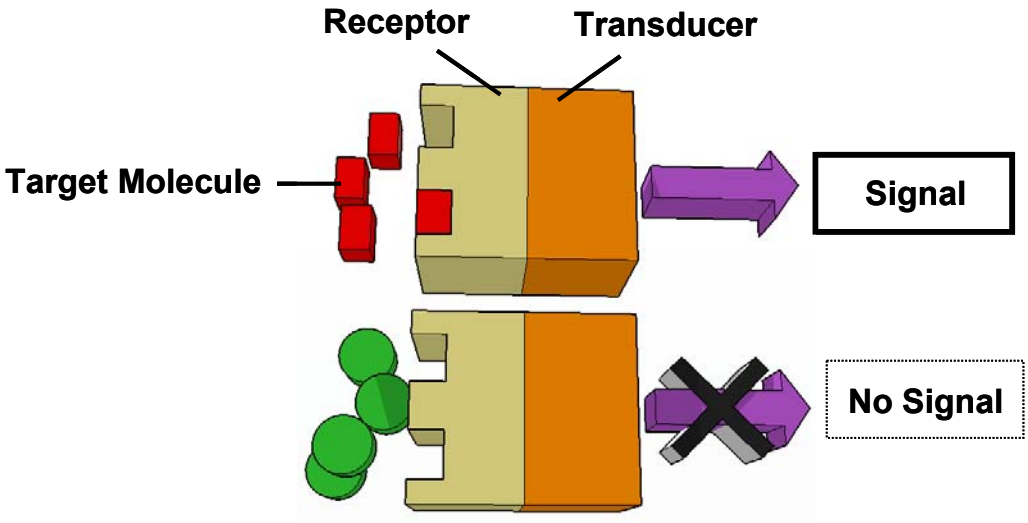

Figure 1.1. Schematic representation of a biosensor.

The molecular sensing element recognizes the target analyte and the transducer converts the recognition event into an electrically measurable signal, related to the build-up of concentration or activity of the analyte in the vicinity of the device.

The most common transducers used for biosensing applications, are electrochemical, amperometric (detect changes in current at constant potential), potentiometric (detect changes in potential at constant current), conductive (detect changes in conductivity between two electrodes), chemically sensitive FETs (field effect transistors), capacitive (used when the biorecognition reaction causes a change in the dielectric constant of the medium), optical (correlate changes in concentration, mass, or number of molecules to direct changes in the characteristics of emitted or absorbed light), mechanical or acoustic (detect changes in mass, strain, surface stress, viscosity), thermal (measure changes in temperature) and magnetic (takes advantage on the magnetic properties of materials).

The main steps in biosensor development include the identification of the target analyte to be detected, the selection of a suitable molecular sensing element (bioreceptor molecule), the selection of a suitable immobilization method of the bioreceptors to the transducer and a suitable transducer. It also has to be considered the design of the sensor, including readout electronics, detection limits, possible interfering sources, linearity of the response, etc. and the design of the sensor packaging.

The main requirements for an ideal biosensor include the clear discrimination of the output signal relatively to the measurement environment, the compatibility between the functional surface and the transducer, high specificity (capability to interact with the analyte of interest) and selectivity (low interference from other molecules), sufficient sensitivity and resolution (low detection and quantification limits), sufficient accuracy and repeatability (no false-positive or false-negative results), sufficient speed of response (preferentially real-time response) and sufficient dynamic range. Another crucial issue is insensitivity to environmental interference or else the effects must be compensated (temperature, chemical

environment, pH, ionic strength, non-specific binding, electric and electromagnetic effects, etc.)

The current work focuses on the development of piezoelectric based biosensors, where the transducer is acoustic and mechanically responds to mass changes. The transducers chosen to develop the biosensors are commonly denominated microgravimetric devices, generally known as quartz-crystal microbalance (QCM), that have already been used for different applications (Pan *et al*., 1996; Etchenique and Brudny, 2000; Ewalt *et al*., 2001; Liss *et al*., 2002; Liu *et al*., 2004; Fabregette *et al*., 2005; Su and Li, 2005; Modin *et al*., 2006). and its advantages, limitations, physical principles and working conditions are next described.

1.2. The piezoelectric effect

In 1880, the Curie brothers demonstrated that the deformation of a Rochelle salt crystal (sodium potassium tartrate) through pressure application results in the generation of a voltage across the crystalline material (Curie and Curie, 1880). This phenomenon was called the piezoelectric effect, based on the Greek word "piezin", that means "to press" (Hankel, 1881). Later the Curies demonstrated the opposite effect: the application of a potential across a piezoelectric material produces a mechanical stress and the distortion of the structure (Curie, 1908). This is still nowadays called the converse piezoelectric effect (Varela *et al*., 2000).

In the beginning of the 20th century it was discovered that quartz crystals exhibiting piezoelectric properties could be used as transducers and receivers of ultrasound in water and from then on the piezoelectric effect was used to develop acoustic based technology: speakers, microphones and sound pick-ups. In the 1920's, it was demonstrated that through

the piezoelectric effect, the resonant vibration of quartz produced an AC electrical signal with a very stable and precise frequency (Cady, 1921; Pierce, 1923). This signal allowed a high precision time reference, and so quartz crystals are still used nowadays in the electronics field as clocking elements.

In 1959, Sauerbrey published an article in which he described that the resonant frequency change of a crystal is directly proportional to the deposited mass on its surface (Sauerbrey, 1959). With the work of Sauerbrey, the first step was taken towards the development of a new small-mass measuring tool: the quartz crystal microbalance (QCM).

In the 60s and 70s the QCM began to be used as a tool to monitor thickness of films in vacuum and air and is still used today to control the thickness during the process of deposition of layers (Janshoff *et al.*, 2000).

But the technology developed until the late 70s for oscillator circuits, to drive the vibration of quartz crystals, was only suitable for measurements in air, not allowing proper operation of the resonators in fluids. In 1982, Nomura and Okuhara built an oscillator circuit that permitted the use of QCM in liquid environments (Nomura and Okuhara, 1982), giving the first instrumental step for the basic development of QCM biosensing tools.

1.3. Quartz crystal microbalance- QCM

Generally, a quartz crystal microbalance is a device that can be induced to vibrate or oscillate at a stable frequency that strongly depends on mass.

The quartz crystals to be used as microbalances are cut with an angle of 35º 10’ to the optical z-axis of a mother crystal (AT-cut) (Fig. 1.2). AT-cut crystals exhibit a high frequency

stability of $\Delta f/f \approx 10^{-8}$ and a temperature coefficient that is almost zero between 0-50ºC. Hence these crystals exhibit small changes in frequency due to temperature variation, making them the most suitable for QCM sensors (Göpel *et al.*, 1991; Sullivan and Guilbault, 1999).

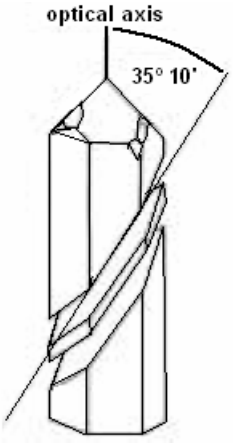

Figure 1.2. AT-cut of a quartz crystal. A quartz plate is cut at an angle of 35º10' with respect to the optical axis. A deviation of only 5' leads to a temperature coefficient that is different from zero in the range of 0-50ºC.

The commercial version of the QCM basically consists of AT-cut thin quartz discs, with circular metal electrodes on both sides (Fig. 1.3) to drive the oscillations.

Due to its piezoelectric properties, when the electrodes are connected to an oscillator and an AC electrical field is applied, parallel to the piezoelectric axis (direction in which tension or compression develops polarization parallel to the strain), a shear wave is generated that propagates through the crystal inducing the oscillation of the crystal (Fig. 1.4) (Chagnard *et al.*, 1996; Sullivan and Guilbault, 1999).

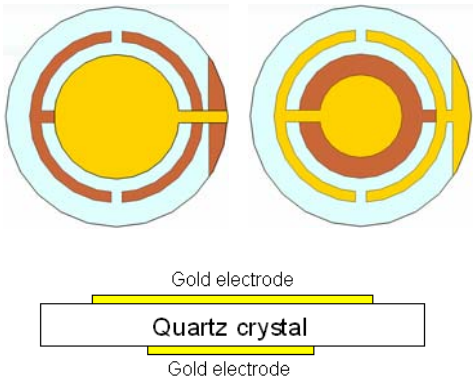

Figure 1.3. QCM top and bottom views showing the metal electrodes and a cross section.

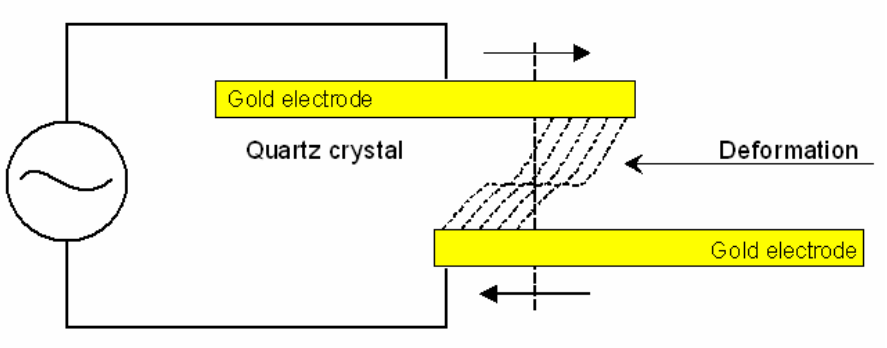

Figure 1.4. Shearing mode of vibration of AT-cut quartz discs due to the application of a potential across the structure of the crystal.

The crystal vibrates at the frequency of the applied AC field. If such frequency is coincident with to the frequency where the impedance of the crystal is minimal, the amplitude of the crystal vibration will be maximized. This is called the crystal's fundamental resonance frequency and an electronic circuit, using feedback (Fig. 1.5), can be used to stabilize the frequency at its resonance value (Chagnard *et al.*, 1996; Sullivan and Guilbault, 1999; Kaspar *et al*., 2000).

For shear mode oscillation there are several frequencies that correspond to resonant conditions, termed harmonic or overtone resonance frequencies (such as 3rd overtone, 5th

overtone, etc.). For all resonant modes, displacement maxima occurs at the crystal faces, however the largest amplitude occurs at the fundamental frequency and as the harmonic number increases the vibration amplitude decreases (Sullivan and Guilbault, 1999).

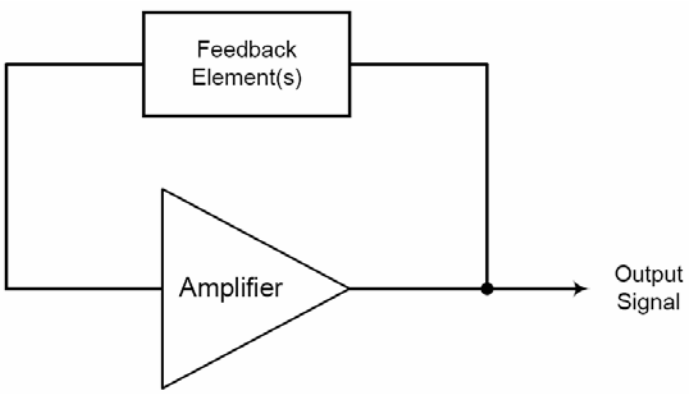

Figure 1.5. Basic structure of an oscillator circuit.

The quartz crystal microbalance is also denominated a Thickness-Shear-Mode Resonator (TSM), because the acoustic wave generated piezoelectrically propagates across the crystal, through the bulk of the material. The thickness of the crystals determines the fundamental resonance frequency, at which the crystal can vibrate mechanically. For instance, a 5 MHz quartz exhibits a thickness of 0.33 mm, while a 30 MHz crystal is only 55 μm thick (Göpel *et al.*, 1991; Sullivan and Guilbault, 1999).

A characteristic of QCM sensors is that when exposed to air exhibit a high quality factor (Q) value, which is the ratio of the energy stored to energy lost during a single oscillation. In terms of frequency signal, it is represented has the ratio between the resonance frequency and the frequency width at half maximum ($Q = f_0/\Delta f_{FWHM}$). Low energy losses in oscillating systems are manifested as high accuracies, *i.e.* feature sharp resonant frequency values with a small bandwidth, allowing the precise measurement of the frequency. For quartz crystals in

gas phase this quantity can exceed 10^5, but in liquid applications however, Q will generally have values in the order of 10^3, indicative of energy damping by the fluid, but the quartz crystals still perform acceptably at these levels (Kanazawa and Gordon, 1985; Chagnard *et al.*, 1996; Sullivan and Guilbault, 1999).

1.4. Physical model of a quartz crystal piezoelectric sensor

As mentioned earlier, piezoelectric materials have the distinctive capability to induce a mechanical strain when an electrical voltage is applied, and vice versa. By stimulating a sensor with an alternating voltage, standing acoustic waves are created within the sensor, and the sensor acts as an extremely responsive resonator (Fig. 1.6).

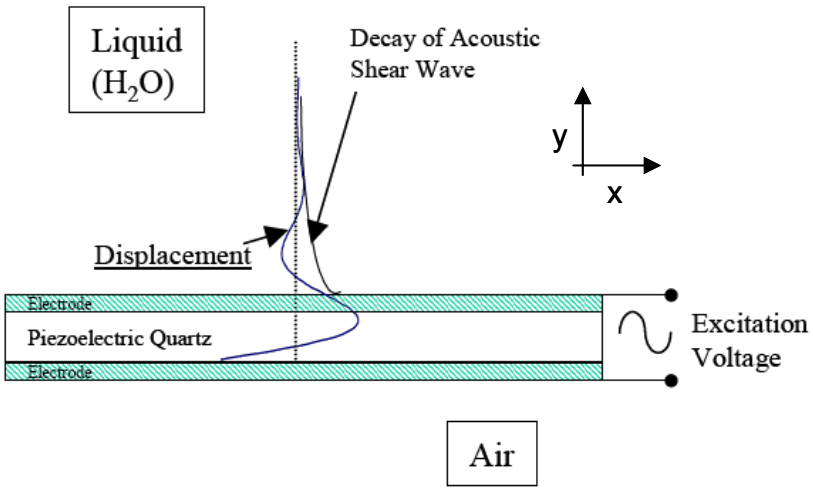

Figure 1.6. Schematic representation of the physical model of the wave motion in the piezoelectric element and the liquid. Adapted from Lec, 2001.

If the sensor is weighed down with a medium, it transmits a shear wave through the medium (Fig. 1.6). The generated shear wave penetrates a very short distance into the liquid, and the influence of the boundary conditions on the behavior of the sensor is extremely dominant. Hence the response of a crystal sensor to changes on its surface is based on corresponding changes in its resonant behavior. The crystal acts as both a mechanical and an electrical resonator coupled through the piezoelectric effect (Ballantine *et al.*, 1997). During an oscillation mechanical energy is transferred from kinetic energy of the moving mass of the crystal to potential energy stored in the elastic deformation of the crystal. As resonance losses are minimized and the vibration amplitude reaches a maximum (Lec and Lewin, 1998; Janshoff *et al.*, 2000). This resonance frequency depends on the crystal properties, on the mass deposited on the crystal surface, and on the coupling between the surface and the surrounding liquid medium.

The linear theory of piezoelectricity regarding wave motion through the quartz crystal is complex, and requires satisfying a set of mechanical and electrical models, that relate the production of electric displacement by applying mechanical stress (piezoelectric effect) and the production of strain in the crystal by applying an electrical field (converse piezoelectric effect) (Martin *et al.*, 1991; Martin *et al.*, 1993; Janshoff *et al.*, 2000; Lec, 2001).

When the acoustic wave is transmitted from the surface of the crystal and propagates through the liquid, an energy loss occurs. The shear wave transmitted into the fluid dissipates quickly as the energy is converted to heat by viscous friction (Martin *et al.*, 1991; Martin *et al.*, 1993; Janshoff *et al.*, 2000; Lec, 2001).

In liquid phase, the description of the propagation of the acoustic waves in terms of one-dimensional mechanical motion relies on two simple boundary conditions. The first condition is the assumption of no slip, that is, the layer of fluid closest to the surface moves at the same

velocity as the surface. The second fluid boundary condition states that fluid motion decays with distance from the crystal surface, vanishing at infinite distance (Martin *et al.*, 1991; Martin *et al.*, 1993; Janshoff *et al.*, 2000; Lec, 2001).

For an oscillatory shear driving force at the solid/liquid boundary, the amplitude of oscillation (A) decays in an exponential form, within a length (δ) in the direction normal to the surface of the crystal (y axis)(Glassford, 1978, Martin *et al.*, 1991). The decay length (δ) that limits the propagation of the damped shear wave into the fluid is dependent on the viscosity (η_L) and density (ρ_L) of the liquid:

$$A = A_0 e^{-\frac{y}{\delta}} \tag{1}$$

$$\delta = (2\eta_L / \omega\rho_L)^{1/2} \tag{2}$$

Where the term A_0 is a constant and ω is the angular frequency ($\omega = 2\pi f$, f is resonance frequency).

For water, the decay length of the acoustic shear wave, at a resonance frequency of 5 MHz, is approximately 250 nm (Ricco and Martin, 1987). This indicates that the quartz resonator responds to the fluid only in the region very near the oscillating surface.

As explained in section 1.3, a TSM sensor can operate at odd harmonics. The resonance frequency at each harmonic generates a different shear wave, and so according to Equation 2,

the crystal sensor can probe the interface at different depths, *i.e.* if the frequency increases, then the depth of penetration is reduced (Fig. 1.7).

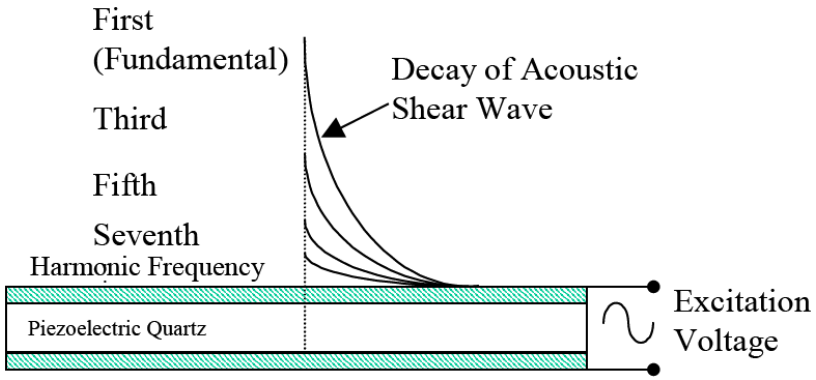

Figure 1.7. Influence of operation frequency (fundamental and harmonics) on shear wave penetration. Adapted from Lec, 2001.

1.5. QCM as a mass sensing tool

The vibrational motion of the quartz crystal results in an acoustic wave that propagates back and forth across the thickness of the crystal, between the crystal faces. At resonance a standing wave condition is established in the quartz resonator and the fundamental resonance frequency, f_0, of the acoustic wave, which is also known as the thickness shear mode or the fundamental mode (Bechmann, 1952), is given by the following equation:

$$f_0 = \frac{\sqrt{\mu_Q}}{2l_Q\sqrt{\rho_Q}} \tag{3}$$

Where l_Q is the thickness of the resonator, ρ_Q is the density of quartz (2.648 g.cm^{-3}) and μ_Q is the shear modulus of quartz (2.947×10^{11} g.cm^{-1}.s^{-2}).

Considering that the mass of the quartz crystal per unit area ($M = m/A$) is given by the product of the crystal thickness and quartz density ($l_Q \rho_Q$), Equation 3 can be written as:

$$f_0 = \frac{\sqrt{\mu_Q \rho_Q}}{2M} \tag{4}$$

The addition of mass (per unit area) ΔM causes a change in resonance frequency Δf:

$$f_0 + \Delta f = \frac{\sqrt{\mu_Q \rho_Q}}{2(M + \Delta M)} \tag{5}$$

Combining Equation 4 with Equation 5 and rearranging:

$$\Delta f = -\frac{f_0 \Delta M}{M\left(1 + \frac{\Delta M}{M}\right)} \tag{6}$$

For a thin deposit, where $\Delta M << M$ equation 6 becomes:

$$\Delta f = -\frac{f_0 \Delta M}{M} \tag{7}$$

Considering the concept of mass change per unit area, Equation 7 can be written as:

$$\Delta f = -\frac{f_0}{l_Q \rho_Q} \frac{\Delta m}{A} = -C_m \Delta m \tag{8}$$

This is the basic Sauerbrey equation (Sauerbrey, 1959), where Δf is the resonance frequency change (Hz), Δm is the surface mass change ($\mu g.cm^{-2}$) and C_m is known as the sensitivity factor dependent on the fundamental resonance frequency. This equation defines the utilization of a QCM as a mass measuring tool due to the simple fact that the resonant frequency decreases with mass deposition on the active area of the exposed electrode.

This model makes the assumption that the attached mass follows the vibration of the crystal and therefore the crystal behaves as if it was simply thicker; the equation is only usable for thin, rigid and uniform films. So in this model a QCM sensor is understood as a multilayer structure of one piezoelectric layer and a certain limited number of non-piezoelectric and non-viscoelastic layers. If the mass is elastic, then it will not rigidly follow the vibration and its viscoelasticity will also contribute to the frequency shift (Tenan and Soares, 1998; Sabot and Krause, 2002).

In the 1980's Kanazawa and Gordon developed a simple mathematical relation that describes the resonant frequency of a QCM dependence on the density and viscosity of liquids

(Kanazawa and Gordon, 1985). The Kanazawa equation predicts that the change in resonant frequency of a QCM is proportional to the square root of the liquid's density-viscosity product (Equation 9).

$$\Delta f = -C'_{\mathrm{f}} \sqrt{(\rho_{\mathrm{L}} \eta_{\mathrm{L}})} \tag{9}$$

Where, C'_{f} is the liquid sensitivity factor (7140.5 $Hz^{1/2}$ $g^{-1}.cm^2$), ρ_{L} is the liquid density and η_{L} is the liquid viscosity.

1.6. Impedance analysis of QCM

Impedance is an important parameter used to characterize electronic circuits, components, and the materials used to make components. Impedance (Z) is generally defined as the total opposition a device or circuit offers to the flow of an alternating current (AC) at a given frequency, and is represented as a complex quantity which can be graphically represented on a vector plane as a magnitude and phase angle: $|Z| \angle \phi$. An impedance vector consists of a real part (resistance, *R*) and an imaginary part (reactance, *X*) and can also be expressed using the rectangular-coordinate form $R + jX$.

Impedance analysis of quartz crystal microbalances is supported on a system modeling of the piezoelectric resonator, which consists on an electrical/mechanical analog. It is important to remember that the piezoelectric resonator is a mechanical structure that is forced to oscillate at a specific set of frequencies and can be modeled mechanically as a simple vibrating

structure. The basic model for a vibrating mechanical structure is that of a mass, spring and damper (Buttry and Ward, 1992) (Fig. 1.8).

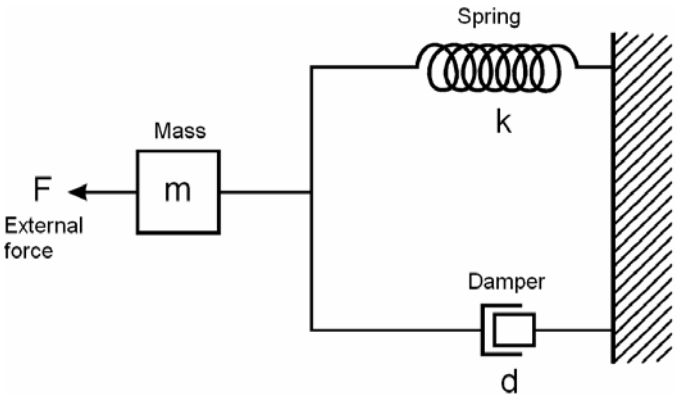

Figure 1.8. Basic mechanical model of a resonator.

For the model presented in Fig. 1.8, there are three fundamental parameters that determine the overall response to the force *F*: the mass of the system (*m*), the spring constant (*k*) and the damping of the damper (*d*). Writing the equation of motion for this system:

$$m\frac{d^2x}{dt^2} = F(t) - d\frac{dx}{dt} - kx(t) \tag{10}$$

Because of the piezoelectric effect, the mechanical system is linked to the electrical domain and Equation 10 can also be expressed in an electrical oscillation. Using Kirchoff's voltage law and by making an analog between displacement (*x*) and charge (*Q*), it is possible to

develop an RLC equivalent electrical circuit for the resonant mechanical structure (Buttry and Ward, 1992; Bandey *et al.*, 1996; Soares *et al.*, 1998, Etchenique and Calvo, 1999):

$$L_m \frac{d^2Q}{dt^2} + R_m \frac{dq}{dt} + \frac{1}{C_m} Q(t) = 0 \tag{11}$$

The different components of this RLC circuit are an inductor (L_m), a resistor (R_m) and a capacitor (C_m). The inductor (L_m) corresponds to the oscillation inertial component and is related to the dislocated mass during vibration (Martin *et al.*, 1991). The resistor (R_m) corresponds to the oscillating energy dissipation to the structure where the crystal is mounted and to the medium which is in contact with (viscous solutions and viscoelastic films) (Martin *et al.*, 1991). The capacitor (C_m) corresponds to the stored energy in oscillation and is related to the crystal's elasticity (Martin *et al.*, 1991). The representation of an equivalent electric circuit of a clean quartz crystal microbalance with metallic electrodes is defined by the Butterworth van Dyke model (BVD) (Fig. 1.9) (Martin *et al.*, 1991).

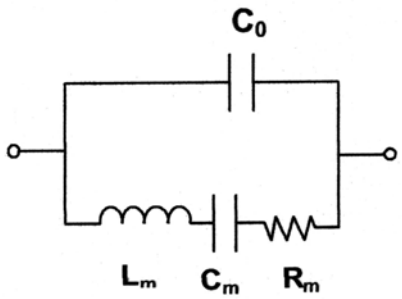

Figure 1.9. The Butterworth van Dyke model (unloaded QCM).

The BVD circuit combines a parallel (static branch) and series resonance circuit (motional branch). The motional branch consists of L_m, C_m and R_m. The electrodes on both sides of the crystal plate provide an additional parallel capacitance C_0, which gives rise to the parallel circuit.

An advanced measurement system like a network analyzer is able to quantify the parameters R_m, L_m, C_m and C_0 and distinguish its different contributions. In order to do so, the network analyzer is tuned to supply the impedance magnitude and phase angle around the crystal's resonance frequency that can be defined by the components L_m and C_m (Martin *et al.*, 1991):

$$f_0 \approx \frac{1}{2\pi\sqrt{L_m C_m}} \tag{12}$$

When using an oscillator circuit to drive a QCM to vibrate, its resonance frequency can be easily read with a simple frequency counter. However when using a network analyzer to follow the resonance frequency of the quartz sensor, the impedance spectroscopy data is much more complex to interpret.

Figure 1.10 shows a representation of typical impedance and phase angle spectrums that can be experimentally obtained for a QCM, using a network analyzer. The figure depicts two cases: QCM exposed to air (A) and to liquid (B). In air, both impedance and phase angle plots are represented has sharp spectrums localized in a frequency range that contains the resonance frequency of the QCM. When the quartz crystal is immersed in a liquid, both spectrums move toward lower frequencies and each peak also diminishes and broadens.

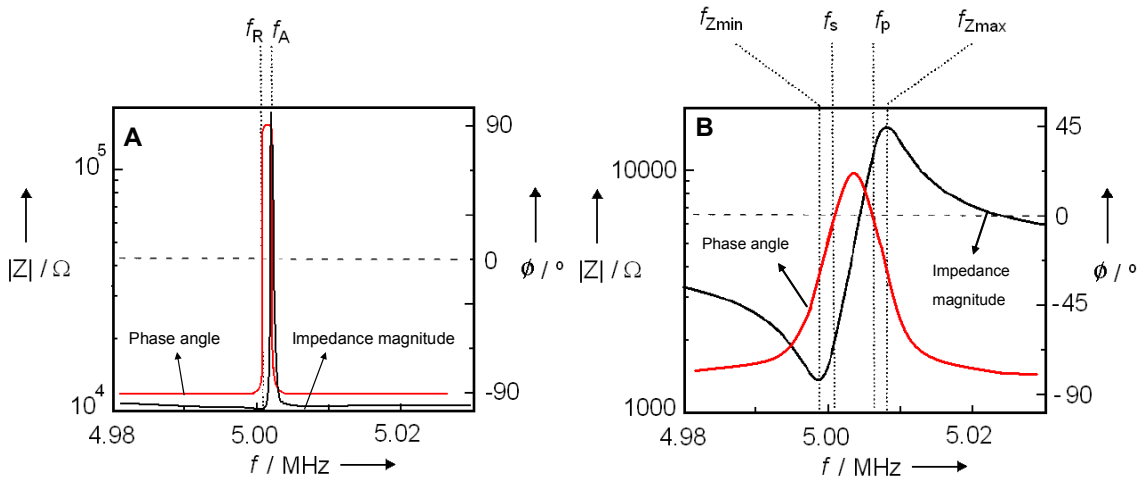

Figure 1.10. Representation of impedance and phase angle spectrums as obtained with a network analyzer, for air (A) and liquid exposure (B) of a QCM. Considering the BVD equivalent circuit, for the case of unloaded sensor ($R_m \rightarrow 0$) there are two marked resonance frequencies: f_R and f_A. For the case of sensor damping ($R_m > 0$) there are four marked resonance frequencies: f_{Zmin}, f_s, f_p, and f_{Zmax}.

For the air exposure case, where the damping is negligible ($R_m \rightarrow 0$), the resonance frequency (f_R) of the QCM, as obtained with an oscillator circuit, is located where the phase angle is zero ($\phi = 0$) and the impedance magnitude $|Z|$ is minimum. At maximum magnitude the frequency is referred as antiresonant frequency f_A, where the phase angle is also zero, but this frequency is not related to mass as defined by the Sauerbrey model (Bottom, 1982; Martin *et al.*, 1991; Martin *et al.*, 1993).

When the QCM is in liquid medium and damping occurs ($R_m > 0$), four different resonance frequencies are discernable (Fig. 1.11). The resonance frequency f_R separates into f_{Zmin}, the frequency at minimal impedance, and f_s, the frequency at zero phase. These two frequencies are of special interest since the operating frequency of oscillator circuit based microbalance systems is located between f_{Zmin} and f_s (Janshoff *et al.*, 2000). The antiresonant frequency f_A separates into the frequencies f_{Zmax}, the frequency at maximum impedance and f_P, the frequency at zero phase angle.

The common procedure to determine the value of each component of the equivalent circuit is to work exclusively with the impedance magnitude spectrum ($|Z|$), but the phase angle spectrum can also give the same information. Because the sensor analysis is based on a parallel circuit, it is mathematically simpler to convert the impedance data into admittance data. So, from each experimental impedance magnitude curve, the admittance magnitude function ($|Y| = 1/|Z| = (G^2 + B^2)^{1/2}$, where G is conductance and B is susceptance) can be determined (Calvo *et al.*, 1997; Etchenique and Weisz, 1999; Zhou *et al.*, 2000). The phase angle is ϕ = arctg (B/G.) For the BVD circuit the complex admittance ($Y = G + iB$) can be represented has:

$$Y_{BVD} = i\omega C_0 + \frac{1}{R_m + i\left(\omega L_m - \frac{1}{\omega C_m}\right)} \tag{13}$$

Thus, the magnitude is:

$$|Y| = \sqrt{\left(\frac{R_m}{R_m^2 + U^2}\right)^2 + \left(\omega.C_0 - \frac{U}{R_m^2 + U^2}\right)^2} \tag{14}$$

Where, $U = \omega.L_m - \frac{1}{\omega.C_m}$ (15)

Considering the situation where C_0 = 0, Equation 12 is verified for the maximum of the admittance magnitude function (Equation 13) and phase angle equal to zero. This condition determines the use of an oscillator circuit, since the system will electrically oscillate at the mechanical resonance frequency of the QCM. Measuring the full admittance spectrum will allow the determination of all 4 parameters, rather than only the product $\sqrt{L_m C_m}$, and will reveal the nature of the medium in more detail. When a liquid is added or mass is deposited on the crystal's surface, a change in impedance/admittance occurs and new elements are simply added to the BVD model (Fig. 1.11) (Bizet *et al.*, 1998; Ha and Kim, 2001).

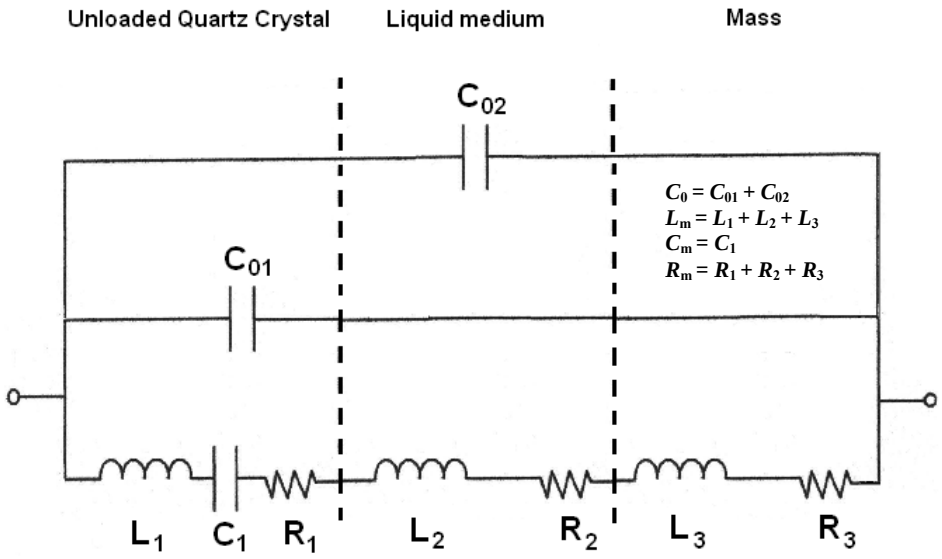

Figure 1.11. Modified Butterworth van Dyke model representing a loaded resonator in liquid medium. The original four BVD electrical elements L_m, R_m ,C_m and C_0 are the sum of different contributions, namely the liquid loading and mass adsorption.

As mentioned previously in section 1.3, the Q factor is the ratio of the energy stored to the energy lost during a single oscillation of the quartz crystal. According to the BVD model the

Q factor drop in liquid because of an increased dissipation of energy in the medium can be defined as:

$$Q = \frac{2\pi f_0 L_m}{R_m} = \frac{X_L}{R} \tag{16}$$

However, also the values of L_m and C_0 change, revealing an increased effective mass at the interface and increased electrode capacitance respectively. Moreover, it has been shown that additional mass deposited on the crystal has different effects for viscoelastic and rigid mass (Martin *et al.*, 1991; Sherrit *et al.*, 1997; Schmitt *et al.*, 1997; Tenan and Soares, 1998; Lucklum and Hauptmann, 2000). Whereas rigid mass only changes the value of the inductance L_m, viscoelastic mass also changes R_m, while a liquid loading of a Newtonian fluid changes the two parameters simultaneously. For Newtonian fluids $\Delta X_L/\Delta R = 1$ ($X_L = \omega L$), hence this is the way to conduct a system check for the network analyzer and evaluate the QCM's electroacoustic response particularly under the influence of viscous energy losses (Janshoff *et al.*, 2000).

An important relation to establish is how acoustic losses, *i.e.* the resistive parameter, influences the resonant frequency value measured when using an oscillator circuit and a frequency counter. The theoretical relation between R and frequency change due to viscoelastic effects Δf_{visc} is (Martin *et al.*, 1991):

$$\Delta R \approx -4\pi L_m \Delta f_{visc} \tag{17}$$

The parameter L_m is the motional inductance of the QCM in air. This relation can be used as a calibration curve for viscoelastic non-mass effects which allows the simple subtraction of its contribution to the total frequency shift, thus allowing the calculus of just the real mass adsorbed on the surface of the crystal.

The complex analysis that impedance spectroscopy provides presents an effective way to detect and quantify the influence of important interferents in the QCM performance, particularly viscoelastic (Martin *et al.*, 1991; Auge *et al.*, 1995; Bouche-Pillon *et al.*, 1995; Etchenique and Weisz, 1999; Lucklum and Hauptmann, 2000; Zhou[a] *et al.*, 2000; Encarnação *et al.*, 2007). Hence, this technique can provide answers that only frequency reading cannot, particularly considering the limitations of the Sauerbrey model.

1.7. Deviations in the QCM response

The use of QCM as a transducer in the development of biosensing tools has been mainly focused on the direct relation between mass and resonance frequency, as described by Sauerbrey. This approach can introduce significant deviations in the interpretation of results, particularly when using biomolecules as receptors, targeting other biomolecules in aqueous mediums.

To better understand all physical aspects behind the piezoelectric response to mass a more complex one-dimensional approach is used to overcome the lack of information in resonant frequency measurements. This approximation relates the acoustic load impedance acting at the surface of the quartz crystal to two directly measurable values: the frequency shift and the

motional resistance. These two values are understood as a measure of acoustic energy storage (film mass contribution) and acoustic energy dissipation (film viscoelastic contribution). In this one-dimensional approximation, a layer is completely characterized by its density (ρ_f), thickness (h_f) and the shear complex modulus G. This modulus contains the information about the viscoelasticity of the film material and so is related to how the shear wave travels through a layer deposited on the crystal. The real part of the complex G is the shear storage modulus (G'- stored energy) and the imaginary part is the shear loss modulus (G"- energy dissipated). These moduli define how elastic (G') and viscous (G'') is the deposited layer (Lucklum *et al.*, 1997; Etchenique and Weisz, 1999). Other elements to account for in the one-dimensional approximation are density, ρ_L, and viscosity, η_L, of a (semi-infinite) liquid.

However even this approach does not describe entirely all the physical phenomena that can contribute to the response of a QCM sensor. The generalized characteristic film parameters have the potential to incorporate effects not present in a one-dimensional description. The relationship to properties of the real film must be established from different models, which can be two- or three-dimensional (Lucklum and Hauptmann, 2003).

Major effects which may affect the sensor signal under real experimental conditions, are summarized in Figure 1.12.

Uniformity is one important condition since it is required in the Sauerbrey model to reliably relate resonance frequency shift to deposited mass. In a non-uniform surface situation, upon shear resonance the waves coupled back into the quartz crystal will have different amplitudes and different wave vectors, as compared to the ideal case where the deposited film is uniform (Auld, 1990).

Surface roughness is always inevitable either on films or the quartz crystal surface itself. A rough top sensor surface tends to trap a significant amount of mass if the sensor is immersed

in a liquid. The drop in frequency is not necessarily the same compared to that measured with a smooth sensor surface and a damping effect on the sensor is usually high under real conditions (Daikhin and Urbakh, 1997). Hydrophilic surfaces can also contribute to the overall detected mass, because they entrap liquids in small cavities. On the other hand hydrophobic cavities are not wetted by the liquid and result in the inclusion of air or vacuum, leading to smaller energy losses than in hydrophilic surfaces (Martin *et al.*, 1993).

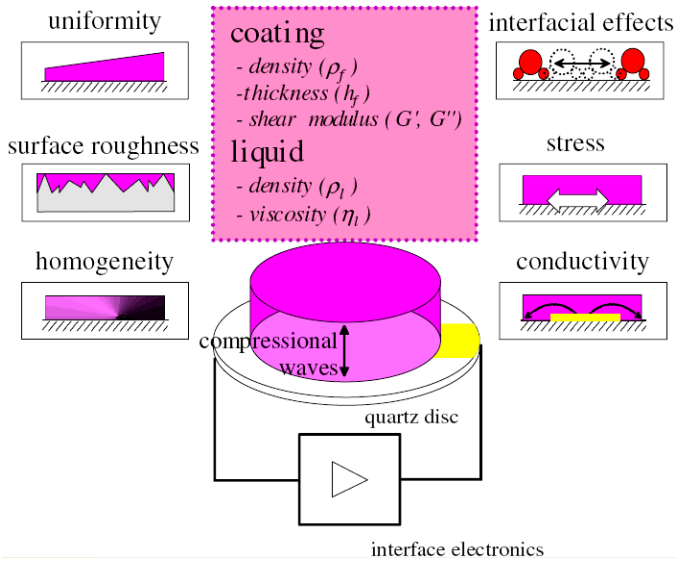

Figure 1.12. Factors influencing the response of a QCM coated with a viscoelastic film and/or working in a liquid environment (Lucklum and Hauptmann, 2003).

Interfacial effects may be expected, for example slip if the sensor has a hydrophobic surface and is immersed in an aqueous environment. These interfacial phenomena are considered to mainly play a more relevant part in acoustic sensors for biological systems (Hayward and Thompson, 1998; Cavic *et al.*, 1997).

Stress can be generated during the film preparation procedure due to shrinking as a result of solvent evaporation, during temperature experiments due to significantly different thermal expansion coefficients or from clamping the quartz in a measurement cell. All these effects can cause the bending of the quartz structure. Thus, these force-related effects can be comparable to pressure differences at both surfaces of the quartz plate, which are known to result in a frequency shift (Kosinski and Pastore, 2001).

Conductive liquids, liquids with a high ionic strength and permittivity can increase the piezoelectrically effective surface of the quartz crystal, even if the liquid is in contact with the grounded electrode only (Shana and Josse, 1994). This effect mainly influences the electrical admittance near the parallel resonant frequency. However, oscillators for liquid applications usually do not work exactly at series resonant frequency (f_s) as discussed before; hence an effect on the sensor response cannot be excluded (Borngraeber *et al.*, 2002). In fact field fringing effects are an important cause for changes in the resonant frequency and the extension of these effects strongly depends on the shape of the electrodes (Rodahl *et al.*, 1996).

Compressional wave generation occurs on the quartz surface and can affect both energy storage and loss (Martin and Hager, 1989). Due to the finite lateral dimensions of the quartz crystal the shear vibration amplitude is not constant over the entire quartz crystal surface. It has its maximum in the center of the electrode and decays toward the edge of the crystal. A compressional wave is generated with its maximum at the point of the largest gradient of the shear wave amplitude. In contrast to a shear wave with its very small penetration depth, the compressional wave can propagate in water and many other liquids without significant attenuation (Benes *et al.*, 1991; Schneider and Martin, 1995).

1.8. Thesis objectives and motivations

The main tasks of this research consisted in the design and testing of a sensing system based on piezoelectric technology, later on used to characterize the interaction of biomolecules with solid surfaces, including biomaterials, and finally applied to the analysis of interfacial phenomena. The sensing system was set up to develop different biosensing methodologies according to the biological molecules to be targeted, with the concern to be able to use it as a valid quantification tool and not only as a mere qualitative detection apparatus.

In order to do that, the first efforts were directed to study all the main steps to build a home-made QCM system for real time molecular analysis, addressing key instrumental issues (Chapter 3). The system was tested considering the theoretical models and interferences described in this Chapter, in order to validate its utilization in liquid medium using frequency and impedance analysis.

Next, the work was focused on the particular problem of the interfacial influence of charged species on the performance of a QCM based biosensor, by the introduction of a resonant frequency signal not related to mass (Chapter 4). An extended equivalent circuit is introduced where a parallel capacitor is added and it is demonstrated how impedance analysis can be used to detect, quantify, and eliminate the influence of charges. The data presented in this chapter originated one publication: João M. Encarnação, Peter Stallinga, Guilherme N.M. Ferreira. *Influence of electrolytes in the QCM response: Discrimination and quantification of the interference to correct microgravimetric data.* Biosensors and Bioelectronics 22 (2007) 1351–1358.

The accumulated knowledge was then used to test the sensing potential of the system (Chapter 5). It is shown how the system follows the real-time chemisorption of alkanethiol

molecules to gold, forming self organized organic films, known as SAMs (self-assembled monolayers) and how this process can be studied in a qualitative and quantitative point of view. The QCM system responds according to the initial concentrations of alkanethiol and the measured data is used to estimate kinetic constants and identify kinetic mechanisms that rule the formation of SAMs. The same approach is demonstrated with a known biological affinity pair: streptavidin-biotin. Biotin molecules immobilized to the QCM surface act as a bioreceptor layer that recognizes streptavidin molecules present in solution.

With the clear demonstration of the potentialities of the developed piezoelectric sensing system, the next step was towards the development of a novel application: the development of an HIV1 biosensor (Chapter 6). The strategy is based on a piezoelectric immunosensor, built with recombinant single chain and single domain antibodies as bioreceptors, to detect the virion infectivity factor (Vif). This target molecule, Vif, is a protein localized in the cytoplasm of HIV1 infected cells and essential for the virus replication. The kinetic binding and equilibrium constants that rule the recognition process for each antibody-antigen pair are estimated and it is also describe how the piezoimmunosensor system potentially can detect Vif molecules in complex cellular extracts.

The data presented in this chapter originated two publications:

I. Guilherme N.M. Ferreira, João M. Encarnaçao, Luis Rosa , Rogério Rodrigues, Roberta Breyner, Sara Barrento, Luisa Pedro, Frederico Aires da Silva, João Gonçalves. *Recombinant single-chain variable fragment and single domain antibody piezoimmunosensors for detection of HIV1 virion infectivity factor*. Biosensors and Bioelectronics 23 (2007) 384–392.

II. João M. Encarnação, Luis Rosa, Rogério Rodrigues, Luisa Pedro, Frederico Aires da Silva, João Gonçalves, Guilherme N.M. Ferreira. *Piezoelectric biosensors for*

biorecognition analysis: Application to the kinetic study of HIV-1 Vif protein binding to recombinant antibodies. Journal of Biotechnology 132 (2007) 142–148.

Chapter 2

Experimental

2.1. Reagents

All chemicals and reagents were ultra-pure, pro-analysis, analytical, electrophoretic or equivalent high purity grade. All solutions were prepared using ultrapure and low conductivity Milli-Q water.

Hydrochloric acid, tris(hydroxymethyl)-aminomethan (Tris), sodium dihydrogen phosphate, disodium hydrogen phosphate, potassium dihydrogen phosphate, sodium, potassium, calcium and magnesium chloride, absolute ethanol, sulfuric acid, hydrogen peroxide, potassium hexacianoferrate (III) (or ferrycianide) and methylene blue (MB) were purchased from Merck. Absolute ethanol and Dimethyl Formamide (DMF) were purchased from Riedel-de-Häen. Dithiobis Succinimidyl Undecanoate (DSU) and 11-hidroxy-1-undecanothiol (HUT) were purchased from Dojindo Molecular Technologies. Streptavidin was purchased from Roche,

biotinyl-3,6-dioxaoctanediamine was purchased from Pierce and 10 nm gold nanoparticles were purchased from Sigma.

2.2. Biologicals

2.2.1. Oligonucleotides

Oligonucleotides (ODN) were designed on the basis of human CTLA4 gene, purchased on-line from Thermo Corporation (www.interactiva.de) and used HPLC pure as received. 5' thiol modified oligonucleotide HS-Pr1 (GCT GAA CCT GGC TAC CAG GAC CTG GCC) was used to functionalize the sensor surface in order to detect: (1) target complementary oligonucleotides -Tgt1 and HS-Tgt1. Tg1 and HS-Tg1 are identical and fully complementary to HS-Pr1 except that HS-Tgt1 is thiol modified to enable labeling with gold nanoparticles (see bellow); (2) Tgt2 - target with a SNP (underlined nucleotide) (GGC CAG GTC CTG GTA GCC AGG TTC AGC); and (3) target B-Tgt1 - a biotin-labelled fully-complementary sequence (enabling labeling with streptavidin). An oligonucleotide sequence with null complementarity with both the probe and target sequences was used as control - Ctr1 (TAG GAG GTC ATC TCG AGC TAT GGC TCT GTT ATT AGC).

2.2.2. Recombinant proteins

HIV1 virion infectivity factor (Vif), anti-Vif single chain antibody (4BL), single domain antibody (VH) and camelized single domain antibody (VHD) were produced in the Biosensors and Bioseparations laboratory of CBME, following methodologies published in

several publications (Yang *et al.*, 1996; Gonçalves *et al.*, 2002; Silva *et al.*, 2004; Ferreira *et al.*, 2007). Western blot analysis of the recombinant antibodies (Fig. 2.1) reveals 100% purity while both SDS page and western of Vif indicate a 75% purity of monomeric form.

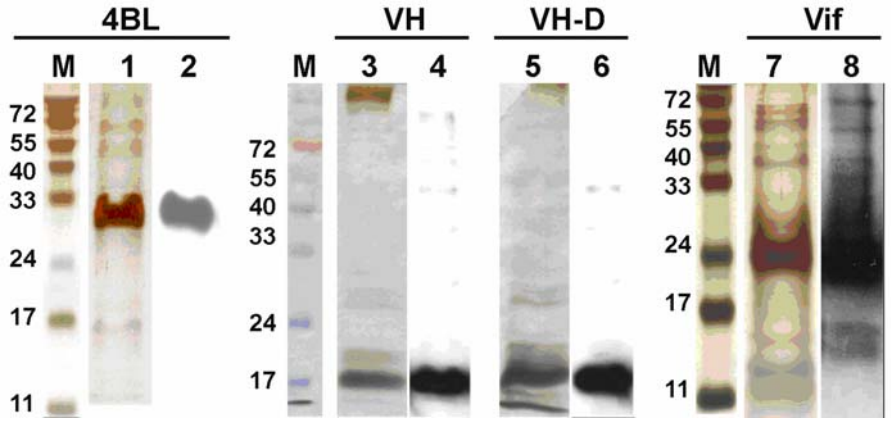

Figure 2.1. Silver-stained SDS-PAGE of purified 4BL (lane 1), VH (lane 3), VHD (lane 5) and Vif (lane 7) and respective western blot autoradiographs (lanes 2, 4, 6, and 8); M-Molecular weight markers. Adapted from Ferreira *et al.*, 2007.

2.2.3. Other biologicals

Human embryonic kidney cells (293T) were produced in the Biosensors and Bioseparations laboratory of Centro de Biomedicina Molecular e Estrutural (CBME).

2.3. Functionalization of gold nanoparticles with oligonucleotides

Oligonucleotides were used to cover gold nanoparticles following a previously published protocol (Csáki *et al*., 2003). Briefly, 35 µl of a 100 µM solution of HS-Tgt1 were diluted in 5 ml of an 8.7 nM colloidal aqueous solution of 10 nm gold nanoparticles and incubated at room temperature for 16 hours. After diluting the reaction mixture with 5 ml of PBS buffer (100 mM phosphate containing 100 mM NaCl, pH = 7.0) and incubating at room temperature for 30 h, 11-hidroxy-1-undecanothiol was added to a final concentration of 50 µM and the mixture was incubated at room temperature for additional 12 h. Modified nanoparticles were recovered by centrifugation for 30 min at 12,000 rpm, washed twice with 5ml PBS, and dispersed in a PBS buffer.

Control gold nanoparticles (Au-SAM nanoparticles) were prepared similarly using Milli-Q water instead of the HS-Tgt1 solution.

2.4. Quartz Crystal Sensors

One inch 5 MHz and half inch 10 MHz AT-cut quartz crystals, coated with optically flat polished gold electrodes on both sides, were purchased respectively from Stanford Research Systems (SRS, Stanford, USA) and International Crystal Manufacturing Co, Inc (ICM, Oklahoma, USA). The sensing gold electrode area is 0.4 cm^2 for the 5 MHz crystal and 0.2 cm^2 for the 10 MHz crystals.

The crystals were cleaned before use by rinsing with absolute ethanol and Milli-Q water before immersion in Piranha solution (30%, v/v, H_2O_2:H_2SO_4 = 1:3) for 15 min, to obtain a clean gold surface. Cleaned crystals were then rinsed with water and dried in a nitrogen stream.

2.5. QCM surface modification

2.5.1. Sensor activation with alkanethiols

The generic strategy used in this work to functionalize the QCM sensors is composed of two main steps: first an alkanethiol self-assembled monolayer covers the gold electrode and finally a bioreceptor layer is immobilized on the organic film.

Alkanethiols are known to spontaneously adsorb to gold surfaces self assembling as oriented monolayers. Alkanethiols self-assembling is initiated by the strong chemical interaction between the sulphur and the metal surface (Karpovich and Blanchard, 1994) which is followed by lateral interactions of neighbour adsorbed molecules, leading to the parallel alignment of the molecules generating a thin, rigid and uniform film at the sensor surface (Liao et al., 2000) (Fig. 2.2).

To activate the surface of quartz crystal sensors with proteins or antibodies, a mixed self assembled monolayer (SAM) of DSU and HUT was generated. DSU was initially deposited and self assembled generating an oriented monolayer with exposed succinimidyl groups. HUT was then deposited in order to fully passivate the gold surface by filling eventual monolayer defects (*e.g.* gaps) (Schwartz, 2001) resulting from steric hindrance effects during DSU deposition.

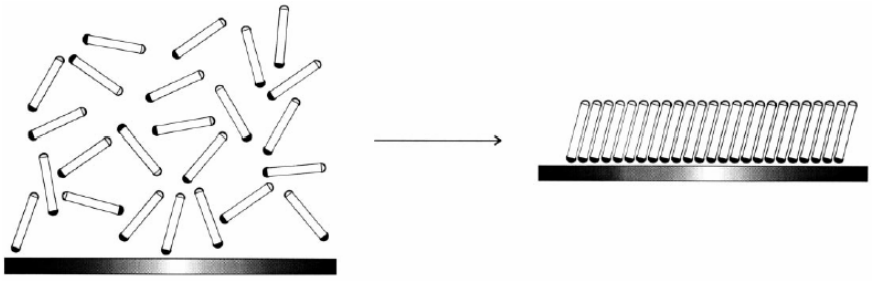

Figure 2.2. Representation of the formation of a self-assembled monolayer (SAM). Alkanethiol molecules present in solution start to spontaneously adsorb to gold surfaces and self assemble as oriented monolayers.

2.5.2. Sensor functionalization with proteins and biotin

A scheme of the immobilization of the molecules on the surface of the quartz sensors is shown in Fig. 2.3.

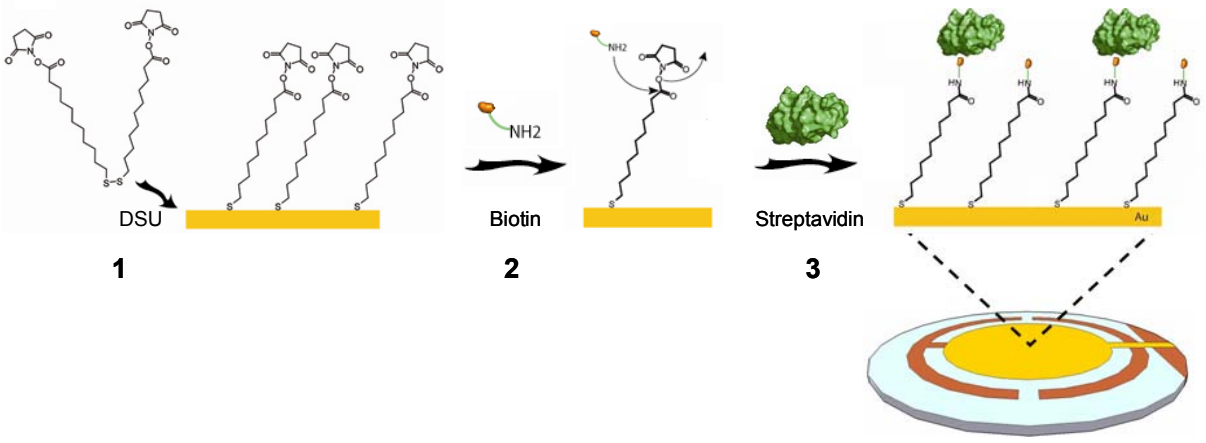

Figure 2.3. Scheme of the steps taken to detect streptavidin molecules in solution using quartz crystals covered with biotin. The same scheme is applicable for all sensors based on protein molecules.

Cleaned crystal sensors were activated with 30 µl of a 100 µM DMF solution of DSU (2 hours incubation at room temperature in a saturated atmosphere). Unbound DSU was removed by washing the activated crystal sensors sequentially with DMF and Milli-Q water. Activated sensors were dried under a nitrogen stream and incubated for additional 2 hours at room temperature with 50 µl of a 50 µM 11-hidroxy-1-undecanothiol ethanolic solution in a saturated atmosphere, washed sequentially with absolute ethanol and Milli-Q water and dried under a nitrogen stream.

Activated sensors were functionalized by covalently immobilizing the proteins (purified 4BL, VH, VHD or commercial biotin) via the formation of an amide bound resulting from a nucleofilic attack of the protein therminal secondary amines to the DSU succinimidyl group. Thirty microliters of a 200 µg/ml phosphate saline buffer (PBS-0.1 M phosphate buffer pH 7.4 containing 0.1 M NaCl) protein solution were pipetted over the activated sensor surface and reacted for 2 hours at room temperature in a saturated atmosphere. Unbounded antibody molecules were further removed by washing sequentially with PBS buffer and Milli-Q water and remaining binding sites at the surface of the sensor were blocked with ethanolamine.

2.5.3. Sensor functionalization with oligonucleotides

To functionalize the surface of the crystal sensors, 50 µl of a 5 µM solution of probe HS-PR1, freshly prepared in PBS buffer, were carefully pipetted onto the surface of a cleaned crystal sensor, and incubated at room temperature for 5 hours in a humidified chamber. Unbounded probe was removed by washing the functionalized crystal sensors sequentially with PBS buffer and Milli-Q water. After drying under a nitrogen flow, the functionalized crystal sensors were incubated overnight, at room temperature in a humidified chamber, with 100 µl

of a 50 μM 11-hidroxy-1-undecanothiol 10% (v/v) ethanolic solution in order to completely cover exposed surface areas, to remove unspecificaly adsorbed HS-PR1 probe, and to better organize the monolayer (Herne, and Tarlov, 1997) (Fig. 2.4).

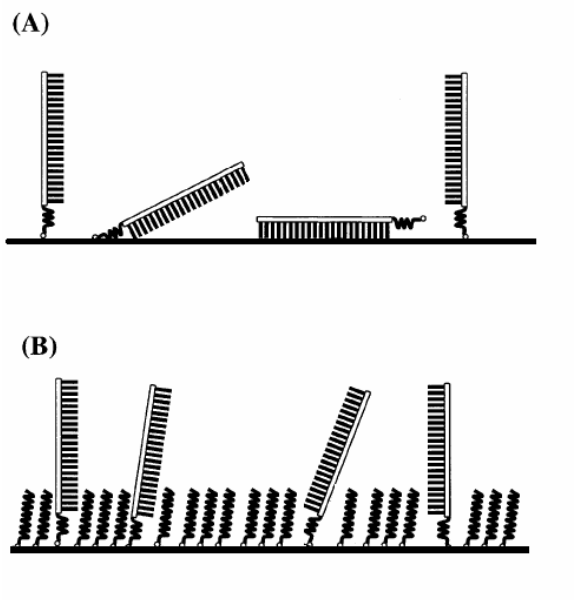

Figure 2.4. Scheme of the functionalization of the gold electrodes with (A) the thiolated ssDNA probe and finally with (B) the alkanethiol, to form a mixed monolayer.

Control sensors were prepared similarly with the sole difference that clean crystals were incubated with 50 μl PBS buffer instead of HS-PR1 probe.

2.6. Experimental set-up

The experimental set-up used to conduct the experiments is depicted in Fig. 2.5. Cleaned or functionalized sensors were assembled on a Kynar crystal holder (Stanford Research Systems, USA) with a home-made acrylic cover to form a 300 μl flow cell exposing just one face of the

sensor to the solution. Viton O-rings were placed underneath the sensor, sealing the flow cell to avoid wetting or flooding the electrical contacts located at the bottom of the crystal holder.

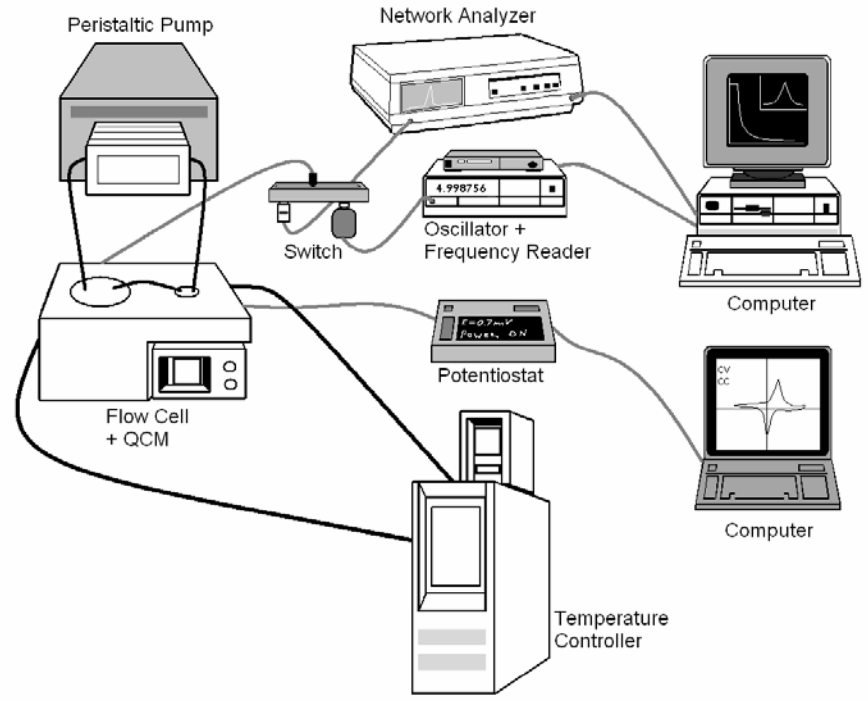

Figure 2.5. Experimental set-up of the 5 MHz quartz crystal microbalance system. Dark lines represent liquid flow tubes and gray lines are electrical connections.

A closed-cycle fluidic circuit was mounted using Tygon tubing to connect the flow cell to an agitated container where all the samples are added. The total volume of the system was 2 ml and the solutions were re-circulated in the system at a flow rate of 500 $\mu l.min^{-1}$ controlled by a Watson-Marlow peristaltic pump. Both the flow cell and the container were installed in a home made 1 liter jacketed beaker to control the temperature of the system at 25±0.1ºC by means of a Thermo Haake temperature controller.

The resonance frequency and impedance spectra were recorded alternatingly using a QCM100 Controller and a QCM25 Oscillator (SRS) connected to a Pendulum CNT-66 frequency counter or using a RF HP8712C Network Analyzer, respectively. The QCM25 consists of

transformer isolated and gain controlled RF amplifiers which maintain the 5 MHz oscillation of the crystal in the holder. It is powered from the QCM100, which also provides the varactor bias to the QCM25 to null the effect of the crystal's static and holder capacitance, allowing the crystal to run at series resonance frequency, as described in chapter 1. The network analyzer and the QCM25 oscillator were electrically connected to the crystal holder through a switch used to select the desired measurement mode (shielded coaxial cables were used in all electrical connections to minimize signal instability arising from electrical interference). The instruments were interfaced to a computer through IEEE boards and a PASCAL program was made for control and to extract experimental data. In order to perform electrochemical measurements, the QCM flow cell was also connected to a PalmSense potentiostat system.

2.7. Impedance Analysis

Impedance spectra were obtained using a 10 kHz frequency span centred near the crystal's resonant frequency with 16 spectra averaging at 1 Hz resolution.

The BVD equivalent circuit parameters were obtained from the experimental data by calculating the conductance function ($|Y|=|Z|^{-1}$; $|Z|$ being the recorded impedance magnitude) and fitting, using a fitting routine written in Matlab, to the equations 14 and 15 of chapter 1.

The analysis is initialized by estimating the four BVD parameters (R_m, L_m, C_m and C_0) for the crystal sensor exposed to air. As examples of typical parameters for air exposed crystal sensors in the experimental set-up used are R_m = 12.925 Ω, L_m = 33.725 mH, C_m = 29.925 fF, and C_0 = 184.575 pF, respectively. Mathematically L_m and C_m are interdependent and so in order to simplify the analysis, and since C_m is related only to the sensor physical material, the

series capacitor it is assumed constant within the experiments. The successive contributions of solvents and adsorbed mass are thus obtained by a 3 parameter fitting (R_m, L_m, C_0) of the respective conductance functions. This procedure is repeated for each stage of the experiment and the BVD parameters of the particular experimental stage, thus of the individual contributions, are calculated by subtracting the global parameters, obtained by fitting, from the respective parameter calculated for the previous stage of the experiment. To facilitate data analysis it is usual to represent a parameter X_L which is the sensor inductance in resistive units (Ω) obtained by multiplying the calculated inductance value by the angular frequency $\omega = 2\pi f$.

2.8. Electrochemical measurements

Cyclic voltammetry (CV) was performed in a 40 ml closed electrochemical cell, using a PalmSense potentiostat, biased to the gold electrode of the quartz crystal sensor. A normal three-electrode configuration consisting of a modified quartz crystal (working electrode), a homemade Ag/AgCl reference electrode, and a platinum counter electrode was used. PBS buffer was used as the supporting electrolyte which was deoxygenated using a nitrogen gas purge for 20 minutes. CV was performed between -0.75 and 0.9 V at a 0.1 V/s scan rate in the presence of 4×10^{-3} M $K_3[Fe(CN)_6]$.

Chapter 3

Instrumental setup of gold QCM sensors for real time molecular analysis

This chapter addresses the key steps involved in the instrumental development of Quartz Crystal Microbalance (QCM) sensors for molecular analysis in solution and its performance optimization in terms of binding monitoring in real time. The focused task was to achieve the best design, performance and validity for our QCM system, according to the theoretical background described in chapter 1.

The properties of the quartz crystal sensors and systematic air and liquid response for its fundamental and overtone frequencies were measured using an oscillating circuit for frequency analysis and a network analyzer for impedance spectroscopy. The sensor performance was studied in liquid environment, during the regeneration process and for temperature variations, liquid evaporation, mechanical interferences and dissolved gases.

For the proper utilization in liquid medium, the Quartz Crystal Microbalance was assembled in a 300 µl flow cell connected to a temperature controlled (± 0.1ºC) closed flow circuit equipped with a peristaltic pump.

3.1. System check- resonant frequency response

In QCM commercial versions, the most commonly advised step for a system check is the evaluation of the crystal's behavior upon immersion in different solutions. In this specific case the evaluation of our system was made using both the oscillator/frequency counter and the network analyzer using aqueous solutions of glycerol.

Upon loading Milli-Q water on a sensor, a 713 ± 12 Hz resonance frequency variation was measured using the oscillator circuit (Fig. 3.1), which is of the same order as predicted by the Kanazawa Equation (Δf = 715 Hz), shown in chapter 1 (Equation 9). Subsequent addition of glycerol dropped the frequency further, showing clearly that the resonant frequency of the crystal decreases dramatically with the increase of density and viscosity of the liquid (Fig. 3.2A).

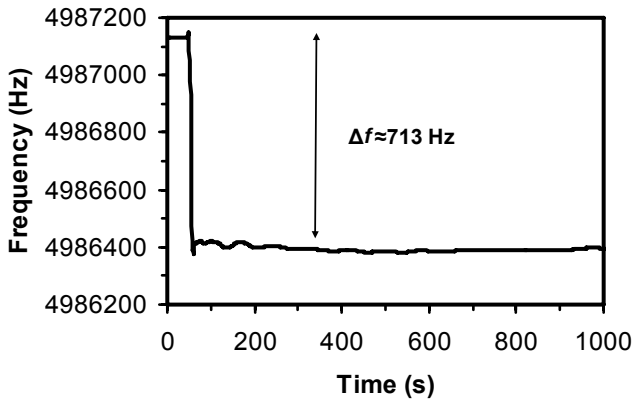

Figure 3.1. Resonant frequency decrease upon immersion of a 5 MHz quartz crystal in Milli-Q water at 20ºC.

However, the information obtained in Fig. 3.2A only shows that the system response is adequate for the increase of the liquid's density and viscosity.

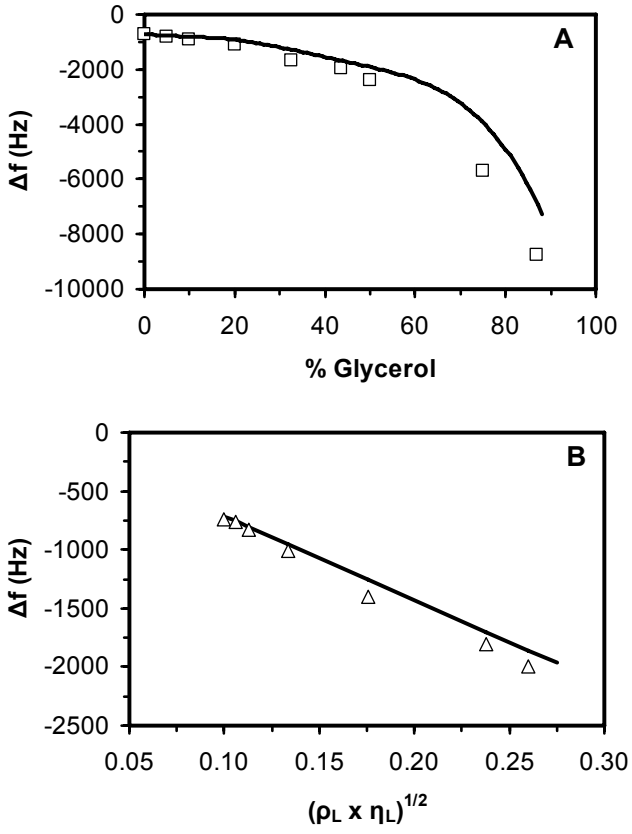

Figure 3.2. A) QCM frequency response to increasing density and viscosity of glycerol solutions at 20ºC and (inset) ethanol aqueous solutions at 20ºC, compared to the correspondent theoretical Kanazawa curve (□ experimental data; ▬ theoretical data). B) Frequency linear dependency on $(\rho_L \times \eta_L)^{1/2}$, for the glycerol solutions case where the black solid line represents the Kanazawa model and the white triangles represent the experimental results. The slope of the solid line corresponds to the Kanazawa liquid sensitivity factor for a 5 MHz crystal.

The true system check must consist in the accurate observation of the Kanazawa model with the experimental results. As shown in Fig. 3.2B, the resonance frequency changes linearly with the increase of the density and viscosity of the solution. The linear regression of the experimental results gives a slope value equal to 7620 $Hz^{1/2}$ $g^{-1}cm^2$ which is close to the theoretical liquid sensitivity factor (7140.5 $Hz^{1/2}$ $g^{-1}cm^2$) for a 5 MHz QCM, thus the microbalance performance with the oscillator was in good accordance with the Kanazawa Equation.

3.2. System check- impedance response

Our QCM apparatus was also tested using a network analyzer that is able to distinguish between different contributions to the piezoelectric sensor response. An example of a typical experimental response of the assembled system is illustrated in Fig. 3.3, that shows the admittance spectrum curves for a dry and clean 5 MHz crystal and for the same sensor in contact with water at 20ºC.

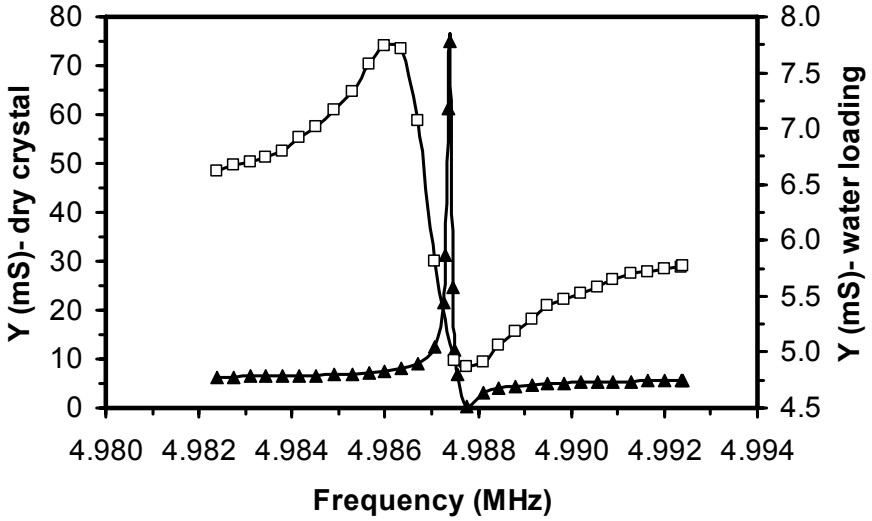

Figure 3.3. Home-made 5 MHz QCM system typical admittance spectrum in air (black triangle) and in Milli-Q water (white square), at 20ºC.

For the dry crystal, the admittance spectrum shows a maximum near the resonance frequency of the sensor. When the same crystal is immersed in water, the admittance curve changes in three distinct ways: i) the maximum admittance decreases in magnitude, ii) is dislocated towards a lower frequency and iii) the curve width increases.

To fully understand the QCM response, hence distinguishing between the case of a crystal in contact with air and then with water, it is necessary to work with the equations that describe the admittance spectrum in the resonance frequency region. The liquid loading effect on the crystal can be modeled with the modified BVD circuit (Fig. 1.11). Applying a least-square-fitting algorithm to the Equation 14 will permit the determination of the BVD parameters, rather than only the product $\sqrt{L_{\mathrm{m}} \times C_{\mathrm{m}}}$ correspondent to the resonant frequency (Fig. 3.4).

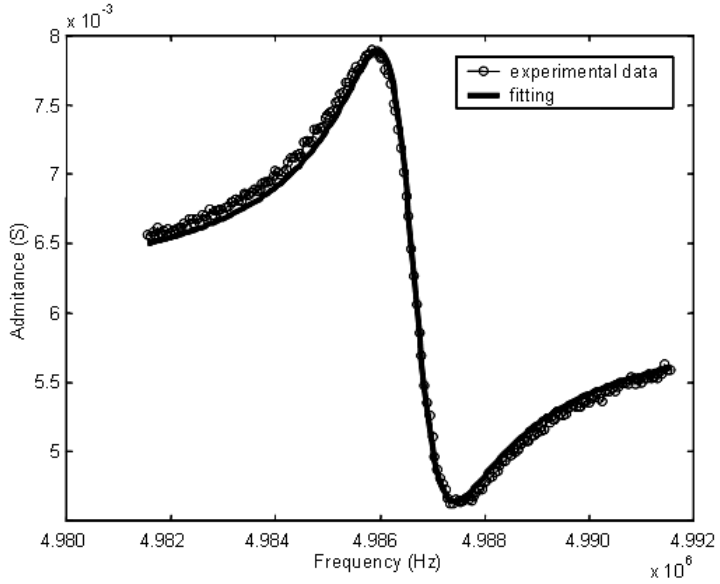

Figure 3.4. Admitance spectrum of the quartz crystal in contact with water (the same as in Fig 3.3). The admittance magnitude equation is fitted to the experimental curve to extract the equivalent circuit components.

The modified BVD reduces to the normal equivalent circuit, considering that $L_{\mathrm{m}} = \sum L_i$, $R_{\mathrm{m}} = \sum R_i$ and $C_0 = \sum C_{0i}$. Liquid loading adds components L_2, R_2 and C_{02} to the existing L_1, R_1 and C_{01} of air, where the total circuit will then follow Kanazawa Equation in terms of resonance frequency (Bizet *et al.*, 1998; Ha and Kim, 2001).

Being a not completely linear element, the crystal has also peaks in its admittance spectrum at harmonics of the fundamental frequency f_0. One very interesting feature of the network

analyzer is the possibility of extracting the crystal's impedance spectrum at those different harmonics (higher overtones). The values obtained with the fitting algorithm from the first ($f = f_0$) to the seventh ($f = 7f_0$) harmonics for the QCM exposed to air and PBS (pH 7.4, 100 mM NaCl) at 30ºC, are shown in Table 1.

Table 1. RLC values obtained after fitting the admittance model to from the first to the seventh harmonic experimental curves obtained with the network analyzer. *The C_m value was assumed to be invariant for each harmonic and that the fundamental resonant frequency is 5 MHz.

BVD components	**Dry crystal 1st harmonic (f_0 = 5 MHz)**	**Dry crystal 3rd harmonic (f_0 = 15 MHz)**	**Dry crystal 5th harmonic (f_0 = 25 MHz))**	**Dry crystal 7th harmonic (f_0 = 35 MHz)**
R_m (Ω)	10.5	22.6	29.9	13.6
L_m (mH)	35.5	30.8	19.1	6.5
C_m (fF)*	28.5	3.7	2.1	3.2
C_0 (pF)	107.5	116.1	140.4	214.6
Q	1.058×10^5	1.284×10^5	1.002×10^5	1.056×10^5
Calculated Freq. (MHz)	4995702	14978951	24962558	34945699
Results with PBS loading (30ºC)				
ΔR (Ω)	315	409	296	82
ΔXL (Ω)	318	407	298	139
ΔC_0 (pF)	14.7	13.1	22.9	77.6
Q	3.541×10^3	6.746×10^3	9.183×10^3	1.499×10^4
Q reduction	97%	95%	91%	86%
Calculated Freq. (MHz)	4996813	14983676	24971088	34957949
Δf (Hz)	-700	-1003	-1242	-1702
S/N (Δf.Q)(Hz)	2.48×10^6	6.77×10^6	11.41×10^6	25.51×10^6

Using the new calculated elements the first thing to note is that when the sensor is immersed in buffer, the Q factor drops because of an increased dissipation of energy to the medium. The resistive element R_m increases and the width of the resonance increases proportionally.

For the first harmonic, at 30ºC the contact with PBS resulted in about a 97% decrease in the resonance Q factor as well as a shift of the peak caused by changes for L_m, correspondent to approximately a change in resonance frequency of 700 Hz, consistent with the frequency counter.

Another fact that should not be forgotten is the increase of parallel capacitance upon immersion in water. This increase is directly related to the properties of the liquid, since resonance frequency of QCM sensors is known to be also influenced by the conductance and permittivity of the solution (Josse *et al.*, 1990). All these acoustoelectric effects combined cause an expansion on the BVD-equivalent circuit, which mainly consists of the modification of the C_0 component (Josse *et al.*, 1990; Shana and Josse, 1994).

As for the harmonics, the obtained results of frequency shift can be normalized, *i.e.* are divided by their respective overtone number (3, 5, 7…) and compared. Thin and rigid films adsorbed to the sensor, show the same normalized frequency response on all overtones. Thus, if the normalized overtones responses differ, the response of the sensor lies outside the validity of Sauerbrey. This is clearly shown in Table 1 for the liquid loading. In these cases liquid loading causes a response dictated by density and viscosity (Kanazawa Equation) and not by a mass rigidly coupled to the vibration of the crystal vibration (Sauerbrey Equation). Hence, the frequency shifts obtained with all harmonics are not proportional to the overtone.

The results for the harmonics also show that for increasing overtones the Q factor decreases less in liquid phase and consequently the signal to noise ratio increases.

Similarly to the check conducted with the oscillator and frequency counter, the QCM system impedance response was also tested against glycerol solutions and the results are depicted in Fig. 3.5.

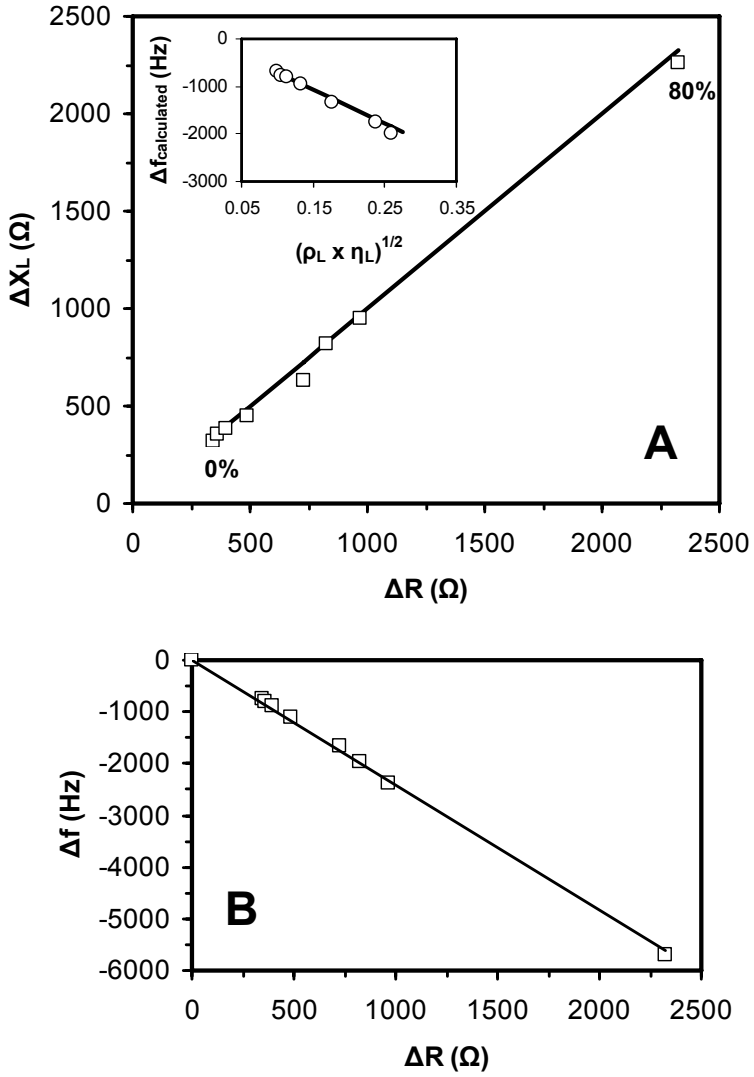

Figure 3.5. A) Parametric plot of ΔX_L vs. ΔR (□ experimental data; ▬ theoretical data), for increasing percentages of glycerol (from left to right = 0 -80%) in aqueous solution in contact with a quartz crystal. The solid line has a slope of unity and represents the predicted behavior of a QCM system in contact with Newtonian fluids of increasing viscosity and density. Inset: calculated frequency linear dependency on $(\rho_L \times \eta_L)^{1/2}$, for the glycerol solutions case (○ experimental data; ▬ Kanazawa model). The deviation obtained with the experimental results for both plots is only 3%. B) For the system-check using glycerol solutions, the obtained frequency shift with the oscillator is linearly related to the resistance shift obtained with the network analyzer, validating the experimental results obtained simultaneously with both instruments according to Equation 17 (□ experimental data; ▬ theoretical data).

As depicted in Fig. 3.5A, representing R and X_L (ωL) variations in a parametric plot, it is shown that not only these components change with the increase of density and viscosity of the liquid medium, but also the condition $\Delta X_L/\Delta R = 1$ for Newtonian fluids is verified (Bouche-Pillon *et al.*, 1995; Kanazawa, 1997).

A significant observation can be made when the impedance readings are obtained for the crystal exposed to different glycerol solutions. With the network analyzer there is only a small deviation of 3% from the experimental results in comparison with the theoretical behavior of Newtonian liquids ($\Delta X_L/\Delta R = 1$).

Another important piece of information that can be extracted from these results is the relation between frequency shifts and resistance changes due to the response of the system to viscoelastic losses. Since both mass and viscoelasticity contribute to the decrease of the resonance frequency, one has to be extremely careful when evaluating and interpreting the obtained results. Viscoelasticity can induce a non-mass effect response, and thus cannot be neglected and its contribution has to be subtracted from the total change in inductance and frequency according to Equations 18 and 19, in order to obtain the real mass signal (Schmitt *et al.*, 1997).

.

$$\Delta X_{\mathrm{Lmass}} = \Delta X_{\mathrm{L}} - \Delta R \tag{18}$$

$$\Delta f_{mass} = \Delta f - \Delta f_{visc} \tag{19}$$

The relation between ΔR and Δf_{visc} due to the net changes in solution density and viscosity for Newtonian fluids is defined by Equation 17, also known as one of Martin's equations. For the

system check the used crystal presented a calculated value of L_m = 33.16 mH, with a theoretical slope value of -2.4 Hz.Ω^{-1}, for Δf versus ΔR. This value is in good agreement with the slope value calculated with the experimental results obtained for the glycerol solutions represented in Fig. 3.5B.

3.3. Crystal cleaning and regeneration

Before conducting a mass adsorption experiment using QCM it is essential to guarantee that the surface of the crystal is absolutely clean and contaminant free, particularly when it is being regenerated to be reused for other assays. Since the main sensor activation strategy used in this thesis starts with the deposition of an alkanethiol layer, this was taken into consideration when choosing the regeneration methodology of the crystals.

To evaluate the behavior of the crystal after successive alkanethiol deposition/cleaning cycles, two different methods were compared: a destructive chemical method using piranha solution and a non-destructive electrochemical method using a fixed potential (Fig. 3.6). In our case, the molecule used to evaluate both methods was the 11-hidoxy-1-undecanothiol, and the resulting reaction with the gold electrode surface is a self assembled monolayer (SAM) (Finklea, 1999).

The use of piranha solution has been generally adopted for cleaning gold surfaces with films adsorbed via the Au-thiol bond (Kim *et al.*, 2001; Pan *et al.*, 1996). Nevertheless, due to its strong reactivity piranha solution is very aggressive to the gold electrode structure. Successive regeneration cycles using piranha solution can cause the gold removal from the surface of the

sensor, eventually leading to its uselessness. The immediate effect is that its resonant frequency is no longer stable.

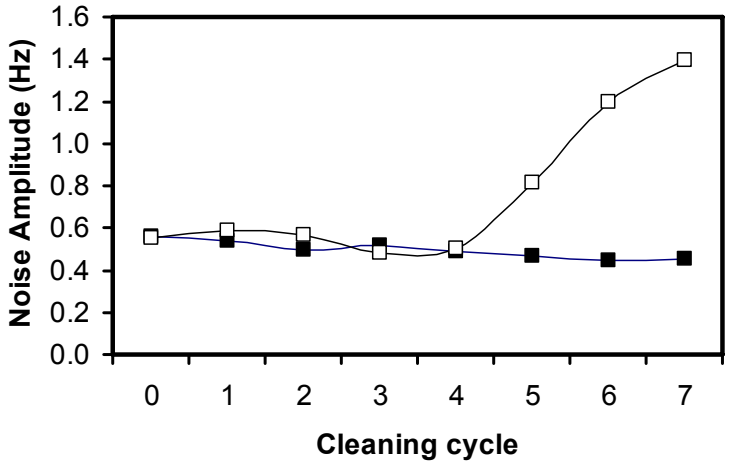

Figure 3.6. Resonant frequency readings noise amplitude obtained after each regeneration cycle procedure to remove a deposited film of 11-hidoxy-1-undecanothiol, using "piranha" solution and a -1.4 V tension (■ electrochemical cleaning; □ piranha solution cleaning).

As shown in Fig.3.6, up to four regeneration cycles with piranha solution were possible, after which resonant frequency becomes unstable. Further regeneration cycles resulted in gold etching and removal, which was visible to the naked eye.

We therefore tested a non-destructive approach, consisting on an electrochemical cleaning procedure in which a -1.4 V tension (relative to an Ag/AgCl reference electrode) is applied to the gold electrode of the crystal.

Cyclic voltammetry was used to evaluate the efficiency of this method to remove the organic layer from the surface of the sensor, since this technique is able to easily distinguish between a clean crystal and one modified with a SAM (Fig. 3.7) (Shen *et al.*, 1997).

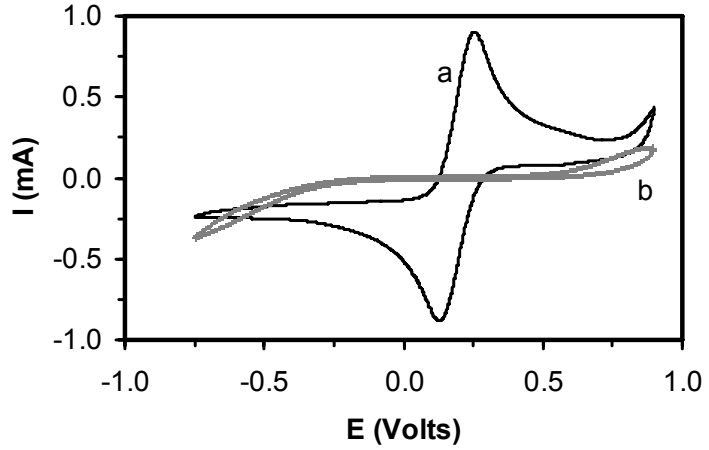

Figure 3.7. Cyclic voltammograms of 4.0 mM potassium hexacianoferrate (III) (a) on a clean crystal (bare gold electrode) and (b) on a crystal covered with a 11-hidroy-1-undecanothiol SAM in PBS buffer (pH 7.0) at a scan rate of 0.1 V/s.

The tested cleaning procedure was conducted in two different stages. First the crystal was immersed in a support electrolyte solution (PBS) and using a potentiostat, a -1.4 V tension was applied for a certain period of time. Finally, the crystal was washed with a 65% (v/v) nitric acid solution, Milli-Q water and dried with N_2.

Subjecting the crystal to successive cyclic voltammetry analysis, it was possible to optimize the period of time during which the crystal has to be submitted to the electrochemical procedure ensuring its effective cleanness (Fig. 3.8). From figure 3.8 it is demonstrated that after about 60 seconds of procedure, the crystal returns to its original cyclic voltammogram profile.

In this way it seems to be possible to extend the lifetime of each crystal and ensure an acceptable cleanliness to allow the reproducibility in chemisorption reactions between thiolated molecules and gold. Not only the resonant frequency remained stable after several interventions (Fig. 3.6), but also no gold removal was observed. This method is also faster,

cheaper and safer, and in principle can be done on-line, without removing the crystal from its measurement environment.

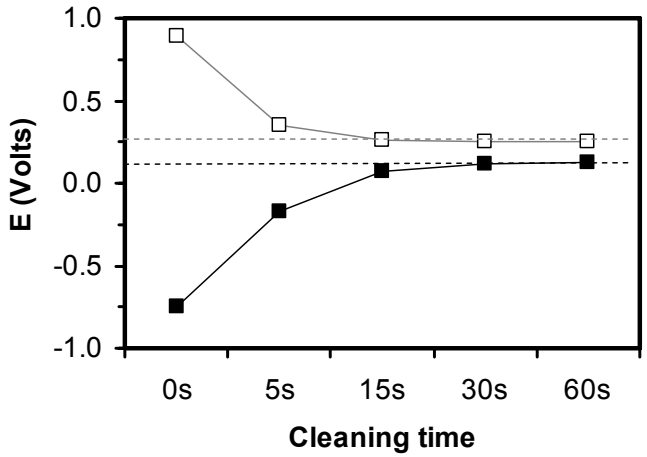

Figure 3.8. Potassium hexacianoferrate (III) reduction and oxidation peaks (■ reduction peak; □ oxidation peak; --- original peaks) obtained with cyclic voltammograms conducted after each electrochemical cleaning procedure of the crystal covered with the alkanethiol SAM.

However, during the course of the experimental work described in this thesis, Piranha solution was used to clean the crystal sensors. The electrochemical cleaning procedure could no be used as the routine cleaning procedure due the unavailability of equipment.

3.4. Interferents

As for any other approach to the validation of analytical methods, studies where conducted in order to determine possible sources for the interferences, and effective mechanisms and strategies for its elimination. In some cases, the interference mimics the expected signals and

therefore can compromise the validity of the analysis. The effects of temperature variation, evaporation, non-degassed fluids and mechanical noise were investigated.

3.4.1. Temperature

There is a temperature dependence of the resonant frequency of quartz crystals, which for AT cut quartz is about 1-3 Hz/ºC exposed to air around room temperature (Janshoff *et al.*, 2000). But larger frequency variations occur when the crystal is in contact with liquids, due to the temperature dependence of density and viscosity. For a crystal immersed in water, the variation coefficient is close to 8 Hz/ºC (Janshoff *et al.*, 2000). Our QCM system response to temperature was tested in liquid environment and the resulting variation coefficient was 7.8 ± 0.4 Hz/ºC. Hence, every experiment conducted in liquid phase must have a temperature control in the 0.1ºC range in order to eliminate this as a source of error in an apparatus with 1 Hz resolution. For better resolutions, a temperature control below the 0.1ºC range is necessary.

3.4.2. Evaporation

To evaluate the possible influence of liquid evaporation, assays where executed in order to observe the response of the QCM sensor exposed to three different media: air, water and ethanol. While in air the crystal has a stable frequency, for water there is a periodic signal variation, which is even higher in ethanol (Fig. 3.9).

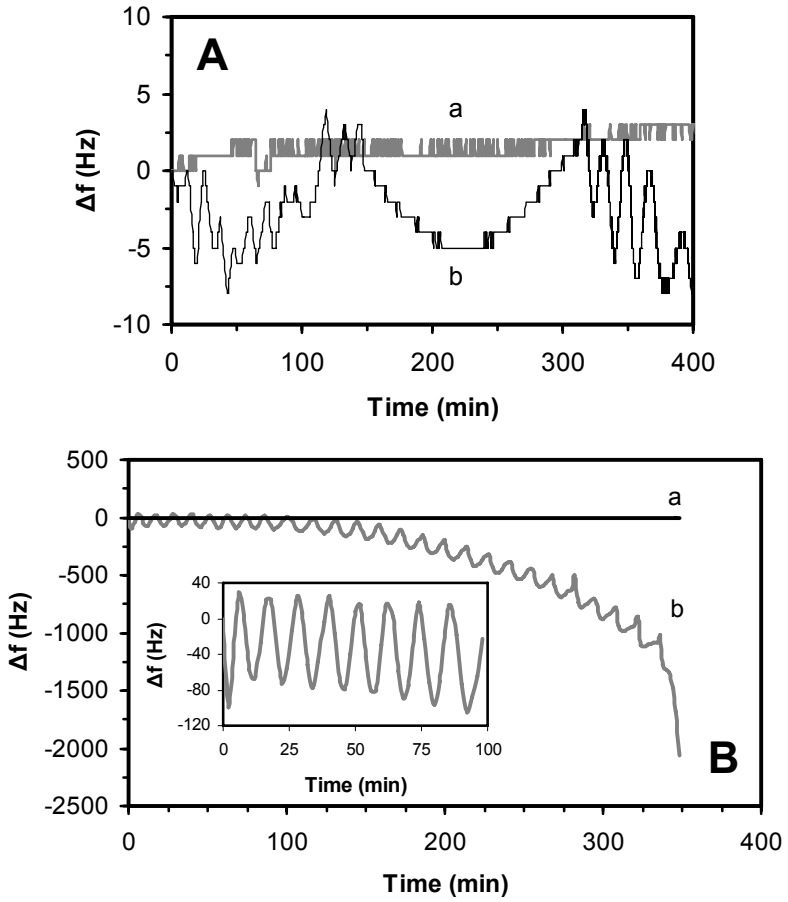

Figure 3.9. A) The quartz crystal response in an open support, to contact with air (a) and water (b), showing clearly a very stable frequency signal for the first case but a periodic shift in the second case. B) Quartz crystal response to contact with absolute ethanol (6 mm liquid height) in (a) a closed support and in (b) an open support. Inset: the first 100 minutes of curve b.

There is an evaporation related phenomena that can be explained by the fact that, with time, the liquid height decreases that is significant in water but overwhelming in ethanol.

A QCM resonating in liquid medium, besides generating shear waves, can also generate longitudinal or compressional waves (sound) (Lin and Ward, 1995; Schneider and Martin, 1995). A nonzero velocity gradient of the shear oscillation along the x-axis or even impurities in the surface can cause a conversion of the shear waves to perpendicular compressional waves that travel from the surface of the sensor into the liquid and can be reflected at an

interface. When the thickness of the medium is an integer number of wavelength of the compressional waves, standing waves occur, causing an increase in loss and a change of resonance frequency (Lin and Ward, 1995; Schneider and Martin, 1995). This phenomenon can constitute an important source of error considering the data in Fig. 3.9, because with liquid evaporation, there is also a decrease of the propagation distance of the longitudinal or compressional waves that are generated at the surface of the crystal sensor (hence a constructive and destructive interference) and travel to the liquid/air interface (Schneider and Martin, 1995). So the cyclic frequency variation is related to the height variation of the liquid.

The experiment b) depicted in figure 3.9B was performed with the QCM assembled in an open support, allowing the ethanol to evaporate, and the frequency reading was accompanied until the total volume evaporated.

For a frequency of 5 MHz and a sound velocity in ethanol of 1207 m/s the wavelength of the compressional wave is 0.24 mm ($v_s = f\lambda$). In this way, one period in figure 3.9B can be interpreted as the evaporation of 0.24 mm of ethanol. The figure shows 26 periods before total evaporation, totalizing 6 mm which was equal to the initial height of the liquid. This way, each peak obtained in the assay simply corresponds to the evaporation of one liquid layer.

While operating with QCM, it is necessary to take into account the significant noise that liquid evaporation produces, since that in the ethanol case the amplitude of the oscillations is about 100 Hz, thus completely drowning expected signals in this interference. To eliminate this effect, and according to the results in curve a) of Fig. 3.9B, a 300 µl flow cell was constructed for the crystal holder, in order to maintain the fluid height constant.

3.4.3. Non-degassed fluids

The presence of air bubbles on the surface of the sensor may induce erratic frequency shifts that sometimes may mimic transient profiles. Experiments where conducted, in which the performance of the sensing system was evaluated in the presence of degassed and non-degassed fluids (Fig. 3.10A), and also in contact with degassed fluids that later where intentionally gassed (Fig. 3.10B).

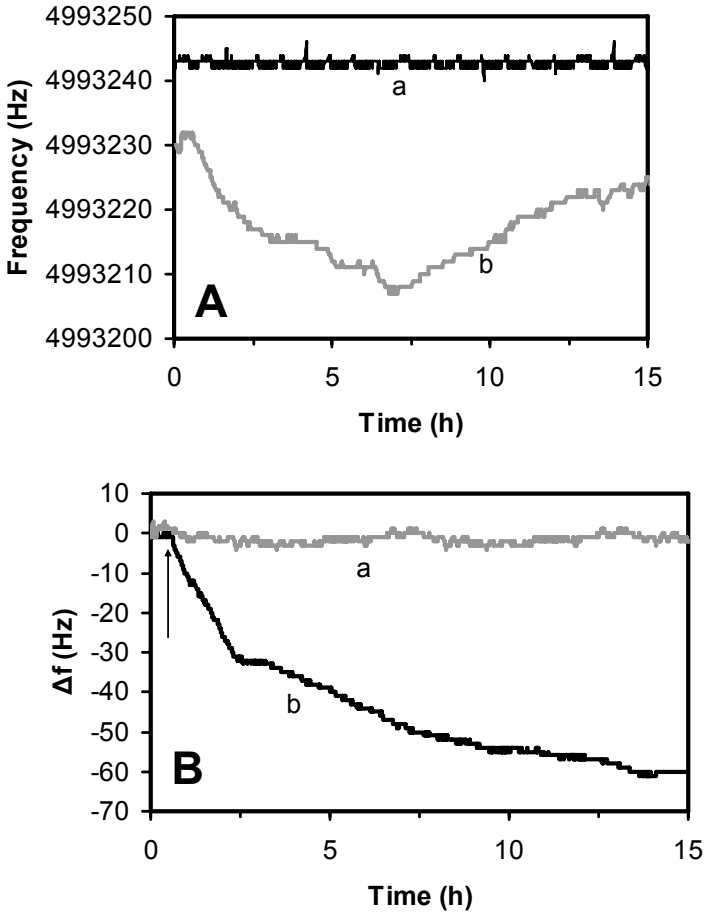

Figure 3.10. A) Batch QCM experiment where the crystals were assembled in a 300 µl closed cell. The quartz crystal frequency response was followed with the sensor in contact with degassed (a) and non degassed water (b). B) Batch QCM experiment where the crystals were assembled in a 300 µl closed cell, and only loaded with degassed fluids. The chamber was first loaded with 200 µl of water and then a 100 µl sample (indicated by arrow) of the same fluid was injected. In one crystal the sample was carefully injected with a syringe (a), but for the other a micropipette was used (b) and one single air bubble was introduced inside the chamber.

By evaluating the crystal response in figure 3.10A it is clear that non-degassed fluids are definitely a very important source of interference that not only renders the building of stable baselines difficult, but can also affect transients during its course. The results in Figure 3.10B indicate that the sample injection method can also introduce an irreversible problem in QCM experiments that can even mimic a transient, easily mistaken for a molecular kinetic process. Thus, it is imperative to use a good injection technique for the samples, to avoid inadvertent injection of air bubbles.

3.4.4. Mechanical noise

The crystals are extremely sensitive to any source of vibration or pressure, which may introduce significant noise in frequency readings. One good example of that was experimentally verified by tightening the crystal retainer, exerting additional stress on the crystal and changes of its frequency of oscillation were observed.

In our apparatus, the crystal sensor is closed in a flow cell, integrated in a closed micro-flow circuit with a buffer vessel where all the samples can be injected away from the sensor. This avoids the possibility of a mechanical perturbation on the surface of the crystal caused by the addition of a sample to the sensing system.

Due to the fact that the 5 MHz QCM system has a fluidic tubing system, assisted with a pump, pressure variation could become an important source of interference. Pressure dependency was investigated using water columns (Fig. 3.11) where a crystal was assembled in a closed flow chamber, to which water was pumped. The extraction tube connected to the crystal chamber was immersed exactly 8 cm in a Milli-Q water column, at 25ºC. As the liquid height dropped, the resonance frequency was monitored and related to the decrease of

hydrostatic pressure ($p = \rho gh$, where ρ is the liquid density, g is the gravitational acceleration and h is the liquid height). From the experiment in Fig. 3.11, the calculus of the pressure dependency factor was of 9 Hz/kPa. The same value was obtained with the inverse experiment, where the increase of water column was tested.

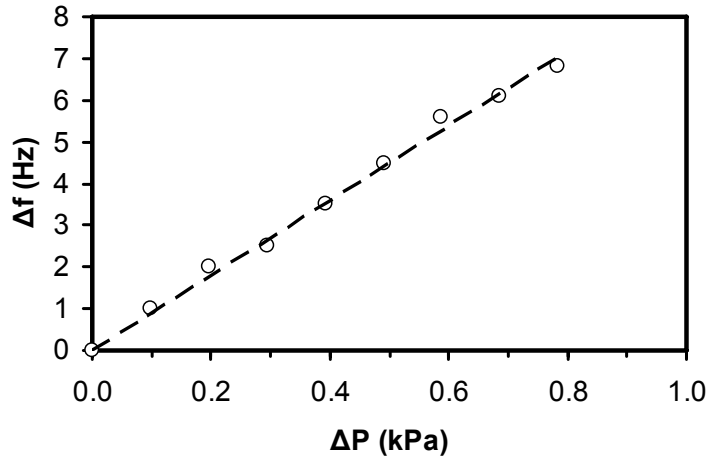

Figure 3.11. QCM response to hydrostatic pressure drops by diminishing the height of a water column to which the sensor, enclosed in a flow-cell, is connected through tubing. (dashed line is an aid to the eye).

Another experiment was made but this time monitoring the quartz crystal response to air pressure (Fig. 3.12). The QCM was placed inside an inox closed chamber connected to a Varian turbomolecular pump, and the frequency response was monitorized during the depressurization immediately followed by pressurization, in a 100 kPa range (Fig. 3.12).

From the results in Figure 3.12, the frequency changes are in the order of 1100 ± 100 Hz for a pressure change of 100 kPa, leading to a pressure factor of 11 Hz/kPa. For both cases and considering the differences in the assays, the two pressure factors estimated are close enough to conclude that indeed the resonance frequency variation is linearly proportional to pressure changes. These results demonstrate that for the implementation of a closed flow circuit, like

the system used in this thesis, all inline pressure fluctuations and/or variations must be avoided.

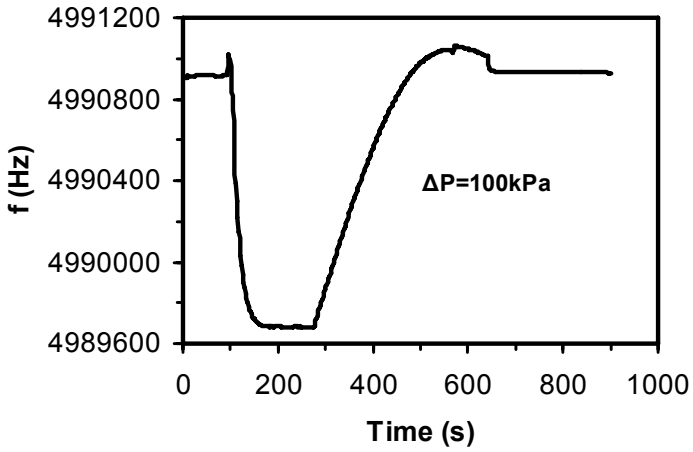

Figure 3.12. QCM response to air pressure. A crystal was assembled in a closed metal chamber, from which air was first pumped out (causing a resonant frequency decrease) and then let in (causing a resonant frequency increase). The pressure differential studied was of approximately 100 kPa.

Considering the pressure dependence of the resonance frequency, the pumping system used in the fluidic circuit of the QCM system can introduce an interference caused by pressure fluctuations. In our system the pump is peristaltic pumps, which is suitable for liquid flow in closed systems but adds noise to the signal, obviously due to its pulses (Fig. 3.13). For the reduction of the periodical noise provoked by the peristaltic pump, the best and cheapest course of action is to use small rotations, working in underpressure mode (the pump extracts fluid from the crystal chamber instead of loading it) and small diameter soft tubing.

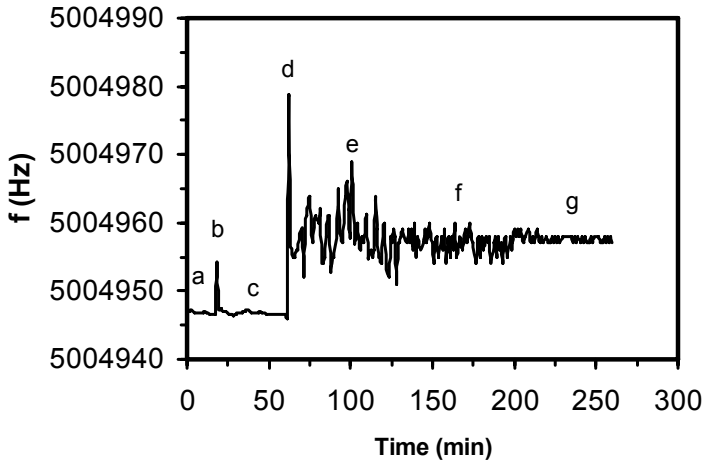

Figure 3.13. QCM in contact with water at 25ºC in batch (a), afterwards 50 µl of water were injected on top of the crystal (b) and then again in a vessel connected by tubing to the crystal flow cell (c). A peristaltic pump was turned on (d), and the water started flowing by overpressure to the crystal chamber, at 1 ml/min in a 1 mm silicone tube (e). The same flow was then achieved but with a 1 mm tygon tube in overpressure mode (f) and then on underpressure mode (g).

3.5. Conclusions

In this chapter, it was shown how to setup a 5 MHz QCM system assisted with two different measuring systems: the frequency counter and the network analyzer.

The validation procedures of the basic response of our QCM system, were successfully demonstrated for both frequency and impedance analysis, according to the theoretical background described in chapter 1.

Some crucial instrumental key steps for the proper use and optimization of QCM sensors were also established.

It was demonstrated how an electrochemical cleaning procedure using a potentiostat, represents a good alternative for the use of piranha solution in the regeneration of crystal sensors.

In liquid environment there are three important elements to take into consideration, which may introduce artifacts in the transduced signals: temperature variation, liquid evaporation and the presence of dissolved gases. It was established that all QCM experiments must be conducted with a stable and controlled temperature (± 0.1ºC), the crystal sensors must be assembled in a flow cell to avoid the evaporation of the solvent and all liquids must be degassed before use.

It was also determined that the quartz sensors respond to pressure changes. Since the QCM system setup is based on a fluidic circuit where the sensors are incorporated, all line pressure fluctuation must be avoided and/or eliminated, specially generated by the use of a pumping system.

Chapter 4

Influence of electrolytes in the QCM response: Discrimination and quantification of the interference to correct microgravimetric data

In this chapter it is demonstrated that the presence of electrolytes in solution generate desorption-like transients when the resonance frequency is measured.

Using impedance spectroscopy analysis and BVD equivalent electrical circuit modeling it is shown that non-Kanazawa responses are obtained in the presence of electrolytes mainly due to the formation of a diffuse electric double layer (DDL) at the sensor surface, which also originates a capacitor like signal.

The BVD equivalent circuit was extended to include additional parallel capacitances in order to account for such capacitor like signal. Interfering signals from electrolytes and DDL perturbations were this way discriminated. It was quantified as 8.0 ± 0.5 Hz/pF the influence of electrolytes to the sensor resonance frequency and this factor was used to correct the data obtained by frequency counting measurements.

The applicability of this approach is demonstrated by the detection of oligonucleotide sequences associated with gold nanoparticles. In this case, after applying the corrective factor to the frequency counting data, the mass contribution to the sensor signal yielded identical values when estimated by impedance analysis and frequency counting.

4.1. Influence of charged species in the response of QCM sensors

The QCM operating in liquid phase also sensitively responds to the presence of charged species, resulting in an undesired parasitic frequency shift, which can be more or less of the same magnitude as the measuring signal itself (Kim *et al.*, 2003).

Considering the fact that QCM devices are used in liquid phase for (bio)molecular sensing and recognition, besides the charges of the biomolecules, in the majority of the situations the analytes are present in buffered solutions containing small amounts of electrolytes. Thus a set of experiments was undertaken to study and characterize the influence of such electrolytes in the sensor signal.

It was experimentally observed that the mere addition of NaCl to a Milli-Q water flow causes significant frequency shifts. Thus, one can conclude that any assays that have or require the presence of ions might be compromised. Examples of such experiments are the ones that areintended to develop QCM biosensors, which have to be able to detect charged biomolecules in buffer or electrolyte solutions.

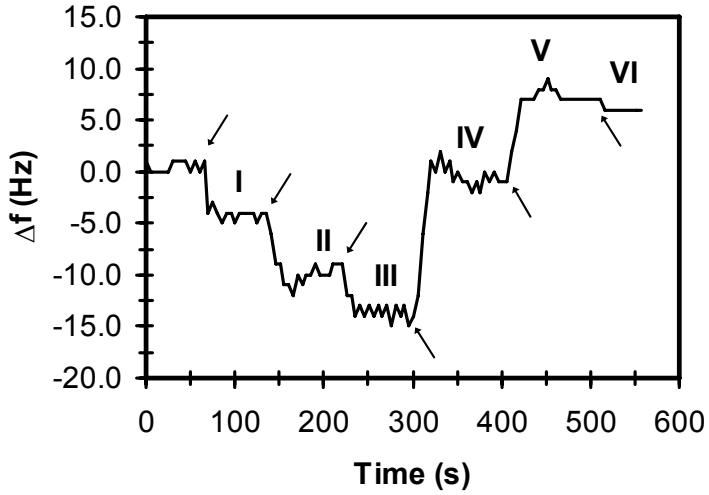

Figure 4.1. QCM resonance frequency response to increasing ionic strength. Experimental result with transient response for successive additions of concentrated NaCl solution (arrows) to the final ionic strengths I- 0.2 mM; II- 1.0 mM; III- 3.4 mM; IV- 9.9 mM; V- 26.5 mM; VI- 52.6 mM.

As shown in Fig. 4.1 the crystal sensor response can be related to significant changes in the ionic strength of the medium. Since the problem of charged species may be particularly important upon the addition of a sample to the QCM system, a simple experiment was conducted to verify the response of the system to the injection of a concentrated solution of NaCl, to a sensor immersed in different buffers (Fig. 4.2).

It was verified that frequency shifts do not occur if in the solution there is already electrolytes present in a considerable concentration (Fig. 4.2). This observation raises the possibility that only sample injections that may contribute to a significant change of ion concentration induce a non-mass resonance frequency response of the QCM.

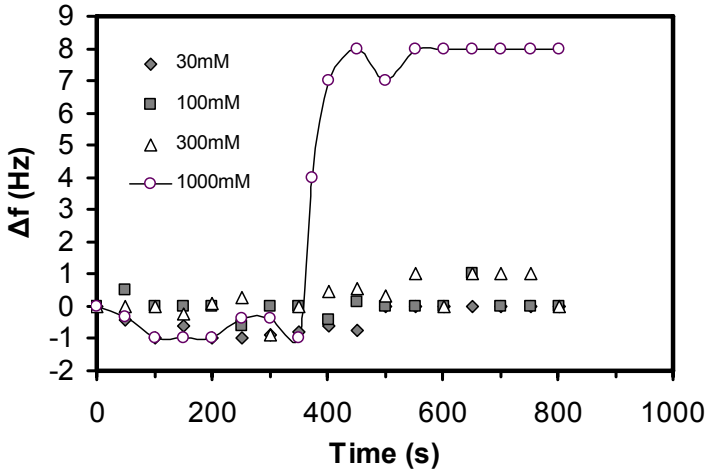

Figure 4.2. Resonant frequency response in function of the addition of injection of 1 ml of NaCl solutions at different concentrations in a PBS 100 mM (pH 7.0) flow (500 µl/min at 25ºC).

A preliminary conclusion is that for QCM assays, the ionic strength of the sample and of the solvent must necessarily be similar to avoid undesirable frequency shifts at the beginning of a mass adsorption transient.

4.2. Effect of small increments of electrolytes

Milli-Q water was circulated in the sensor flow chamber and, after establishing a stable resonance frequency signal, small volume amounts of concentrated solutions of NaCl, KCl, $MgCl_2$ or $CaCl_2$ were successively added in the sample container in order to achieve the desired ionic strength in the system.

As shown in Fig. 4.3, the QCM sensor responds strongly to small variations on the solution electrolyte concentration when the resonance frequency is directly measured by frequency counting. To evaluate wether this response was related to possible variations of the hydrostatic pressure owing to the small volume increments, control experiments were

performed adding similar volume amounts of Milli-Q water instead of electrolyte solutions. No frequency variations were observed for these control experiments, which indicate that the frequency variations observed are related to nothing more then the presence of the electrolytes.

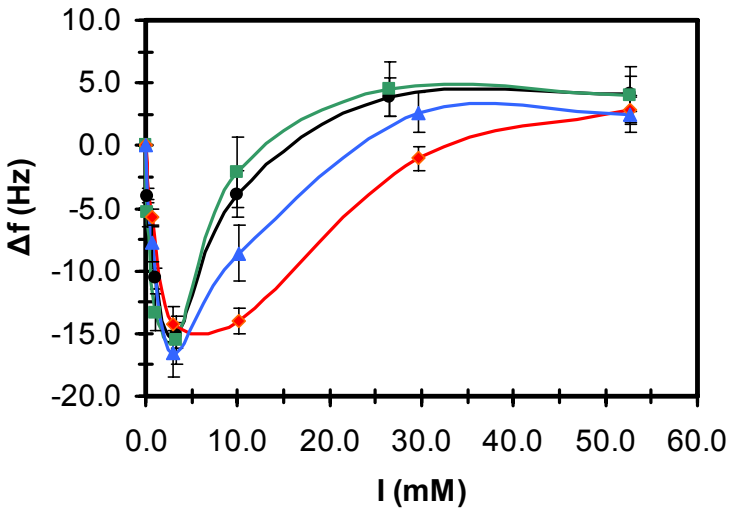

Figure 4.3. QCM resonance frequency response to increasing ionic strength. Average resonance frequency variation (Δf) with increasing ionic strength for (●) NaCl, (■) KCl, (♦) $CaCl_2$ and (▲) $MgCl_2$, resulting from n = 6 independent measurements for each salt.

Fig. 4.3 also shows that, by representing the frequency variation (Δf) as a function of the ionic strength (I), it is possible to differentiate between the effect of monovalent and divalent cations. Even though the general tendency is the same, with frequency decreasing for the initial variations and increasing after reaching a minimum, the frequency increase rate is higher for monovalent cations (Na^+ and K^+) when compared to divalent cations (Mg^{2+} and Ca^{2+}).

If one adopts the mathematical models usually used to interpret frequency variation data (Sauerbrey and Kanazawa models), the increase in the frequency observed (Fig. 4.3) should be related either to a decrease of the mass over the crystal surface or to a decrease in the

solution viscosity and/or density. However, considering that (i) the bulk solution viscosity and density are unchanged during the experiments; (ii) no mass is deposited over the crystal; and (iii) the addition of such small quantities of salt has negligible or no effect on the overall system hydrostatic pressure, this thesis proposes, in accordance with a previously published work (Etchenique and Buhse, 2000; Etchenique and Buhse, 2002), that the anomalous frequency response observed is correlated to the increment of the charge density in the solution due to the addition of electrolytes.

The admittance data associated with the experiments described above were recorded, in order to investigate in more detail the origins of the frequency variation, to differentiate the effect of the different interferences, and to calculate the values of the parameters of the BVD equivalent electrical circuit.

Fig. 4.4 shows the variation of each parameter relatively to Milli-Q water, with the small increments of the solution ionic strength. In accordance with previously published data (Etchenique and Buhse, 2000; Ghafouri and Thompson, 2001; Ghafouri and Thompson, 2001; Etchenique and Buhse, 2002), the calculated inductance and resistance increase with increasing ionic strength. This increase occurs up to reaching a certain ionic strength, after which the inductance stabilizes while resistance decreases considerably (Fig. 4.4A and 4.4B). On the basis of the BVD parameters, it is possible to predict the resonance frequency variation ($f_0 = (4\pi^2 \times L_m C_m)^{-1/2}$). Fig. 4.4C shows that the predicted frequency variation with the solution ionic strength is not consistent with the measured values of Fig. 4.3. Even though sharing a similar tendency for the low ionic strengths, with resonance frequency decreasing with increasing ionic strengths, for the higher ionic strengths the predicted resonance frequency variation stabilizes close to its minimum value while the measured resonance frequency variation considerably increases before stabilizing.

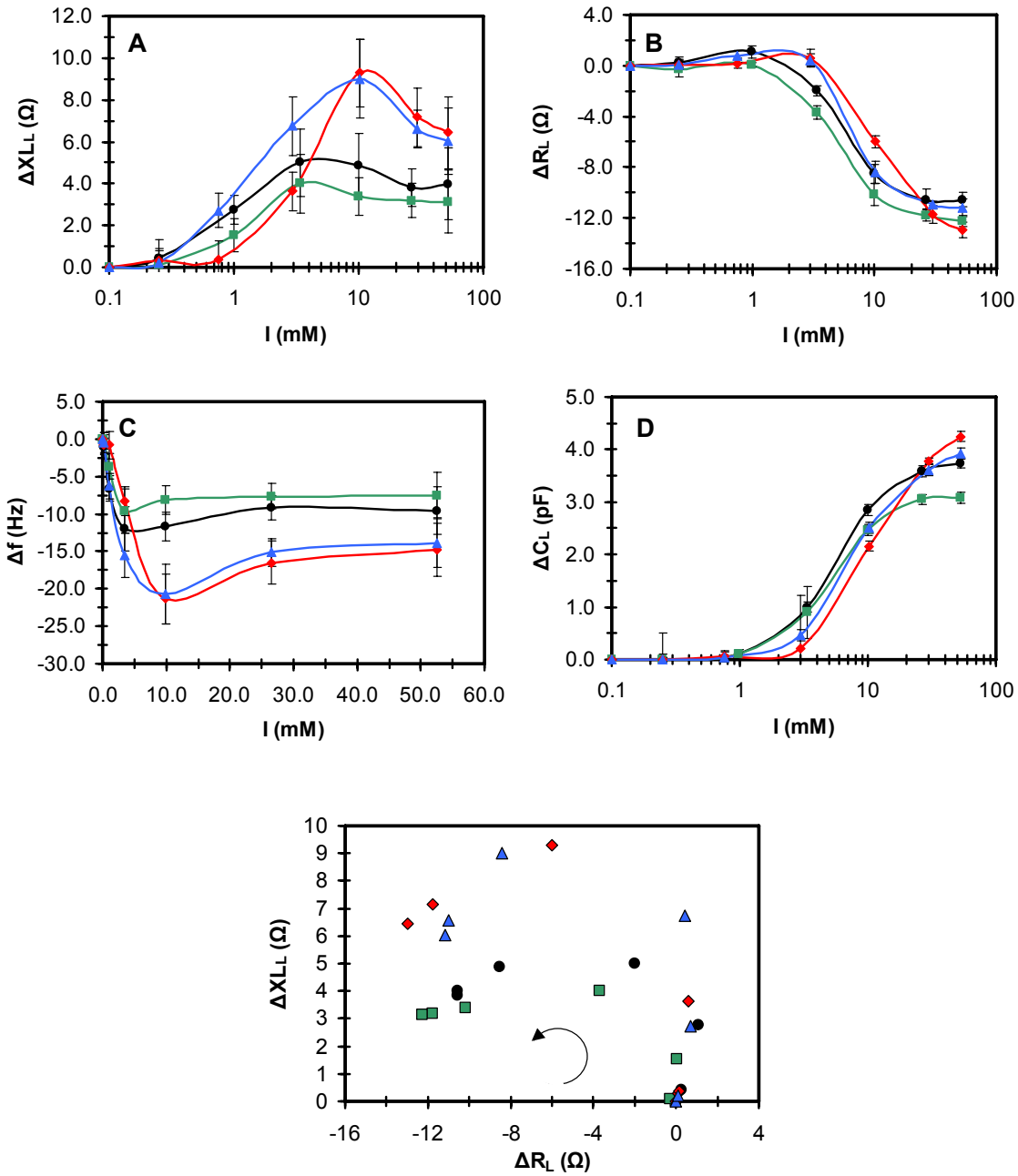

Figure 4.4. Variation of the Butterworth van Dyke model parameters in liquid (subscript L), relatively to the crystal loaded with Milli-Q water, with the ionic strength for (●) NaCl, (■) KCl, (♦) $CaCl_2$ and (▲) $MgCl_2$. (A) inductance; (B) resistance; (C) calculated resonance frequency variation, (D) parallel capacitance and (E) parametric polar impedance plot where the ionic strength increases counter-clockwise, as indicated by the arrow. The figures correspond to the average of impedance analysis data resulting from three independent experiments with each salt.

Furthermore, contrary to the measured resonance frequency data, impedance analysis predicts different sensor responses to mono and divalent cations (Fig. 4.4C). These results suggest that QCM frequency counting data is affected by interfering signals which can be avoided or eliminated by using full impedance analysis.

Owing to the assumption that the parallel capacitance (C_0) is related to the physical properties of the system components, such as electrodes, cables, connectors, and holders, this capacitance should be expected to be constant within the experiments. However, there is an increase of parallel capacitance with the loading of Milli-Q water due to a fringing-field effect that augments the ideal parallel-plate capacitance.

This effect is well known since it affects the performance of crystal oscillators and it is advised by QCM manufacturers (Ex. Stanford Research Systems) that capacitance cancellation is essential for accurate measurements and should be checked and readjusted every time the environment of the crystal is changed (for example when transitioning from air to a liquid phase) since it dominates the electrical behavior of the crystal away from resonance (Schneider and Martin, 1995). The problem is that the capacitance cannot be adjusted during the measurements.

Only a few QCM users take this increase in parallel capacitance into consideration (Kim *et al*., 2003), since basically, if it is properly annulled, it no longer represents an interference and most importantly, no more increases relatively to the original value of C_0 are expected to occur. Contrary to these expectations, total parallel capacitance increases with increasing ionic strength (Fig. 4.4D). This result suggests that variations in the electrolyte composition of the solution results in a capacitive response characterized by a specific addition to C_0. To account for such sensor response, in accordance with previously published experimental work

(Xie *et al.*, 2001), we extended the generally used BVD model to include additional parallel capacitances for each stage of the experiment (Fig. 4.5).

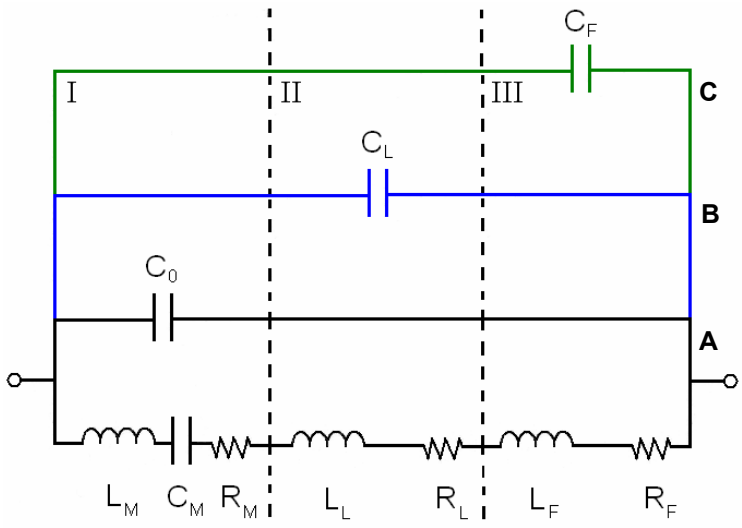

Figure 4.5. Butterworth van Dyke equivalent circuit model (A) and proposed Butterworth van Dyke equivalent circuit (adding B and C) of QCM sensors. I - unloaded resonator; II - elements added due to liquid medium exposure; and III - elements added due to the adsorption of mass on the surface of the sensor.

It is expected that these additional capacitances will enable the differentiation of the influence of charged species added or removed at each stage, thus the correction of calculated parameters upon rendering the parasitic capacitance (C_0) constant. According to this modification, the parallel capacitance calculated corresponds to the total parallel capacitance of the system ($C_T = C_0 + C_L + C_F$) and includes the contributions from the static capacitance (C_0), and the additional capacitances due to charge variation upon liquid loading (includes the effect of solutes) (C_L) and/or mass loading (C_F). The influence of the charge variation at a given stage is this way discriminated after subtracting the capacitance values calculated for the previous stages. Fig. 4.4D shows the variation of C_L relatively to the Milli-Q water capacitive contribution, with the increase of ionic strength.

Further interpretation of the calculated parameters reveals no variation of the resistance (R) or the capacitance (C_0) with the cation valence (Fig. 4.4B and 4.4D). On the other hand, the simultaneously determined inductance values (Fig. 4.4A) reveal a strong influence by the cation valence, a result that is consistent with the data gathered by frequency counting (Fig. 4.3). As shown in Fig. 4.4A, the resonator inductance increases to a further extent, both considering the amplitude and the ionic strength, when divalent cations are present. Since the resonance frequency is affected by the motional inductance and capacitance ($f_0 = (4\pi^2 \times L_m C_m)^{-1/2}$) these results show that, for the same ionic strength, divalent cations generate higher frequency drops and slower responses to ionic strength variations which are driven just by the inductive contribution of the resonator.

4.3. Piezoelectric resonators sense and respond to modifications of the diffusive electrical double layer

Considering the physical meaning of the BVD parameters, in particular the fact that XL is related to vibrating mass, hence reflecting mass displacement, and that R is related to acoustic energy loss owing to medium damping (viscous losses), a more detailed analysis of the experimental data reveals that the recorded profiles, both by frequency counting and impedance measurements, can be divided into two distinct regions. In the low ionic strength region (I < 1 mM) the resonant frequency drops while both the calculated inductance and resistance rise, which is compatible to an increase of the density and/or of the viscosity near the crystal's surface. On the other hand, for higher ionic strengths (I > 1 mM) the resonant frequency increases and the resonator impedance is characterized by $X_L >> R$ which indicates the formation of a rigid enough layer that moves in phase with the resonant surface.

It seems thus that a layer is formed at the crystal surface whose viscosity/rigidity depends on the solution electrolyte nature and composition. The viscoelastic behavior of this layer can be characterized by the parametric polar impedance plots, which are graphical representations of the variation of the calculated inductance with the variation of the calculated resistance (Fig. 4.4E). In general, parametric polar impedance plots of Newtonian or viscoelastic fluids are characterized by linear dependencies of *XL* and *R* whose slope equals one for Newtonian fluids (Etchenique and Buhse, 2002). On the other hand, fluids or layers of variable viscosity or elasticity are characterized by a curvature in the *XL vs. R* plots (Etchenique and Buhse, 2002). As such, the circular shape of the *XL vs. R* plots of Fig. 4.4E leads to the conclusion that a thin film with variable viscosity/elasticity is formed between the crystal surface and the solution bulk.

Considering the fact that the solutions that are in contact with the crystal surface consist of water and electrolytes, the only possible layer being formed or "deposited" on the crystal surface is a diffuse electrical double layer (DDL). The thickness of the DDL, the Debye length, is known to be influenced by the concentration and by the valence of electrolytes (Atkins, 1990). By increasing the solution ionic strength, or by using ions with higher valences, the Debye length decreases, resulting in a reduced distance between charged particles, as well as the entire double layer drawing nearer the surface, resulting therefore in the accumulation of charges at the surface of the electrodes. Thus, more rigid layers and higher charge accumulation are expected to be formed close to the sensor surface for higher ionic strengths and valences, detected by higher inductance values (Fig. 4.4A). Moreover, higher capacitances (Fig. 4.4D) are measured as a consequence of the additional parallel capacitances.

4.4 Use of modified BVD data as corrective tool to evaluate and quantify DNA hybridization

To further demonstrate the applicability of the proposed modification to the BVD model, the sensor response as a DNA detector was evaluated. DNA fragments, and oligonucleotides, are polyelectrolytes in neutral aqueous solution and a strong interfering signal resulting from DDL perturbation can be expected. Crystal sensors were functionalized with oligonucleotides, mounted in the experimental setup, and used to detect complementary oligonucleotides (Fig. 4.6).

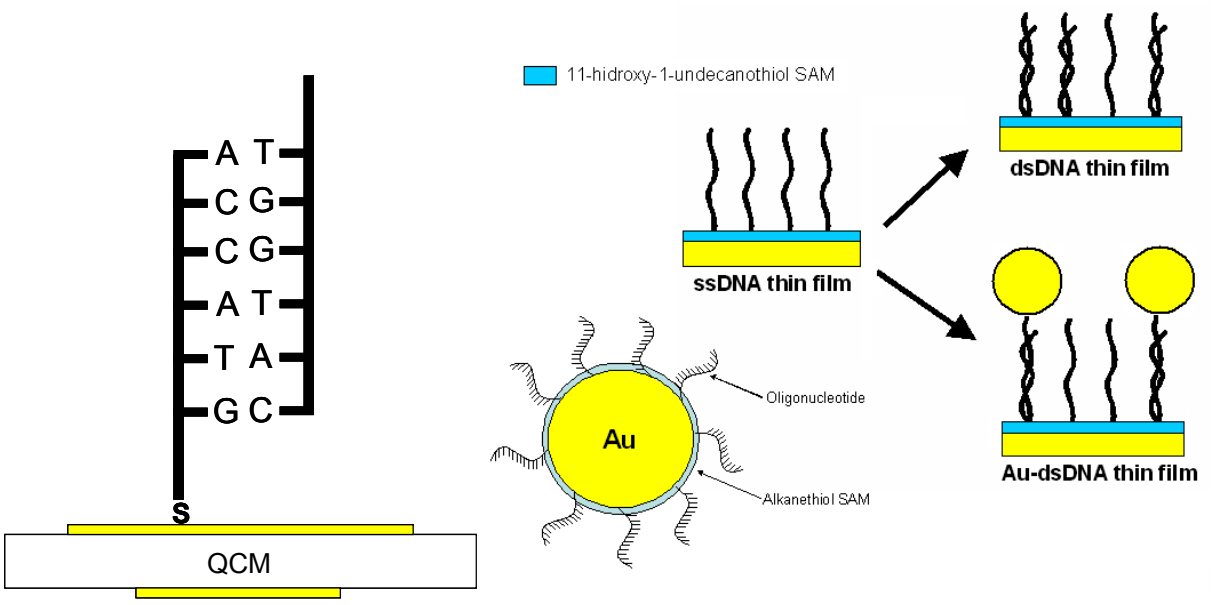

Figure 4.6. Scheme representing the strategy used to develop a piezoelectric DNA sensor. The crystals were first functionalized with a thiolated oligonucleotide, forming a ssDNA film, used to target the complementary sequence. The complementary oligonucleotide was detected non-labeled and labeled with 10 nm gold nanoparticles.

As shown in Fig. 4.7A, the signals measured by frequency counting for unlabeled oligonucleotides and for the controls are similar. Such a result leads to the conclusion that either the sensor is not fully operational or no complementary sequences are present. The lack of signal variation in frequency counting measurements when using unlabeled oligonucleotide or DNA fragments has been reported by other authors that used gold nanoparticles as labels for mass amplification in order to force a signal resulting from DNA hybridization at the sensor surface (Zhou[b] *et al.*, 2000; Su and Li, 2005).

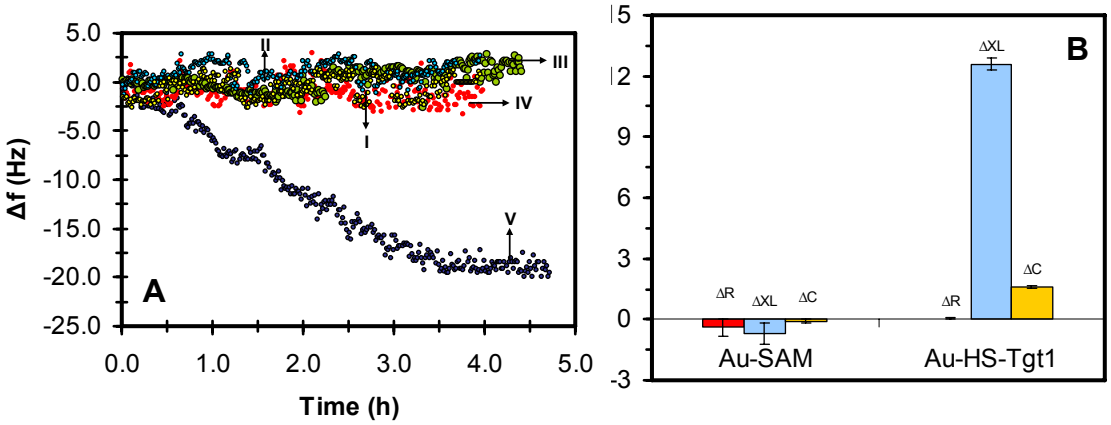

Figure 4.7. Crystal sensor response to DNA hybridization. All crystal sensors used were functionalized with HS-Pr1 probe and blocked with 11-hydroxy-1-undecanothiol: (A) resonance frequency recorded for crystal sensors incubated with (I) PBS buffer, (II) 1 μM of Ctr1, (III) 1 μM of Tgt1, (IV) 1.7 nM of Au-SAM nanoparticles, (V) 1.7 nM of Au–HS-Tgt1 nanoparticles; (B) impedance data acquired for crystal sensors incubated with gold nanoparticles modified with 11-hydroxy-1-undecanothiol (Au-SAM) and gold nanoparticles functionalized with complementary target HS-Tgt1 (Au–HS-Tgt1).

Even though resonance frequency variations are measured when using gold labeled targets (Fig. 4.7A, curve V), target labeling withdraws from piezoelectric sensors the advantages of direct transduction of unlabeled targets. Moreover, the total frequency variation obtained for the gold labeled oligonucleotides measured by frequency counting is Δf = 19 Hz (Fig. 4.7A) which only accounts for 63% of the frequency change predicted by impedance analysis (Fig.

4.7B). This discrepancy indicates that quantitative calculations based on frequency counting (*e.g.* mass determination) can be underestimated due to the interfering signal resulting from the effect of the charges on the sensor surface and adjacent layers.

In order to account for the effects of charges it is proposed the calculation of the respective interfering capacitances C_L and C_F (Fig. 4.5). The total frequency variation (Δf_T) due to mass loading (Δf_M), viscoelasticity of the adsorbed/deposited mass (Δf_V), liquid (Δf_L) and charge interference (Δf_C) should be thus obtained by,

$$\Delta f_T = \Delta f_M + \Delta f_V + \Delta f_L + \Delta f_C \quad (20)$$

When operating the QCM in the oscillator/frequency counting mode in liquid phase Δf_M, Δf_V, Δf_C can not be differentiated, and the measured frequency variations is given by Δf_T - Δf_L. In analogy to the case of the generally accepted correction for the liquid loading effects, where the contribution of the buffer viscosity/elasticity and density to the total frequency change (Δf_L) is estimated from a linear relation established between Δf and ΔR (Martin *et al*., 1991; Zhou[a] *et al*., 2000), a parameter was sought that could be used to correct the underestimation of frequency counting quantification. Considering, once again, that the frequency variations shown in Fig. 4.3 and Fig. 4.4 result only from charge interferences ($\Delta f_M = \Delta f_L = \Delta f_V = 0$), the data from these figures was used to estimate the values of such a parameter. A plot of the measured frequency variation against the calculated interfering capacitance (Fig. 4.8) shows that these parameters are linearly correlated within the range investigated, leading to the conclusion that the frequency variation is linearly dependent on the calculated capacitance

variation (demonstrated by the close to one correlation coefficients and by the very low p values).

Moreover, the similarity of the slopes may indicate that the observed frequency variations are due to the capacitive effect and could be independent of the charged species involved. Thus, calculating the average of the slopes, a frequency variation of 8.0±0.5 Hz per pF is found resulting from charge interference. To test the applicability of this hypothesis, this corrective factor was applied to the data gathered for the gold labeled oligonucleotide detection. For this case, the charge interference was quantified as C_F = 1.60 ± 0.02 pF (Fig. 4.7.B) which results in an estimated contribution to the frequency variation of Δf_C = 12.8±0.8 Hz.

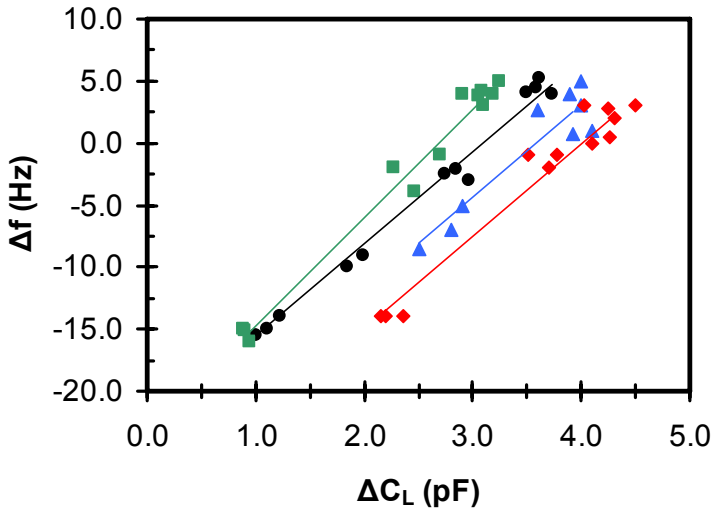

Figure 4.8. Relation between measured resonance frequency variation and calculated parallel capacitance in the range of 1 mM ≤ I ≤ 50mM. Triplicate independent experiments for (●) NaCl (12 experimental points), (■) KCl (12 experimental points), (♦) $CaCl_2$ (12 experimental points), and (▲) $MgCl_2$ (9 experimental points) were performed; Linear regression of experimental data yielded the correlations Δf = (7.8±0.4)×ΔC + (-24±1); r = 0.9862; p < 0.0001, for NaCl; Δf = (8.7±0.3)×ΔC+ (-23.6±0.8); r = 0.9935; p < 0.0001, for KCl; Δf = (7.8±0.5)×ΔC+ (-31±2); r = 0.9790; p < 0.0001, for $CaCl_2$; and Δf = (7.7±0.9)×ΔC+(-28±4); r = 0.9372; p = 0.0002.

Since the immobilized mass has a negligible viscous effect ($\Delta R \approx 0$, Fig. 4.7B), the use of Equation 31 estimates the frequency variation due to mass load as $\Delta f_M=\Delta f_T-\Delta f_L+\Delta f_C$=31.8 Hz. The similarity between this value and the 30 Hz estimated from the impedance data demonstrates that charge interferences can reliably be corrected by using the parameter obtained from Δf *vs*. C_L correlations.

4.5. Conclusions

In this chapter, it was demonstrated that the response of QCM is affected by the presence of electrolytes in solution. This interference leads to transients mimicking desorption, with frequency variations (Δf) decreasing with increasing densities of charges in solution, and can thus have a considerable impact in biosensor applications, up to the point of leading to less accurate conclusions. The influence of electrolytes results in non-Kanazawa response, which, for the low ionic strengths, is characterized by a frequency drop and by an increase of the sensor inductance and resistance owing to the increase of the density and viscosity near the sensor surface as a diffuse electric double layer develops.

For high ionic strengths, charge effects predominate, leading to increasing resonance frequencies, while the resistance drops and the parallel capacitance increases. We propose a modification to the Butterworth–Van Dyke model to include additional parallel capacitances in order to account for the influence of charges to the sensors response. Such influence is linearly correlated to the measured resonance frequency variation in the range of 1 mM $\leq$ I $\leq$ 50 mM and is characterized by a desorption-like signal of 8.0±0.5 Hz pF^{-1}. The use of this factor allows for the correction of the mass-frequency variation, which otherwise is close to

40% underestimated, resulting in a convergence of the values measured by frequency counting and impedance analysis.

Estimating the influence of electrolytes and its contribution to the measured frequency variation thus enables the acquisition of more accurate data and this represents a step forward in the use of piezoelectric sensors for quantitative direct transduction of molecular recognition events.

Chapter 5

Electroacoustic impedance complemented piezoelectric quantitative analysis of molecular systems: self assembled monolayers and streptavidin-biotin binding

In this chapter electroacoustic impedance analysis is used to complement resonance frequency variation data obtained from piezoelectric crystal sensors under organic mass adsorption experiments. Resonance frequency signal is deconvoluted by electroacoustic impedance data to identify interfering signals as well as to assess and remove their influence, according to what was discussed in previous chapters. This approach enables the accurate use of the Sauerbrey correlation to establish a direct relation between mass deposited at the sensor surface, or solution concentration, and measured frequency variations. Kinetic models can thus be evaluated and kinetic constants estimated directly from measured data, without the risk of reaching overestimated or underestimated values due to non-mass effects.

This approach is also used to the study of the formation of alkanethiol self assembled monolayers (SAM) and to the binding of streptavidin to immobilized biotin. Kinetic and

equilibrium parameters were estimated from transient analysis, adsorption isotherms, Scatchard and Hill plots obtained from the frequency data for both the alkanethiol and streptavidin films. The resulting analysis shows that the SAM formation is characterized by a positive cooperativity while streptavidin recognition process is characterized by a negative cooperativity. Finally, the approach used in this chapter enabled the estimation of the dissociation rate constant for the interaction of streptavidin with immobilized biotin (k_{-1} = $(2.7\pm0.5)\times10^{-4}$ s^{-1}, which is the first dissociation rate constant calculated directly from experimental surface binding data using a non-labelled target.

5.1. Formation of a Self Assembled Monolayer (SAM)

Alkanethiols spontaneously adsorb to gold surfaces self assembling as oriented monolayers, through a strong chemical interaction between the sulphur and the metal surface (Karpovich and Blanchard, 1994,) followed by lateral interactions of neighbour adsorbed molecules, leading to the parallel alignment of the molecules generating a thin, rigid and uniform film at the sensor surface (Liao *et al*., 2000). Thus, the formation of alkanethiols SAMs was selected to illustrate the use of piezoelectric sensors in quantitative monitoring of thin, rigid films within the assumptions of the Sauerbrey equation. Impedance analysis of self-assembled monolayers on the gold electrodes of the crystal sensors could also be put to practice in this case, particularly focused on the viscoelastic and charge effects discussed previously.

In order to monitor the real-time response of the sensor to the formation of SAMs, increasing concentrations of 11-hydroxy-1-undecanothiol were recirculated over the sensor surface and the frequency variation was measured (Fig. 5.1A).

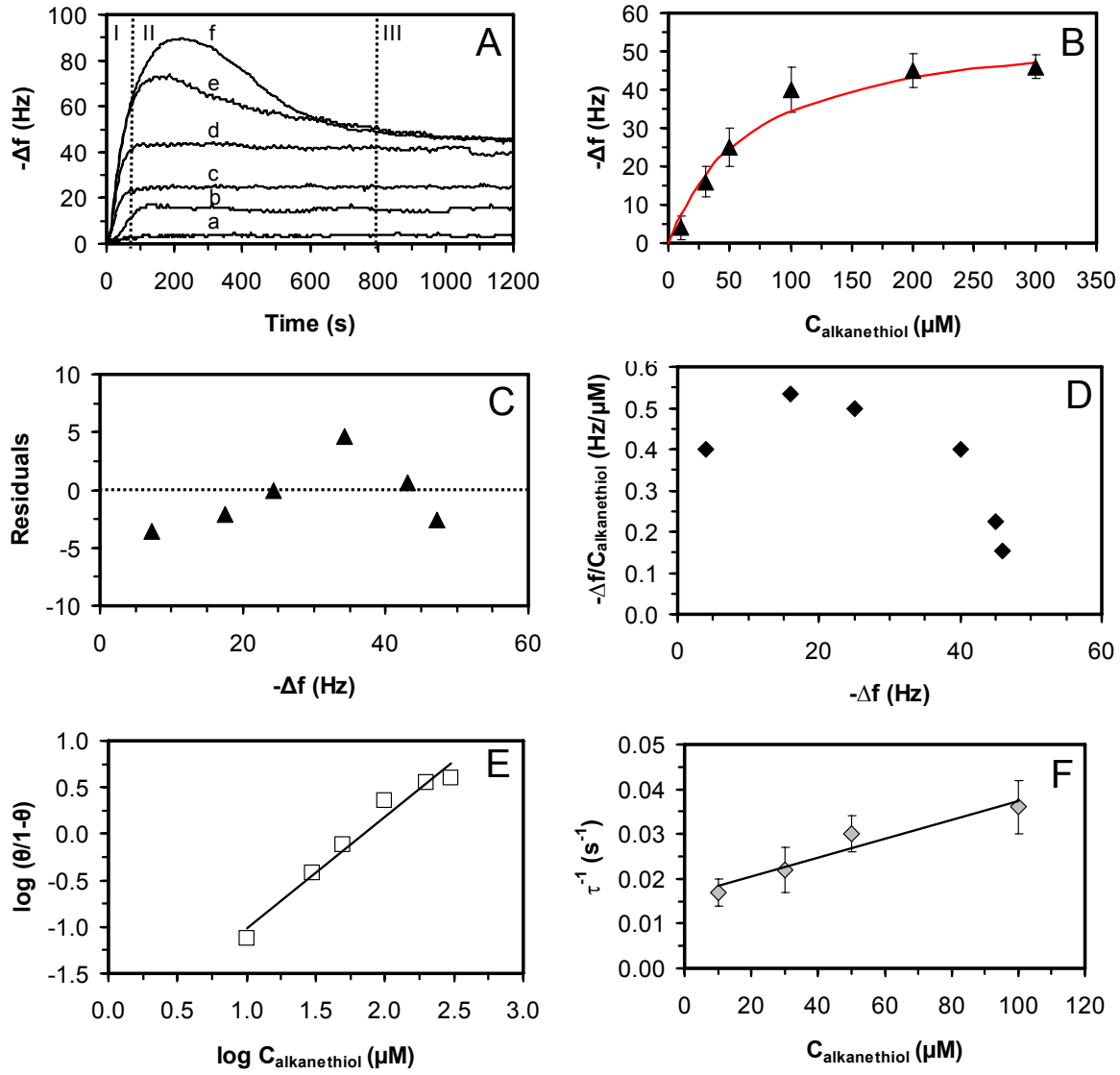

Figure 5.1. (A) Frequency shift response of quartz crystal gold sensors to the exposure to increasing bulk concentrations (a- 10 μM; b- 30 μM; c- 50 μM; d- 100 μM; e- 200 μM; f- 300 μM) of 11-hydroxy-1-undecanothiol. (B) Saturation curve showing the total frequency shift obtained for each concentration of alkanethiol used. The curve represents the non-linear interpolation of the data to the saturation component of the molecular model presented in Equation 22, with accepted goodness for $Chi^2 = 9.14 <$ critical $Chi^2 = 11.07$ ($\alpha = 0.05$, $n = 5$). (C) The residuals data for the interpolation presented in B. (D) Scatchard plot and (E) Hill plot for the data presented in B. (F) Linear dependence of the 1:1 molecular model calculated constant τ (relaxation time of binding), to the lowest bulk alkanethiol concentrations used (10-100 μM). Linear regression of experimental data yielded the correlation: $\tau = (2.1\pm0.4)\times10^{-4}\ \mu M^{-1}\ s^{-1} \times C + (1.6\pm0.2)\times10^{-2}\ s^{-1}$; r = 0.9659; ANOVA analysis accepts linear interpolation for F statistic $p = 0.034 < \alpha = 0.05$. Each presented data is the average result of three independent experiments.

Time-dependent resonance frequency transients indicate alkanethiol adsorption, which occurs rapidly up to the establishment of equilibrium (Fig. 5.1A). Three distinct regions are identified in the adsorption transients (Fig. 5.1A): An initial period (region I), characterized by excess surface binding sites to which alkanethiols adsorb very rapidly; In region II, fewer binding sites are available as the surface is closer to saturation. This region is characterized by a slow organization of the SAM which may result in the release of excess adsorbed molecules as shown for the higher alkanethiol concentrations; Finally, region III corresponds to the equilibrium of the chemisorption process.

As shown in Fig. 5.1A, steeper frequency transients are obtained for higher alkanethiol concentrations and alkanethiol adsorption follows a standard saturation-like isotherm (Fig. 5.1B) where the final frequency drop is plotted vs. concentration. When analyzing these data using a Langmuir isotherm, sensor saturation at ~58±5 Hz dissociation constant (K_D) of ~69±16 μM were calculated. Even though acceptable distribution of the residuals (Fig. 5.1C) is obtained and data fitting to a Langmuir isotherm is accepted by the Chi^2 statistical test (95% confidence level and 5 degrees of freedom), significant deviations are shown (Fig. 5.1B).

This fact reveals the possible influence of molecular phenomena, such as mass transfer and cooperativity, which are not predicted by the Langmuir model. While no conclusion may be drawn regarding the influence of mass transfer, the convex shape of the Scatchard plot (Fig. 5.1D) indicates positive cooperative effects during the adsorption process which is consistent with the 3-stage mechanism proposed above. Positive cooperativity of alkanethiol adsorption is further demonstrated by the Hill coefficient (n_H = 1.2±0.1) obtained from the slope of the respective Hill plot –Fig. 5.1E.

In order to evaluate the usefulness of frequency variation data to calculate the amount of mass adsorbed at the sensor surface by the Sauerbrey equation, the sensor acoustic impedance was measured at the end of each of the adsorption processes shown at Fig. 5.1A. The acoustic impedance parameters were then estimated from impedance spectra using the BVD equivalent model proposed in Chapter 4, Fig. 4.5. As expected, increasing variations of the inductive component of the BVD model (ΔXL_F) were calculated as increasing mass amounts are adsorbed onto the sensor surface. On the other hand, the variation of both impedance resistance (ΔR_F) and capacitance (ΔC_F) were negligible indicating the formation of a rigid film with no charge influence. Therefore no viscoelastic (Martin *et al.*, 1991) or charge (Encarnação[a] *et al.*, 2006) interferences affect the measured frequency variation, and thus the Sauerbrey equation can be directly applied to the measured frequency variation enabling adsorbed mass quantification. The results concerning the main measurable parameters, given by the quartz crystal sensor, are summarized in Table 2.

Table 2. Impedance analysis parameters calculated for 11-hidroxy-1-undecanothiol SAMs obtained with increasing bulk concentrations of alkanethiol, and respective immobilized mass calculated from the frequency data in Fig. 5.1A using the Sauerbrey model.

Concentration (μM)	**ΔXL_F (Ω)**	**ΔR_F (Ω)**	**ΔC_F (pF)**	**Immobilized mass (μg/cm^2)**
10	1.8±0.4	0.4±0.2	0.08±0.02	0.07±0.05
30	7.1±0.8	1.0±0.3	0.06±0.01	0.28±0.07
50	11±1	0.8±0.4	0.06±0.03	0.44±0.09
100	17±1	1.5±0.7	0.10±0.06	0.7±0.1
200	19±2	1.9±0.6	0.11±0.04	0.80±0.08
300	20±2	1.8±0.4	0.15±0.09	0.81±0.05

The validity of the Sauerbrey model demonstrated by the acoustic impedance analysis can also be used to estimate binding constants from transient data. The kinetic constants were calculated from frequency transients by non-linear fitting to a 1:1 binding model (Equation. 21).

$$d\theta / dt = k_1(1-\theta)C - k_{-1}\theta \tag{21}$$

Where θ is the relative amount of surface coverage, C is the initial ligand concentration, and k_1 and k_{-1} are the association and dissociation rate constants, respectively. Upon integration of the rate equation, an expression is obtained to describe the time dependency of the sensor surface coverage:

$$\theta = \frac{C}{C + \frac{k_{-1}}{k_1}} \theta_\infty \left[1 - \exp\left(-t/\tau\right)\right] \tag{22}$$

Where θ_∞ is the total available binding sites at the sensor surface and $\tau = [k_1 \times C + k_{-1}]^{-1}$ is the relaxation time of binding. The rate constants k_1 and k_{-1} are then calculated from the slope and intercept of linear regression of the reciprocal of the relaxation time variation with the ligand concentration.

Because mass in the Sauerbrey equation is proportional to the sensor surface coverage (θ), the measured frequency variation can be used to calculate the binding relaxation time (τ) from which the binding rate constants can be further calculated. However, as discussed above, this

model may not be appropriate to interpret the presented SAM formation. Nevertheless, given its simplicity, this model was used with the linear region of the adsorption isotherm (up to 100 μM). As shown in Fig. 5.1F, a plot of τ^{-1} vs. $C_{alkanethiol}$ yields a straight line with slope k_1 = 211±40 $M^{-1}s^{-1}$ and intercept k_{-1} = (1.6±0.2)×10^{-2} s^{-1} from which a dissociation equilibrium constant $K_D = k_1/k_{-1}$ = (8±2)×10^{-5} M. Even though this dissociation equilibrium constant is ~20% higher from the one calculated from the isotherm, which may be the result of deviation from the ideality, as discussed previously, the rate constants calculated are consistent with previously published data for self assembled monolayers of other alkanethiol molecules (Karpovich and Blanchard, 1994; Liao *et al.*, 2000; Kim *et al.*, 2001).

5.2. Piezoelectric detection and analysis of Streptavidin binding to Biotin

Streptavidin is a homotetrameric molecule folded in such as way that the four biotin binding sites are grouped in pairs located at opposite faces of the protein. The very high specific binding affinity between streptavidin and its ligand biotin makes this system a very attractive model to study surface recognition processes (Ewalt, *et al.*, 2001; Muzykantov, *et al.*, 1994; Yao *et al.*, 1995; Rosebrough and Hashmi, 1996; Schechter *et al.*, 1999). Binding of streptavidin to immobilized biotin is known to result in well ordered biofilms (Chilkoti *et al.*, 1995; Qureshi *et al.*, 2001). Therefore, in this work streptavidin detection was selected to demonstrate the usefulness of piezoelectric sensors to specifically detect proteinaceous analytes in solution. Piezoelectric sensors were functionalized with biotinyl-3,6-dioxaoctanediamine, assembled in the experimental set-up and used to detect streptavidin injected in the buffer flow and the obtained data is shown in Fig. 5.2.

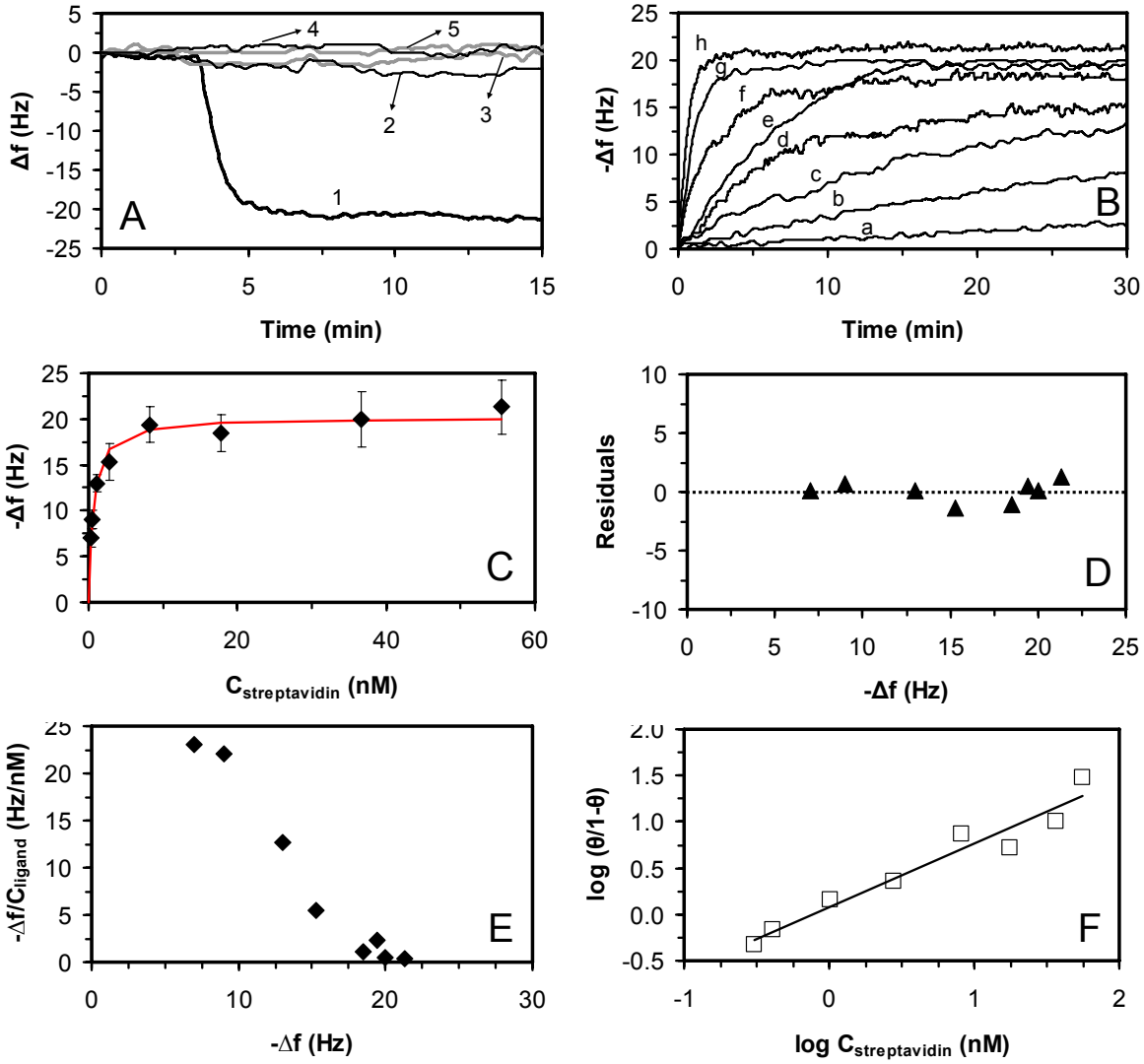

Figure 5.2. (A) Blank assays compared to biotin-streptavidin molecular recognition: (1) crystal with biotin exposed to streptavidin at 3 µg/ml, (2) crystal with biotin exposed to BSA at 50 µg/ml (3) clean crystal exposed to streptavidin at 3 µg/ml, (4) crystal with biotin exposed to PBS and (5) crystal with SAM exposed to streptavidin at 3 µg/ml. (B) Biotin functionalized QCM resonance frequency response, to different streptavidin concentrations (µg/ml): (a) 0.025, (b) 0.05, (c) 0.1, (d) 0.2, (e) 0. 5, (f) 1.0, (g) 2.0 and (h) 3.0. Each presented curve represents the average of three transients obtained experimentally. (C) Saturation curve showing the total frequency shift obtained for each concentration of streptavidin used. The curve represents the non-linear interpolation of the data to the saturation component of the molecular model presented in Equation 22, with accepted goodness for $Chi^2 = 0.79 <$ critical $Chi^2 = 14.07$ ($\alpha = 0.05$, $n = 7$). (D) The residuals data for the interpolation presented in C. (E) Scatchard plot and (F) Hill plot for the data presented in C.

The biofilm of immobilized biotin specifically captures streptavidin from solution: no sensor response is obtained for a mixture of BSA, ribonuclease A, and cytochrome c (Fig. 5.2A), while significant frequency variations are monitored for streptavidin binding (Fig. 5.2B).

Fig. 5.2A also includes controls to evaluate the eventual unspecific binding of streptavidin to any of the sensor surface components other than biotin. As shown, no streptavidin binding is seen to clean or SAM modified gold surfaces.

Streptavidin binding to biotin biofilms tends rapidly to the equilibrium according to a saturation isotherm (Fig. 5.2C), with an acceptable distribution of the residuals (Fig. 5.2D).

As before, the data was fitted to a Langmuir isotherm yielding a saturation, capacity, corresponding to Δf_{max} = (20.2±0.4) Hz and a dissociation equilibrium constant K_D = (5.8±0.7)×10^{-10} M which is comparable to most of the published equilibrium constants.

Table 3 contains a collection of published estimated rate and equilibrium constants, using different techniques and methodologies, for the biorecognition process between streptavidin and biotin molecules.

Similarly to the study of SAM formation, Scatchard plots and Hill analysis were performed to evaluate cooperative effects during streptavidin recognition (Fig. 5.2E and 5.2F, respectively). The data indicates that streptavidin binding to immobilized biotin films is characterized by a negative cooperativity (n_H = 0.69±0.07). This result is consistent with binding mechanisms of biomolecules binding to natural receptors (Nesbitt *et al.*, 1982; Chazenbalk *et al.*, 1996 ; Urizar *et al.*, 2005) where, upon binding, the formation of the affinity pair may partially or completely hinder adjacent binding sites (receptors).

Table 3. Rate and equilibrium kinetic constants determined for the pair streptavidin-biotin in different published studies and in this work. n.d.- constants not calculated; *- off-rate not calculated and K_D obtained using k_{-1} published by Green in 1990.

$k_1 \times 10^{-7}$ ($M^{-1}.s^{-1}$)	$k_{-1} \times 10^{5}$ (s^{-1})	K_D (M)	Experimental Method	Reference
7.0	0.28	4.0×10^{-14}	Radiolabled exchange reaction	(Green, 1990)
n.d.	n.d.	1.0×10^{-12}	Paramagnetic beads	(Fujita and Silver, 1993)
n. d.	n. d.	$\approx 10^{-10}$	Elisa	(Chilkoti *et al.*,1995)
n. d.	n. d.	4×10^{-7}	Reflectometric interference spectroscopy	(Piehler, *et al.*, 1996)
50	*	5.5×10^{-13}	SPR	(Qureshi, *et al.*, 2001)
n. d.	n. d.	1.0×10^{-6}	Light scattering	(Raschke, *et al.*, 2003)
n.d.	n.d.	1.0×10^{-11}	SPR	(Han and Van Duyne, 2004)
460±30	27±5	$(5.8 \pm 0.7) \times 10^{-10}$	5 MHz QCM with Impedance Analysis	This thesis

Acoustic impedance analysis was performed to identify the presence of viscoelastic and charges interferences in the frequency variation transients obtained for streptavidin binding (Fig. 5.3).

As expected, the inductance variation (ΔXL_F) follows a concentration dependent trend similar to the adsorption isotherm obtained from frequency measurements, which reveals the binding of streptavidin to the immobilized biotin biofilms (Fig. 5.3). Resonant energy dissipation due to viscoelastic interference can be neglected as indicated by the ~0 variation of the impedance resistance (ΔR_F). Viscoelastic effects, however, are observed for the highest streptavidin concentrations, which, according to the Martin model (Martin *et al.*, 1991), $\Delta R = -4\pi L_m \Delta f_m$, results in a frequency variation interference of 2 Hz. Even though having some importance at the molecular level, the resulting viscoelastic interference results in a neglected frequency

overestimation (positive value) since it is within the noise level, and thus the uncertainty, associated with the frequency measurements.

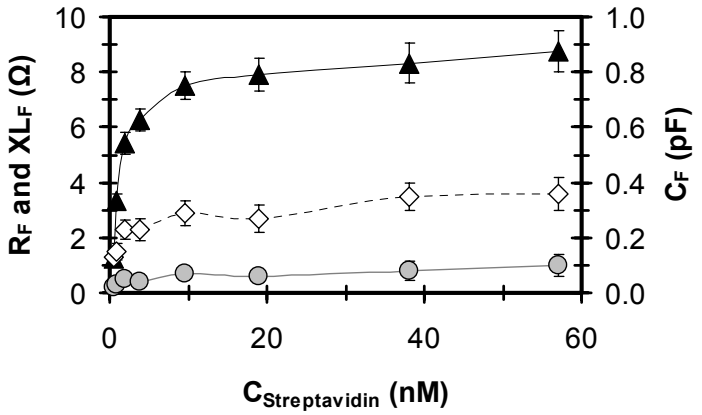

Figure 5.3. Impedance measurements for each streptavidin concentration. The (▲) inductance XL_F , (●), resistance R_F and (◊) parallel capacitance C_F contribution of streptavidin film to the BVD equivalent circuit, for each tested concentration.

Information concerning charge interferences is given by the parallel capacitance C_F, which results in desorption-like signals of 8.0±0.5 Hz/pF (Encarnação[a] *et al.*, 2007). As shown in Fig. 5.3, the maximum capacitance variation monitored during streptavidin binding was 0.36±0.06 pF resulting in an equivalent 3 Hz frequency underestimation (negative value) during frequency counting. Since viscoelastic and charge frequency interferences are additive (Encarnação[a] *et al.*, 2007), the combined viscoelastic and charge effects result in a maximum 1 Hz interference and is within the instrumental resolution of frequency counting and noise level. Hence, we can conclude from this acoustic impedance analysis that the Sauerbrey model can be used to relate frequency counting and mass quantification and therefore to quantitatively measure the amount of streptavidin as well as the streptavidin-biotin binding kinetics. Similarly to what was described for the SAM formation, upon fitting the frequency variation transients to a 1:1 binding model, the association (k_1 = (4.6±0.3) $\times 10^5$ $M^{-1}s^{-1}$) and

dissociation (k_{-1} = (0.3±5) $\times 10^{-5}$ s^{-1}) kinetic constants are estimated from the slope and the intercept of the linear relation between the reciprocal of the binding relaxation time (τ^{-1}) and streptavidin solution concentration (Fig. 5.4).

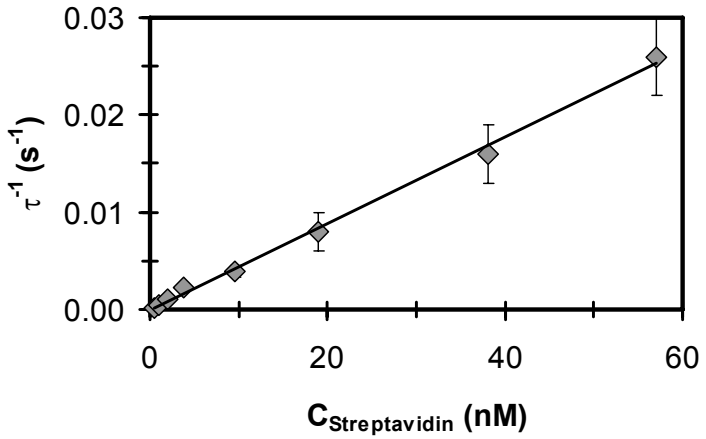

Figure 5.4. Linear dependence of the 1:1 molecular model calculated constant τ (relaxation time of binding), to the streptavidin concentrations used (0.5-57 nM). Linear regression of experimental data yielded the correlation: $\tau = (4.6\pm0.3)\times10^{5}\ M^{-1}s^{-1} \times C + (0.3\pm5)\times10^{-5}\ s^{-1}$; $r = 0.9882$; ANOVA analysis accepts linear interpolation for F statistic $p < 0.0001 < \alpha = 0.05$. Each presented data is the average result of three independent experiments.

While a good linear correlation was obtained for the variation of the reciprocal of the binding relaxation time (τ^{-1}) with the streptavidin solution concentration, which suggest the applicability of the 1:1 model, the association rate constant calculated is one order of magnitude lower as the one previously published estimated from surface plasmon resonance (SPR) data (Qureshi, *et al.*, 2001). The difference between these values can easily be explained by the fact that we verified the existence of a negative cooperativity in our biosensing system, leading to a situation where, as the sensor surface becomes more and more saturated with target molecules, available adjacent binding sites may become less exposed, leading to an apparent slower recognition process.

To verify if the calculated kinetic parameters were also influenced by other mechanisms besides negative cooperativity, further investigation was carried out. The defined aim was to determine the extent of the influence of mass transfer in the binding mechanism of streptavidin molecules to the biotin film. In order to do this, streptavidin binding experiments were performed with increasing flow rates, for it is known that in fluidic systems this can minimize the effects of mass transport phenomena (Myszka *et al.*, 1997; Myszka, 1999; Kortt *et al.*, 1997; Barak-Shinar *et al.*, 2000; Khaled and Vafai, 2004) (Fig. 5.5).

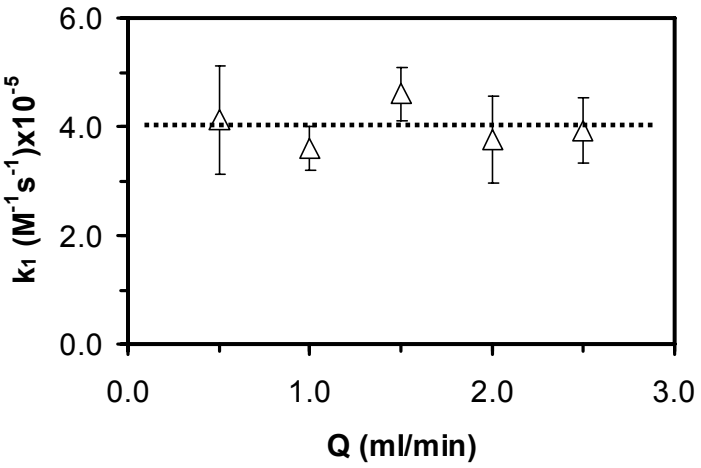

Figure 5.5. Dependence of the calculated streptavidin-biotin association kinetic constant k_1 to increasing flow rates (Q) of carrier buffer used during piezoelectric biosensing experiments.

Fig. 5.5 shows that, in fact, the association kinetic constant does not change significantly with the increase of the carrier flow rate, thus showing that, for our biosensing system, diffusional effects do not exert a relevant influence on the calculated constants. Regarding the dissociation rate constant, it was found to be smaller than the associated experimental error removing any significance from the calculated constant. This work ran into similar problems as for SPR determination (Qureshi, *et al.*, 2001) which are related to the limiting values that can be obtained for high affinity binding reactions where the desorption rate is very slow. The

dissociation rate constant, however, can be calculated from the product of the dissociation equilibrium constant given above (K_D = (5.8±0.7)×10^{-10} M) to the association rate constant, yielding k_{-1} = (2.7±0.5)×10^{-4} s^{-1}.

Table 3 compares previously published data for streptavidin/biotin binding. The high affinity is indicated by the dissociation equilibrium constant, in the nano- to pico-molar range for most cases. Table 3 evidences the high dispersion of equilibrium constant values and their dependence on the experimental conditions and methodologies. Even though diffusional and cooperativity effects may contribute to this dispersion, it is mostly due to the very slow dissociation process, which, as also experienced by us, renders the determination of dissociation rate constants from binding data difficult. Nevertheless, the first published estimation of streptavidin/biotin binding constants were based on an extrapolation from experimental association rate constants of avidin binding to biotin (Green, 1990), it is still most commonly used and referenced. Data reporting the experimental determination of streptavidin/biotin binding constants are scarce or make use of such extrapolated constants (Qureshi *et al.* 2001) On the contrary, the approach shown in this thesis enables the direct estimation of streptavidin/biotin binding constants and, to the best of our knowledge, represents the first measurement of the dissociation rate constant for the case of immobilized biotin, using a biosensing surface approach.

5.3. Conclusions

In this chapter piezoelectric sensors were used to study the process of 11-hydroxy-1-undecanothiol SAM formation and the recognition of streptavidin in aqueous medium.

By measuring simultaneously the resonant frequency variation and electroacoustic impedance of the sensors, quantitative analysis was enabled. Interfering signals from viscoelastic forces and electroacoustic coupling effects were found to be absent or negligible for the systems studied. Hence for both cases it was possible to directly use the Sauerbrey relation for the analytical quantification of the mass adsorbed at the sensor surface, essential in data analysis tools based on models that necessary require this information. The approach used enabled the estimation of both kinetic and equilibrium binding constants with possible insights into the molecular mechanisms involved. Furthermore, it was shown that alkanethiol self assembling process involves positive molecular cooperativity while, on the other hand, streptavidin binding to biotin involves negative cooperativity.

In summary, it was demonstrated that a full electroacoustic impedance analysis can significantly improve quantitative biosensing analysis with piezoelectric crystals in liquid environments. The modified equivalent circuit approach proposed can be further extended to the study of biomolecules with particular properties and even to potentially identify other surface molecular phenomena that can affect the response of piezoelectric sensors. This procedure can then easily be used in the study of affinity interactions, to identify interaction mechanisms, and/or to estimate equilibrium constants with a higher level of accuracy and confidence. This methodology thus potentially contributes to the future applicability of quartz crystal sensors in quantitative procedures, like the evaluation of affinity pairs for separation applications, the detection and quantification of molecules present in solution as a stand-alone analytical instrumentation and as a molecular screening technique in processes.

Chapter 6

Piezoimmunosensors based on recombinant single-chain and single domain antibodies for detection of HIV1 virion infectivity factor

In this chapter single chain (scFv), single domain and camelized single domain recombinant antibodies generated against HIV1 virion infectivity factor (Vif), were used to develop piezoimmunosensors for HIV1 recognition. Mixed self assembled monolayers were generated at the surface of gold coated crystal sensors to which the antibodies were immobilized. Impedance analysis was used to discriminate interfering signals from frequency variation data. The elimination of interfering signals enabled the quantification of the amount of antibody immobilized and also identified some flexibility of immobilized scFvs. All immobilized antibodies were able to specifically recognize HIV1 Vif in liquid samples. The results indicate that lower sensitivities are obtained with single domain antibodies possibly due to their higher hydrophobic character. The sensitivity obtained when using scFvs is reestablished when camelized single domains were used. The camelized single domain

piezoimunosensors were effective in recognizing HIV1 Vif from protein mixtures and from cell extracts of human embryonic kidney cells expressing HIV1 Vif.

Impedance analysis enabled the quantitative use of the piezoelectric immunosensors to estimate antigen binding and equilibrium constants. In spite of the possible limitation regarding mass transport and other related molecular phenomena, which were not considered in the binding model used, this work demonstrates the usefulness of piezoelectric biosensors in biorecognition analysis and evidences the advantages of using simultaneous impedance analysis to bring analytical significance to measured data, and thus to improve piezoelectric sensors sensitivity and applicability. The results presented in this chapter demonstrate the potential applicability of the developed piezoimmunosensors to monitor HIV1 infection evolution.

6.1. HIV1-Vif and anti-Vif recombinant antibodies

The target analyte is the HIV1 virion infectivity factor (Vif), a ~23 kDa phosphorilated protein localized in the cytoplasm of HIV1 infected cells and essential for HIV1 replication and spread in peripheral blood lymphocytes, primary macrophages, as well as in T-cell lines (Silva *et al.*, 2004). HIV1 Vif enhances infectivity of virus particles by inhibiting intracellular antiviral defenses apparently by inducing the degradation of the anti-retroviral cellular factor APOBEC3G (Gonçalves and Santa-Marta, 2004). 7 to 20 Vif molecules are incorporated into each HIV1 virion (Camaur and Trono, 1996) and thus its detection and the monitoring of its variation in infected cells may be used to follow-up HIV1 infection. HIV1 Vif and anti-Vif scFv 4BL, single domain VH and camelized single domain VHD are depicted in Fig. 6.1.

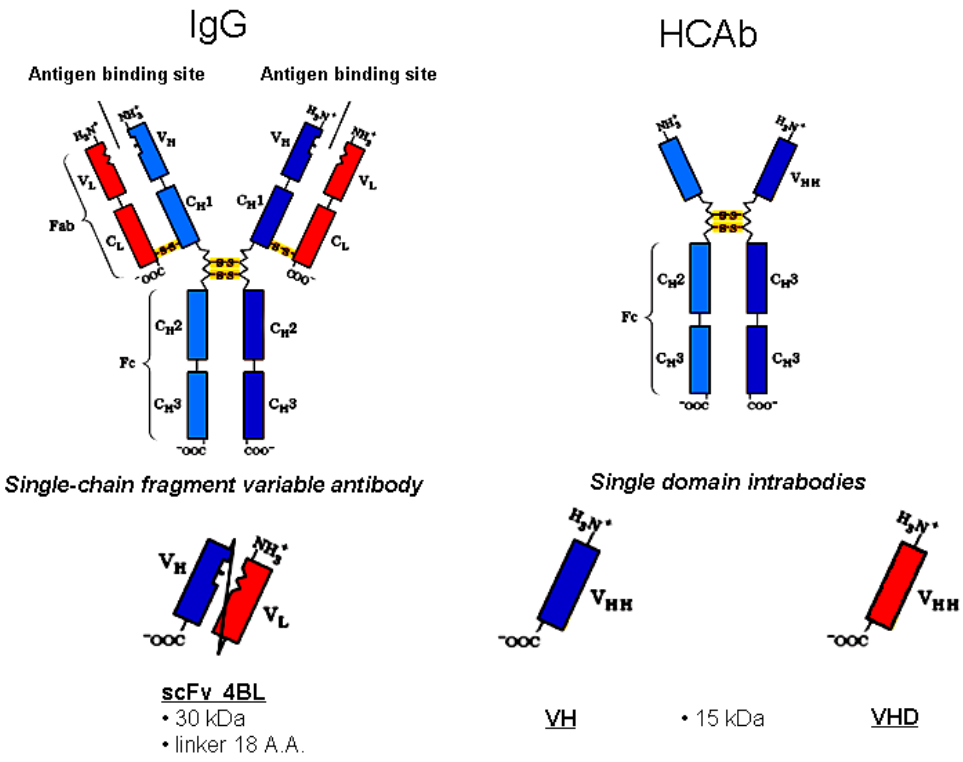

Figure 6.1. Representation of the antibodies 4BL, VH and VHD produced to develop the piezoimmunosensor. IgG- Immunoglobulin G; HCAb- Humanized Chimeric Antibody. Adapted from Gonçalves *et al.*, 2002 and da-Silva *et al.*, 2004.

6.2. Immobilization of antibodies

Owing to their small size and homogeneity, recombinant antibodies can be coupled at high density and order onto the sensor surface, therefore reducing the possibility of unspecific adsorption and trapping of contaminant molecules and thus enhancing the capacity of the sensor to recognize the target molecule (Shen *et al.*, 2005).

Quartz crystals activated with the mixed DSU/HTU SAMs were assembled onto the sensor flow cell and the experimental setup was used to follow the immobilization of the antibodies. PBS solutions with increasing concentrations (50×10^{-6} to 200×10^{-6} g/ml) of each antibody,

4BL, VH, and VHD were recirculated over the activated sensors and the resonance frequency variation over time was monitored (Fig. 6.2A-C).

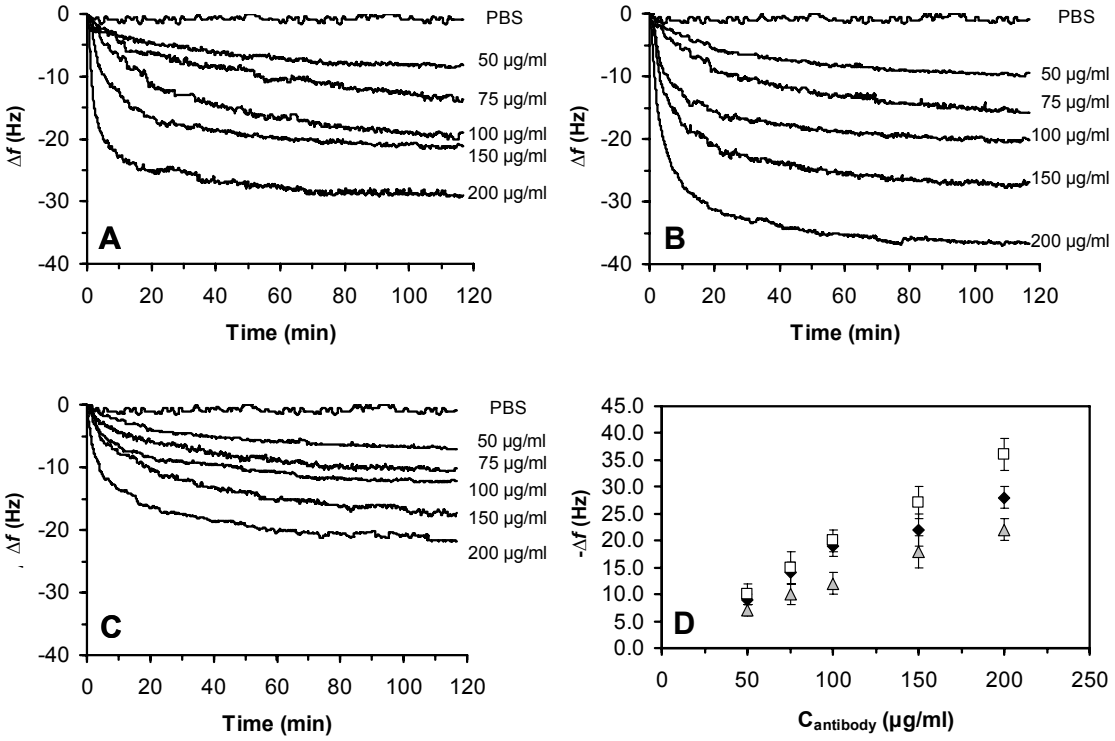

Figure 6.2. Immobilization of the recombinant antibodies on the surface of activated sensors. Measured resonance frequency variation during antibody immobilization using solutions of increasing concentration of (A) anti-Vif ScFv 4BL, (B) anti-Vif VH single domain, and (C) anti-Vif VHD camelized single domain; (D) immobilization isotherms of 4BL, VH, and VHD.

As shown in Fig. 6.2D, no saturation of the sensor was achieved within the concentrations evaluated and the immobilization of the antibodies followed a linear isotherm. The amount of antibody immobilized in each experiment can be estimated from the total frequency variation provided that the Sauerbrey relation is valid. However, as mentioned earlier, measurements of resonance frequency variation in quartz crystal resonators are known to be affected by viscoelastic effects, both from solution and adsorbed films (Etchenique and Weisz, 1999; Lucklum and Hauptmann, 2000; Kanazawa and Gordon, 1985; Martin *et al.*, 1991), as well as

by the presence of electrolytes and local charge variations (Etchenique and Buhse, 2000; Ghafouri and Thompson, 2001; Encarnação[a] *et al.*, 2007)- Chapter 4. These interferences limit the use of quartz crystal sensors for analytical detection and quantification of biological materials mass in liquid phase. Acoustic impedance analysis of the resonator enables the isolation and quantification of such interfering signals.

As previously published (Encarnação[a] *et al.*, 2007), the measured frequency variation (Δf_T) is the total of the contributions of mass loading (Δf_M), viscoelasticity (Δf_V), and charge interference (Δf_C): $\Delta f_T = \Delta f_M + \Delta f_V + \Delta f_C$. The use of experimental correlations to quantify Δf_V (Martin *et al.*, 1991) and Δf_C (Encarnação[a] *et al.*, 2007), translated to $\Delta f_V = 2.4 \times \Delta R$ and $\Delta f_C = 8 \times 10^{12}$ Hz/pF$\times \Delta C_0$ for the sensors used in this study, respectively, enabling the elimination of interfering signals from experimental data and thus the quantification of adsorbed mass through the application of the Sauerbrey relation to mass loading contribution (Δf_M). To do so, acoustic impedance analysis and equivalent electrical circuit modeling were used to study the immobilization of the antibodies (Fig. 6.3 and Fig. 6.4).

As expected, the resonator inductance increased upon antibody immobilization as an indication of mass deposition at the sensor surface (Fig. 6.3, up row). Viscoelastic (Martin *et al.*, 1991) and charge interferences (Encarnação[a] *et al.*, 2007) are identified by variations of the resonator resistance and capacitance, respectively.No variation in the parallel capacitance was observed for all immobilized antibodies within the concentration range investigated (Fig. 6.3, bottom row), which indicates that charge interferences are negligible. On the other hand, the resonator resistive component was found unchanged for VH and VHD antibodies for all tested antibody concentrations (Fig. 6.3, middle row and Fig. 6.4). This indicates that, for these cases, the immobilized antibodies behave as a rigid film and its amount can thus be analytically quantified from frequency variation data through the Sauerbrey relation.

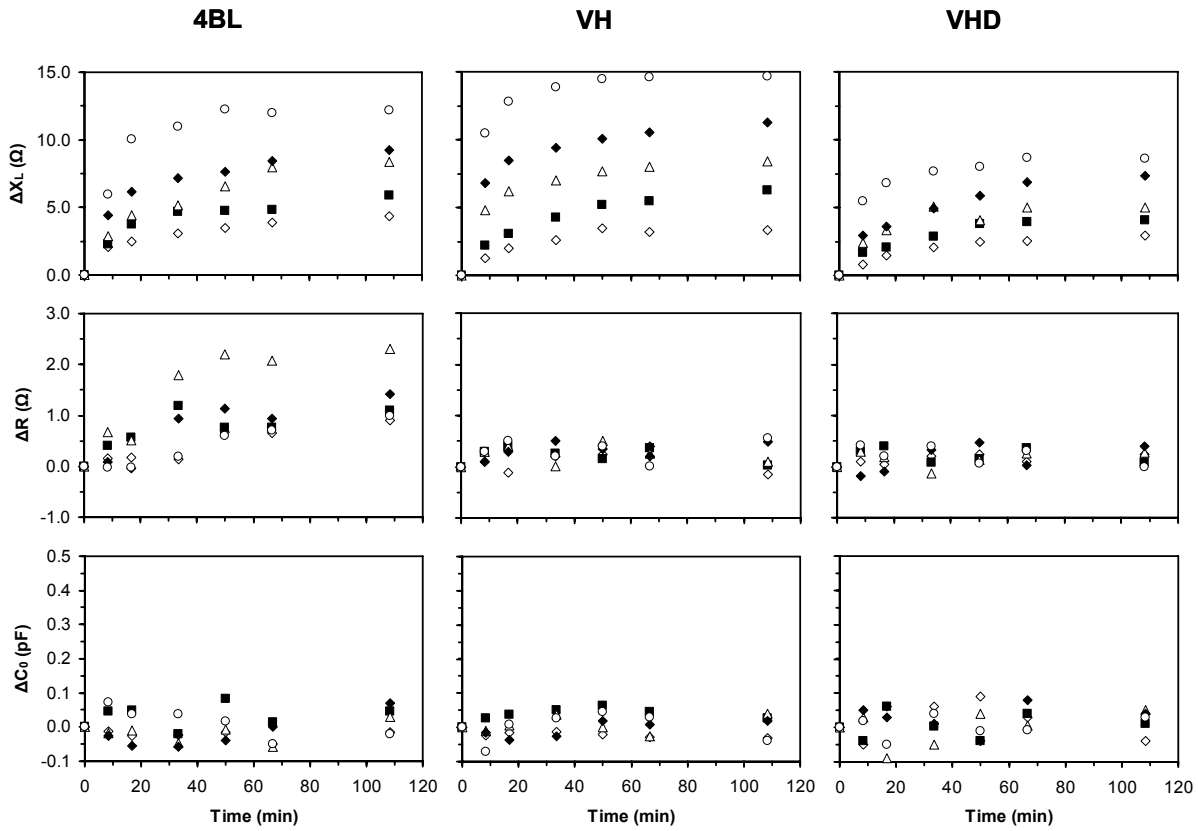

Figure 6.3. Variation of BVD parameters during antibody immobilization at 50 µg/ml (◊),75 µg/ml (■),100 µg/ml (Δ), 150 µg/ml (♦), and 200 µg/ml (○).

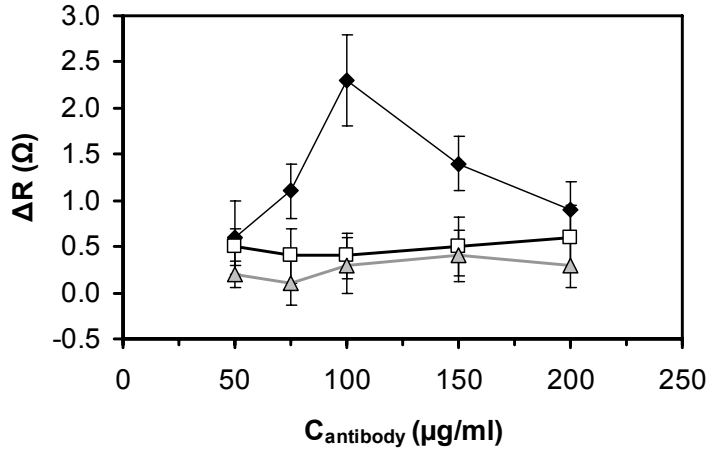

Figure 6.4. Total variation of the resonator resistance obtained after at the equilibrium for immobilization of (♦) 4BL, (□) VH and (▲) VHD.

In the cases where the scFV 4BL antibody was immobilized a different conclusion is taken from the measured data. As shown in Fig. 6.4, the resonator is characterized by variations of the resistive component with an antibody concentration dependency. Viscoelastic interference cannot be neglected and its contribution to the total frequency shift has to be accounted for if the quantification of immobilized antibody is aimed. The different behavior of immobilized 4BL can be explained considering its structural differences as compared with VH and VHD. Since 4BL contains two domains attached by a linker, we hypothesize that immobilized 4BL has some flexibility which results in acoustic energy losses, thus in viscoelastic interferences, as indicated by increasing resistance variations (Fig. 6.4). As the surface density of immobilized antibody increases, higher packaging is achieved resulting in a stereochemical induced rigidity as indicated by the decrease of the resonator resistive component observed after a given antibody concentration (Fig. 6.4).

Considering the linear antibody isotherm immobilization (Fig. 6.2D) it was decided to use 200 μg/ml to functionalize the activated sensors. For this antibody concentration, after eliminating interfering signals, the antibody surface density was analytically quantified to be 462±40 ng.cm^{-2}, 615±50 ng.cm^{-2}, and 377±40 ng.cm^{-2} for 4BL, VH and VHD, respectively.

6.4. Selective detection of HIV1 Vif

The performance of antibody functionalized sensors to detect the target antigen (Vif) was evaluated. PBS buffer was recirculated over the sensor surface and, upon stabilization of the measured frequency signal, increasing concentrations of Vif were applied and the sensor resonance frequency was monitored over time until the equilibrium was reached (Fig. 6.5).

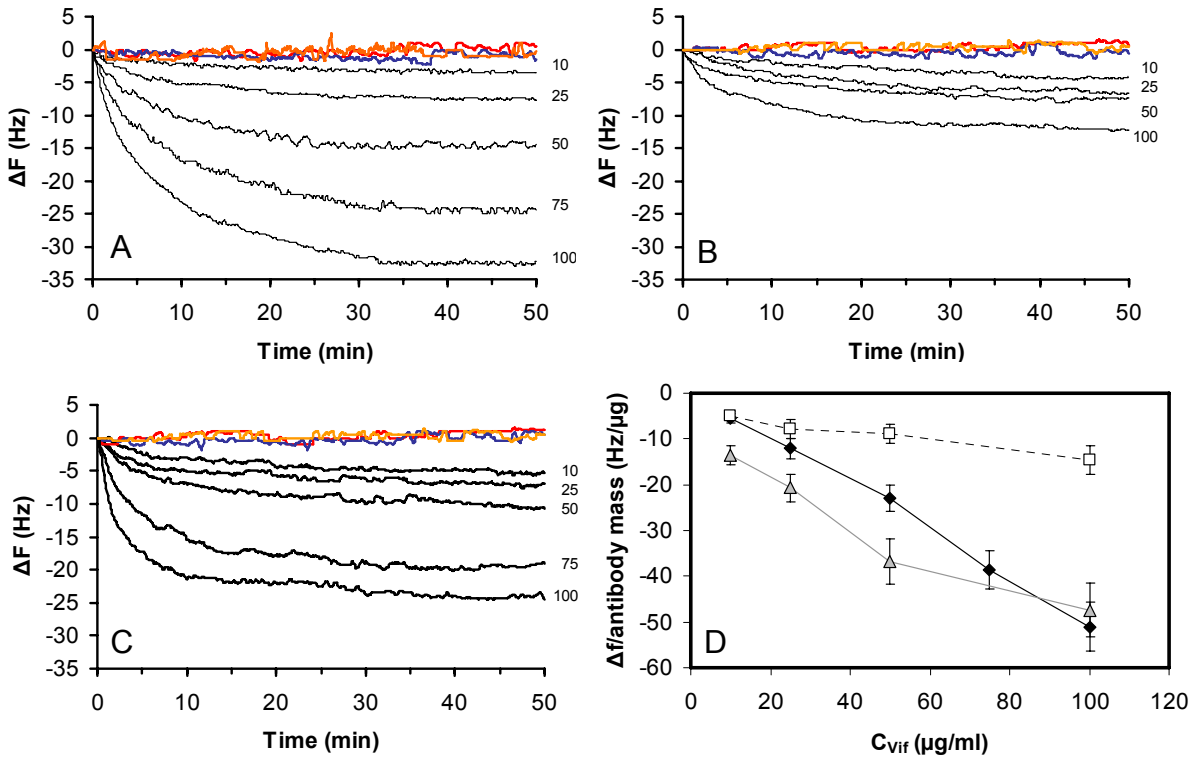

Figure 6.5. Binding of HIV1 Vif preparations of increasing concentrations (values next to each curve with units µg/ml) to sensors modified with (A) anti-Vif scFV 4BL, (B) anti-Vif single domain antibody VH, and (C) anti-Vif camelized single domain antibody 4BL; (D) specific equilibrium frequency signal for each antibody concentration (♦) 4BL, (□) VH, (▲) VHD. The data presented correspond to average transients from 6 independent measurements for each Vif concentration. Indicated concentrations refer to total protein quantification in purified HIV1 Vif preparations and not to HIV1 Vif monomeric isoforms. Cytochrom C (—), BSA (—), and Ribonuclease A (—), all at a concentration of 100 µg/ml, were used as controls.

To evaluate the selectivity to the target antigen, the sensors were challenged with protein solutions without Vif. As shown in Fig. 6.5, no frequency variation is observed when 100 µg/ml cytochrome C, BSA, or ribonuclease A are applied. Unspecific binding of Vif to the mixed SAM monolayer was also evaluated using activated sensors with no immobilized antibodies, in which case no frequency variations were monitored. Taken together these

controls demonstrate the selectivity of immobilized biofilms of 4BL, VH and VHD to detect Vif.

Fig. 6.5 also reveals that 4BL, VH and VHD modified sensors detect the target antigen differently. While similar frequency variations are obtained for 4BL (Fig. 6.5A) and VHD (Fig. 6.5C) biofilms, approximately half the signal is achieved with single domain VH biofilms (Fig. 6.5B) under similar conditions. The apparent contradiction with the calculated immobilized antibody surface density can be explained considering the hydrophobic properties of this antibody. The grand average of hydropathicity (GRAVY) is a factor used to measure the tendency of proteins to seek an aqueous or a hydrophobic environment, negative or positive values, respectively (Kyte and Doolittle, 1982). A bioinformatics analysis of the recombinant antibodies sequences (ProtParam at www.expasy.org) calculate GRAVYs as -0.113, -0.247, and -0.214, for VH, VHD and 4BL anti-Vif antibodies, respectively.

Therefore, it can be hypothesized that the higher hydrophobicity of VH molecules results in a surface conformation where the antibody binding residues are oriented in such a way that they become closer to the hydrophobic aliphatic chains of the SAMs. As such, VH binding sites are hindered and less antigen binds to the biofilm. On the other hand, when using VHD single domains, which are derived from VH single domains by protein engineering (Silva *et al.*, 2004) resulting in a ~2.2 fold increase of the hydrophilicity as indicated by the hydropathicity factor, higher frequency variation signals are obtained that, in addition to the surface density data, indicates that more antigen binding sites are exposed.

The data obtained for the selective detection of HIV1 Vif is consistent with qualitative Elisa analysis (Silva *et al.*, 2004). As shown in Fig. 6.5D, the measured signal for QCM sensors modified with VH single domains is considerably lower (< 3 fold) then the one measured with anti-Vif 4BL scFv modified sensors. Furthermore, the signal obtained with single domain

antibodies is considerably improved when using the camelized VHD single domain in which case signals of similar order of magnitude as 4BL scFv are measured.

6.5. Kinetic analysis of antigen recognition

A 1:1 binding model (Equations 21 and 22) was used to estimate the binding rates of HIV1-Vif to the modified immunosensors, where θ is the relative amount of antibody-Vif complex (*i.e.* surface coverage), C is the initial Vif concentration, and k_1 and k_{-1} are the association and dissociation rate constants, respectively. The rate constants k_1 and k_{-1} can be calculated from the sensor data whenever θ is proportional to the measured frequency variation. As mentioned earlier, the Sauerbrey relation provides such proportionality, provided that the validity of the assumptions of the Sauerbrey relation is guaranteed. As before, such, interfering signals resulting from the viscoelasticity of the films attached to the sensor and to the aqueous environment, as well as from electroacoustic coupling owing to local charge variations, must be eliminated.

Impedance analysis was performed, as before, in order to identify and eliminate interfering signals. As shown in Fig. 6.6, the change of damping resistance owing to viscoelastic effects is negligible ($\Delta R \sim 0$) in all cases. Together with the increase of the inductive component (ΔXL), these results demonstrate that Vif is recognized and binds to the modified sensors, resulting in biofilms exhibiting a rigid behavior.

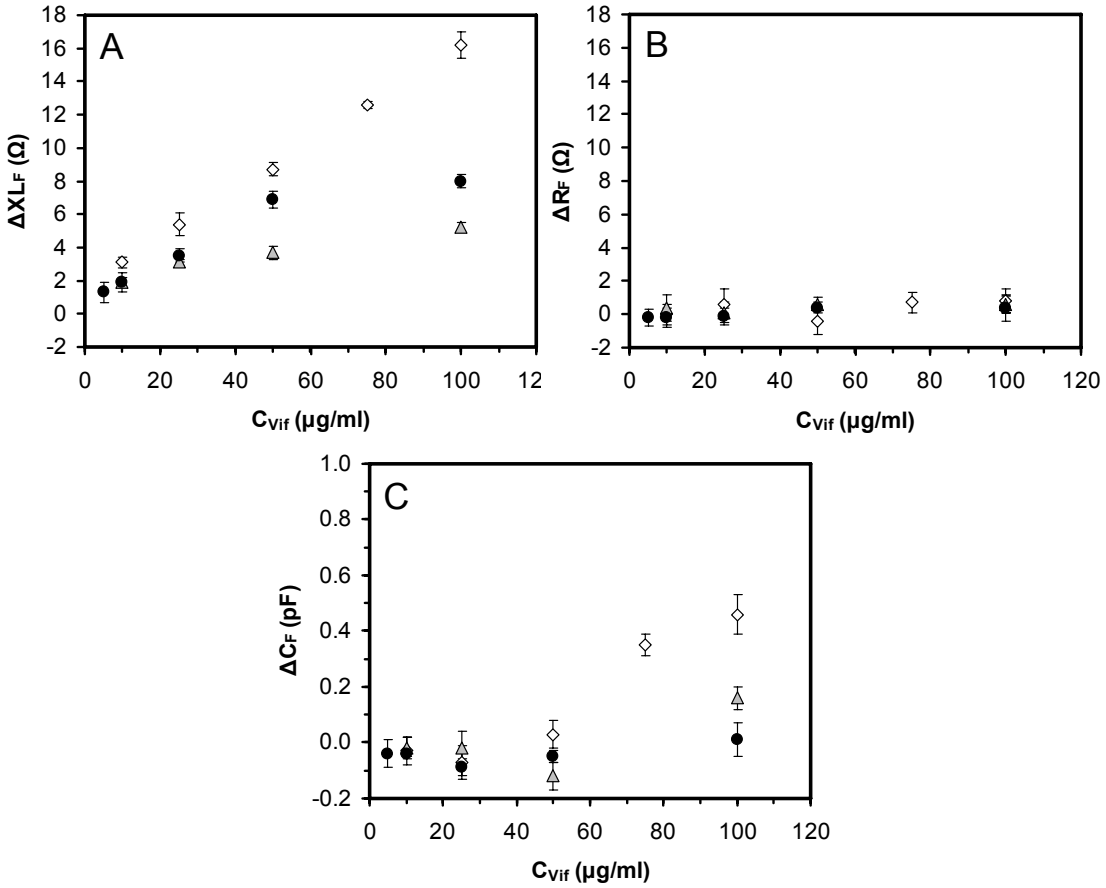

Figure 6.6 Figures A (Δ*XL*), B (Δ*R*), and C (Δ*C*) present the variation of the Butterworth van Dyke model parameters, relatively to the response of the three immunosensors (◊) 4BL, (▲) VH and (●) VHD to different concentrations of Vif. Each presented data is the average result of six independent experiments.

Electroacoustic interferences were also found to be negligible for the majority of the cases. However, for the highest Vif concentrations evaluated for the 4BL and VH modified sensors, as much as 16% of the measured frequency variation signal corresponds to electroacoustic interferences (Fig. 6.6C).

The impedance analysis data was used to correct the measured frequency data variation in order to eliminate interfering signals (Fig. 6.7).

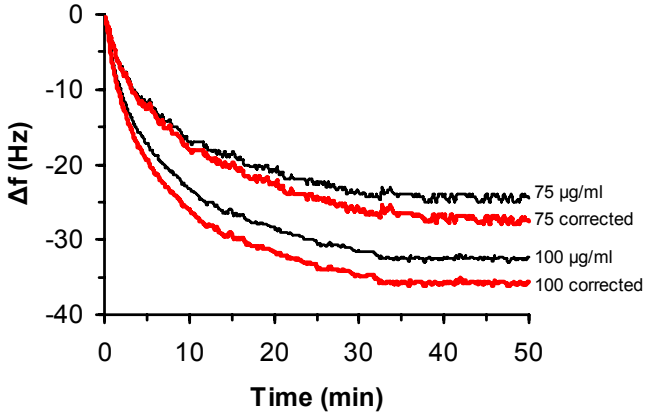

Figure 6.7. Corrected frequency transients for the binding of HIV1 Vif to 4BL biofilms.

Corrected frequency variation is related to the sensor surface coverage (θ) and thus the relaxation time of binding (τ) can be estimated for each Vif concentration by non-linear fitting of Equation 22 to frequency variation transients. According to the binding model proposed the binding rate constants, k_1 and k_{-1} are obtained, respectively, from the slope and intercept of the linear relation of the reciprocal of the relaxation time (τ^{-1}) versus Vif concentration (Fig. 6.8).

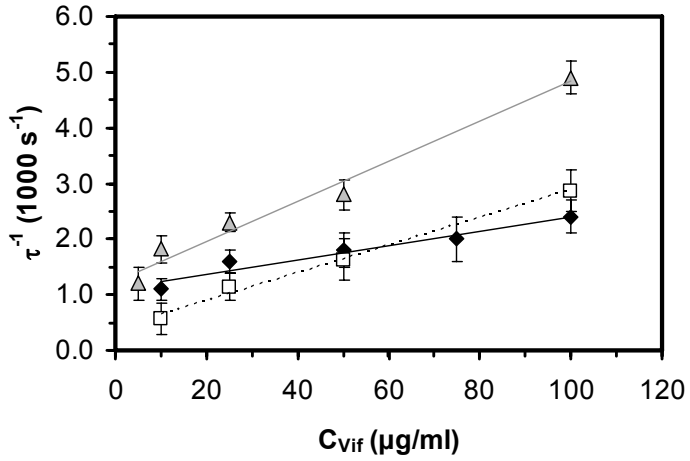

Figure 6.8. Linear dependence of the 1:1 molecular model calculated constant τ^{-1}, to the bulk Vif concentrations used for each immunosensor: (♦) 4BL, (□) VH and (▲) VHD. Linear regression of experimental data yielded the correlations: $\tau^{-1} = (1.3\pm0.2)\times10^{-5}\times C + (1.1\pm0.1)\times10^{-3}$; $r = 0.9697$; $p = 0.0063$, for 4BL; $\tau^{-1} = (2.5\pm0.2)\times10^{-5}\times C + (0.4\pm0.09)\times10^{-3}$; $r = 0.9963$; $p = 0.0037$, for VH; $\tau^{-1} = (3.6\pm0.3)\times10^{-5}\times C + (1.2\pm0.2)\times10^{-3}$; $r = 0.9885$; $p = 0.0015$, for VHD. Each presented data is the average result of six independent experiments.

The values of the rate constants are summarized in Table 4 together with the dissociation equilibrium constant ($K_D = k_{-1}/k_1$).

Table 4. Rate and equilibrium constants for the binding of Vif to immobilized recombinant antibodies.

Antibody	k_1 ($M^{-1}.s^{-1}$)	k_{-1} (s^{-1}) × 10^3	K_D (M) × 10^6
4BL	305 ± 47	1.1 ± 0.1	3.6 ± 0.8
VH	587 ± 47	0.41 ± 0.09	0.7 ± 0.2
VHD	845 ± 70	1.2 ± 0.2	1.5 ± 0.4

Even tough the dissociation rate constants are of a similar order of magnitude as other affinity partners using scFvs and single domain antibodies (Pribyl *et al.*, 2003; Hengerer *et al.* 1999), surprisingly the association rate constants for the antibodies studied was found to be ~3 orders of magnitude less. In conjunction with the low equilibrium constant (K_D), in the micro-molar range as compared to the nano-molar range described with other affinity pairs using recombinant antibodies (Hengerer *et al.*, 1999), these results suggest that anti-Vif 4BL scFv, VH and VHD single domains, although selective, are not strong binders to Vif. We also hypothesize that other factors, which are intrinsic to the system used, such as steric hindrance and mass transfer effects, may also contribute to the low calculated kinetic and equilibrium constants. Unfortunately, there is a lack of published quantitative affinity data for the antibodies used in this study and, therefore, no definitive conclusion regarding the origins of the low kinetic constants obtained can be drawn at this moment.

6.6. Detection of HIV1 Vif in complex mixtures

The data presented shows that piezoelectric sensors modified with anti-HIV1 Vif 4BL scFv, VH single domain, and with VHD camelized single domains are able to selectively recognize HIV1 Vif in solution. The detection of target analyte in complex mixtures constitutes a step forward towards the eventual applicability of HIV1 Vif immunosensors to real-life situations such as in the follow-up of HIV1 clearance during anti-retroviral therapy. In order to evaluate the ability of the piezoimmunensors developed in this study, to detect intracellular HIV1-Vif, human embryonic kidney cells (HEK293T) were transfected with an expression vector encoding HIV1-Vif (VifpAmCyan1-N1). This expression vector was obtained by cloning HIV1 Vif amplified from the pD10Vif, the bacterial expression vector used to produce the protein, into pAmCyan1-N1 expression vector. This results in a fusion protein in which HIV1 Vif is N-terminally fused to the cyan fluorescent protein (CFP). HIV1 Vif expression can thus be easily monitored by visualizing CFP fluorescence. Two controls were established: (i) HEK293T cell cultures with no expression vector were used as control for protein expression; (ii) HEK293T cell cultures expressing CFP, therefore which were transfected with the vector pAmCyan-N1, were used as control for CFP unspecific adsorption to the piezoimmunosensor.

Due to its performance the anti-HIV1 Vif VHD camelized single domain modified sensor was selected challenged with a mixture of pure proteins and with cellular extracts obtained from HIV1 Vif producing animal cell cultures (Fig. 6.9).

A 50 ug/ml HIV1-Vif preparation spike to a mixture of BSA, cytochrome C and ribonuclease results in a frequency variation of ~23 Hz (Fig. 6.9A), which constitutes a further evidence of the sensor selectivity. Going further in increasing the analyte complexity, a ~10 Hz frequency variation was measured when the sensor was challenged with cell extracts obtained from

control cells cultures (Fig. 6.9B). Although this might reveal eventual unspecific binding of components from such complex mixture, impedance analysis shows a major signal contribution (up to 7 Hz) from viscoelastic interferences.

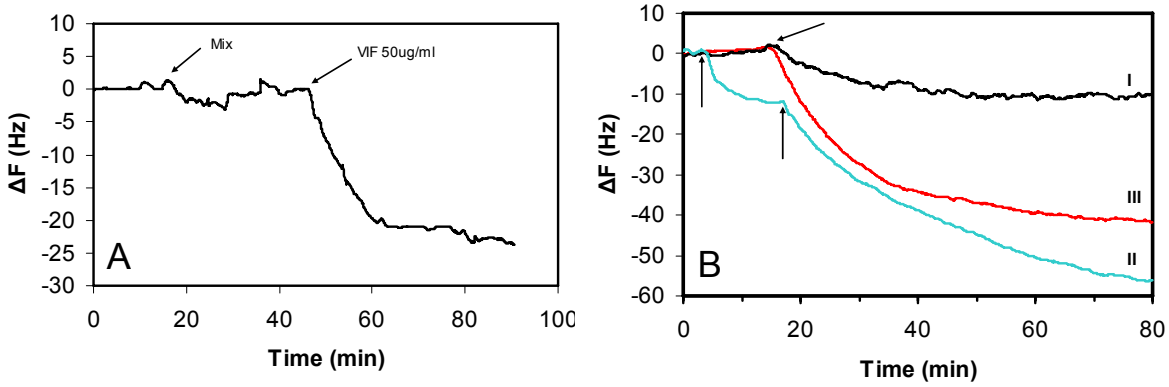

Figure 6.9. Detection of HIV1 Vif in complex mixtures with VHD camelized single domain antibody piezoimmunosensors. Arrows indicate the moment of sample application to the sensor. (A) A mixture of 100 µg/ml BSA, Cytochrom C, and Ribonuclease A was added to the crystal and the frequency was monitored for a period of time before spiking with 50 µg/ml HIV1 Vif preparation; (B) sensor response obtained for cell extracts: HEK293 cell extracts from the control cell cultures (cells only expressing CFP) were applied to the sensor (curve I) and spiked with 50 µg/ml HIV1 Vif preparation (curve II); curve III shows the sensor response for cell extracts obtained from HEK293T cell cultures expressing HIV1 Vif.

A spike of HIV1 Vif preparation (Fig. 6.9B), as before, results in a ~5 fold increase of the measured frequency variation as the protein is specifically recognized and binds to the anti-HIV1 Vif VHD single domain immunosensor. Fig. 6.9B also shows that the anti-HIV1 Vif immunosensor developed in this work detects the presence of HIV Vif in cell extracts from cell cultures expressing this protein intracellularly. Considering the fact that cells expressing intracellularly HIV1 Vif were used to mimic HIV1 infected cells, the ~4 fold increase in the measured frequency variation, as compared to the control cell extracts, is an additional

evidence of the immunosensor's selectivity and of its ability to recognize HIV1 Vif in complex cellular mixtures, therefore rendering its use as HIV1 sensor possible.

6.7. Conclusions

This chapter described the work directed to develop a new detection tool for the HIV1 virus. Piezoelectric immunosensors based on scFvs and single domain recombinant antibodies were developed to recognize HIV1 virion infectivity factor (Vif). All modified sensors were able to selectively recognize HIV1 Vif. The sensors were stable and antigen specific even when using complex protein mixtures.

Quantitative analysis was possible by simultaneously measuring both the sensors resonant frequency variation and acoustic impedance. Interfering signals from viscoelastic forces and electroacoustic coupling effects were identified and quantified. Frequency variation data were corrected accordingly in order to enable the use of the Sauerbrey relation for the analytical quantification of the mass adsorbed at the sensor surface. An additional advantage of acoustic impedance analysis is that, to some extent, structural aspects of the immobilized antibodies can be derived. In particular, insights were taken regarding the molecule-to-surface orientation and alterations of the molecular conformation upon antigen recognition and binding. This approach increases the usefulness of piezoimmunosensors rendering possible its use for quantitative analysis and detection of target antigens, kinetic parameters, and equilibrium constants.

This study showed that HIV1-Vif recognition by modified sensors with anti-Vif 4BL scFv, VH single domain, and VHD camelized single domain, can be modeled by a 1:1 binding

model from which kinetic and equilibrium constants were calculated. Even though the low calculated kinetic constants suggest that the antibodies studied are poor binders to HIV1 Vif, no final and definitive conclusion can be taken yet. Other phenomena such as mass transfer, steric hindrance and sensor sensitivity may also contribute to such low constants. Nevertheless, the study presented in this thesis provides a valuable insight into Vif molecular recognition by anti-Vif ScFv 4BL, VH and VHD single domains with impact in ongoing research focused on the use of these recombinant antibodies as intrabodies for the functional neutralization of the Vif protein as a strategy to strongly neutralize HIV1 infectivity. Furthermore, this chapter demonstrates the applicability of piezoelectric sensors in biorecognition analysis and evidences its potential as a quantitative biosensor. Using the methodology described and the VHD camelized anti-HIV1 Vif single domain antibodies, a piezoimmunosensor was developed and proven to be effective in the detection of HIV1 Vif in human cell extracts.

Chapter 7

Concluding remarks

This thesis deals with the application of piezoelectric sensors, namely quartz crystal microbalances (QCM), for the study of molecular interactions and for the development of biosensing systems for biomedical purposes. A major aspect is the expansion of the physical understanding of the behavior of these kinds of sensors in liquid medium and also how organic or biological layers can affect the results and its interpretation.

In this work, it was shown how to evaluate the performance of quartz crystal microbalances with two different measuring systems: the frequency counter and the network analyzer. Also some instrumental key steps were established that are crucial for the proper development and use of QCM sensors:

i. The electrochemical cleaning procedure using a potentiostat, ensures not only the cleanness of the crystals, but also its durability, representing a good alternative for the use of piranha solution in the removal of thiol based SAMs;

ii. All QCM experiments must be conducted with a stable and controlled temperature (± 0.1ºC), to avoid artifacts in the transduced signals;

iii. In liquid operations, the evaporation of the solvent must be avoided at all costs, and so the QCM must preferably be assembled in a flow cell connected to a closed flow circuit;

iv. All the liquids used must be degassed to prevent anomalous frequency shifts;

v. Any kind of mechanical interference source coupled to the QCM system must be eliminated, *i.e.* pressure changes;

vi. When conducting an experiment in liquid medium, the salt concentration of both the injected sample and the solvent must be similar to avoid anomalous frequency shifts.

This thesis shows that the response of QCM is affected by the presence of electrolytes or other charged species in solution. This interference leads to transients mimicking surface desorption, with frequency variations (Δf) decreasing with increasing densities of charges in solution, and can thus have a considerable impact in biosensor applications. A modification to the Butterworth–Van Dyke model was proposed that includes additional parallel capacitances to account for the influence of charges to the sensors response. Such influence is linearly correlated to the measured resonance frequency variation in the range of 1 mM $\leq I \leq$ 50 mM and is characterized by a desorption-like signal of 8.0±0.5 Hz/pF. The use of this factor allows for the correction of the mass-frequency variation, which otherwise is significantly underestimated, resulting in a convergence of the values measured by frequency counting and impedance analysis. Estimating the influence of electrolytes and their contribution to the measured frequency variation thus enables the acquisition of more accurate data and this

represents a step forward in the use of piezoelectric sensors for quantitative direct transduction of molecular recognition events.

By simultaneously measuring the resonant frequency variation and electroacoustic impedance of the sensors, quantitative analysis is enabled. Therefore it is possible to directly use the Sauerbrey relation for the analytical quantification of the mass adsorbed at the sensor surface. This approach enables the use of piezoelectric biosensors for the estimation of both kinetic and equilibrium binding constants with possible insights into the molecular mechanisms involved.

Considering the potentialities of the system, it was tested by studying the process of 11-hydroxy-1-undecanothiol SAM formation and the recognition of streptavidin in aqueous medium. The kinetic and rate constants for both processes were estimated with the QCM data and it was also shown that the alkanethiol self assembling process involves positive molecular cooperativity while, on the other hand, streptavidin binding to biotin involves negative cooperativity.

Finally this thesis describes how the established 5 MHz QCM system was used to develop a new detection tool for the HIV1 virus. Piezoelectric immunosensors based on scFvs and single domain recombinant antibodies were developed to recognize HIV1 virion infectivity factor (Vif). All modified sensors were able to selectively recognize HIV1 Vif. The sensors were stable and antigen specific even when using complex protein mixtures.

This study showed that HIV1-Vif recognition by modified sensors with anti-Vif 4BL scFv, VH single domain, and VHD camelized single domain, can be modeled by a 1:1 binding model from which kinetic and equilibrium constants were estimated. This is a major contribution to the ongoing research focused on the use of these recombinant antibodies as

intrabodies for the functional neutralization of the Vif protein as a therapeutic strategy to strongly neutralize HIV1 infectivity.

Using the methodology described and the VHD camelized anti-HIV1 Vif single domain antibodies, a piezoimmunosensor was developed and proven to be effective in the detection of HIV1 Vif in human cell extracts.

In summary, it was demonstrated that a full electroacoustic impedance analysis can significantly improve quantitative biosensing analysis with piezoelectric crystals in liquid environments. Quantitative analysis is possible by simultaneously measuring both the sensors resonant frequency variation and acoustic impedance. Interfering signals from viscoelastic forces and electroacoustic coupling effects can be identified and quantified. Frequency variation data can be corrected accordingly in order to enable the use of the Sauerbrey relation for the analytical quantification of the mass adsorbed at the sensor surface. Thus, the approach proposed can be further extended to the study of affinity interactions, to identify interaction mechanisms, and/or to estimate equilibrium constants with a higher level of accuracy and confidence. This sensing methodology thus presents a high potential for the evaluation of affinity pairs for separation applications, for the detection and quantification of molecules present in solution possibly associated with other instrumental apparatus (like chromatographic columns) or even as a stand-alone analytical instrumentation and/or as a contaminant screening technique in processes.

Chapter 8

Future work…

This thesis opens a series of possibilities concerning the development of piezoelectric biosensing tools.

Ongoing work includes efforts to efficiently detect the hybridization of unlabelled oligonucleotides and the detection of single-nucleotide polymorphisms (SNPs). To do this, a novel biosensing platform is being investigated, based on an impedance assisted electrochemical quartz crystal microbalance (IEQCM) system, where both piezoelectric and electrochemical detections are made in real time and in continuous flow.

This approach is of the same basic nature as electrochemical impedance spectroscopy (EIS) with the difference that our system is focused on the interpretation of an equivalent circuit at a specific region of high frequencies (defined by the resonance of the crystals) instead of a wide region of low frequencies.

The present thesis was completely based on a 5 MHz QCM system, but currently efforts are being made to develop a new QCM system, more sensible and also portable. The core crystals

of the new system are smaller and have a fundamental resonance frequency of 10 MHz. A new fluidic system is being developed, composed of a flow cell with a working volume of only 70 µl (as compared to the 300 µl of the 5 MHz system) and a crystal based diaphragm micropump. The new temperature control system is also being miniaturized and is based on a peltier system associated with a PID controller. All transducer systems are also of reduced size, and include an oscillator, a vector network analyzer and a potentiostat.

References

Agilent Technologies, 2003. The Impedance Measurement Handbook- A Guide to Measurement Technology and Techniques. Agilent Technologies Co.Ltd.

Aizawa, H., Kurosawa, S., Tozuka, M., Park, J., Kobayashi, K., 2004. Sens. Actuators B 101, 150-154.

Atkins, P.W., 1990. Physical Chemistry, 4th ed., Oxford University Press, UK.

Auge, J., Hauptmann, P., Hartmann, J., Rösler, S., Lucklum, R., 1995. Sens. Actuators B 24, 43-48.

Auld, B.A., 1990. Acoustic Fields and Waves in Solids 1-2 (Malabar, FL: Krieger).

Bandey, H.L., Gonsalves, M., Hillman, A.R., Glide, A., Bruckenstein, S., 1996. J. Electroanal. Chem. 410, 219-227.

Ballantine, D.S., White, R.M., Martin, S.J., Ricco, A.J., Zellers, E.T., Freye, G.C., Wohltjen, H., 1997. Acoustic Wave Sensors, Academic press, San Diego.

Barak-Shinar, D., Rosenfeld, M., Zisman, E., Abboud, S., 2000. Annals Biomed. Eng. 28,

565-571.

Bechmann, R., 1952. J. Sci. Instrum. 29, 73-76.

Benes, E., Schmid, M., Kravchenko, V., 1991. J. Acoust. Soc. Am. 90, 700-706.

Bizet, K., Gabrielli C, Perrot H.,1998. Biosens. Bioelectron. 13(3-4), 259-269.

Bottom, V.E., 1982. Introduction to Quartz Crystal Unit Design, van Nostrand Reinhold, New York.

Borngraeber, R., Lucklum, R., Hauptmann, P., 2002. IEEE Trans. Ultrason. Ferroelectr. Freq. Control 49, 1254–1259.

Bouche-Pillon, D., Gabrielli, C., Perrot, H., 1995. Sens. Actuators B 25, 257-259.

Buttry, D.A., Ward, M.D., 1992. Chem. Rev. 92, 1355-1379.

Cady, W.G., 1921. Phys. Rev. 17, 531-533.

Calvo, E.J., Etchenique, R., Bartlett, P.N., Singhal, K., Santamaria, C., 1997. Faraday Discuss. 107, 141-157.

Camaur, D., Trono, D., 1996. J. Virol. 70, 6106-6111.

Cavic, B.A., Chou, F.L., Furtado, L.M., Ghafouri, S., Hayward, G.L., Mack, D.P., McGovern, M. E., Su, H., Thompson, M., 1997. Faraday Discuss. 107, 159–76.

Chagnard, C., Gilbert, P., Watkins, N., Beeler, T., Paul, D. W., 1996. Sens. Actuators B 32, 129-136.

Chang, H., Cheng, T., Wu, T., Lin, T., 2000. Sens. Actuators B 66, 296-298.

Chazenbalk, G., Kakinuma, A., Jaume, J., McLachlan, S., Rapoport, B., 1996. Endocrinology 137, 4586-4591.

Chilkoti, A., Tan, P.H., Stayton, P.S., 1995. Proc. Natl. Acad. Sci. 92, 1754–1758.

Csáki, A., Kaplanek, P., Möller, R., Fritzche W., 2003. Nanotechnology 14, 1262-1268.

Curie, P., Curie, M., 1880. Bull. Soc. Min. de France 3, 90-102.

Curie, P., 1908. Oeuvre de Pierre Curie. Gauthier-Villars, Paris.

Daikhin, L., Urbakh, M., 1997. Faraday Discuss. 107, 27–38.

Encarnação[a], J.M., Stallinga, P., Ferreira, G.N.M., 2007. Biosens. Bioelectron. 22, 1351-1358.

Encarnação[b], J.M., Rosa, L., Rodrigues, R., Pedro, L., da Silva, F.A., Gonçalves, J., Ferreira, G.N.M., 2007. J. Biotechnol. 132, 142-148.

Etchenique, R., Weisz, A.D., 1999. J. App. Physics. 4 (86), 1994-2000.

Etchenique, R., Brudny, V.L., 2000. Langmuir 16, 5064-5071.

Etchenique, R., Buhse, T., 2000. The Analyst 125, 785-787.

Etchenique, R., Buhse, T., 2002. The Analyst 127, 1347-1352.

Etchenique, R., Calvo, E.J., 1999. Electrochem. Commun. 1, 167-170.

Ewalt, K.L., Haigis, R.W., Rooney, R., Ackley, D., Krihak, M., 2001. Anal. Biochem. 289, 162–172.

Fabreguette, F.H., Sechrist, Z.A., Elam, J.W., George, S.M., 2005. Thin Solid Films. 488(1-2), 103-110.

Ferreira, G.N.M., Encarnação, J.M., Rosa, L., Rodrigues, R., Breyner, R., Barrento, S., Pedro, L., da Silva, F.A., Gonçalves, J., 2007. Biosens. Bioelectron. 23, 384-392.

Finklea, H.O., 1999. Encyclopedia of Analytical Chemistry, R.A. Meyers, John Wiley & Sons Ltd. Chichester.

Fujita, K., Silver, J., 1993. BioTechniques 14 (4), 608-617.

Ghafouri, S., Thompson, M., 2000. Electroanalysis 12(5), 326-336.

Ghafouri, S., Thompson, M., 2001. The Analyst 126, 2159-2167.

Glassford, A. P., 1978. J. Vac. Sci. Technol. 15, 1836-1843.

Gomes, M., Silva, A., Duarte, A., Oliveira, J., 1998. Sens. Actuators B 48, 383-386.

Gonçalves, J., Santa-Marta, M., 2004. Retrovirol. 1, 28.

Goncalves, J., Silva, F., Freitas-Vieira, A., Santa-Marta, M., Malhó, R., Yang, X., Gabuzda, D., Barbas, C., 2002. J. Biol. Chem. 277, 32036-32045.

Göpel, W., Hesse, J., Zemel, J.N., 1991. Sensors: A Comprehensive Survey. VCH Verlagsellschaft mbH: Weinheim, Vol 2.

Green, N., 1990. Methods Enzymol. 184, 51-67.

Ha, T.H., Kim, K., 2001. Langmuir 17, 1999-2007.

Han, A., Van Duyne, R., 2004. Rev. Mol. Diagn. 4 (4), 527-537.

Hankel, W.G., 1881. Abh. Sachs. 12, 457-458.

Hayward, G.L., Thompson, M., 1998. J. Appl. Phys. 83, 2194–201.

Hengerer, A., Kößlinger, C., Decker, J., Hauck, S., Queitsch, I., Wolf, H., Dübel, S., 1999. BioTechniques, 26, 956-964.

Herne, T., Tarlov, M., 1997. J. Am. Chem. Soc. 119, 8916-8920.

IUPAC, 1999. "Recommended Definitions and Classification" Pure Appl. Chem. 71(12), 2333-2348.

Janshoff, A., Galla, H.-J., Steinem, C., 2000. Chem. Int. Ed. 39**,** 4004-4032.

Gopel, W., Jones, T.A., Kleitz, M., Lundstrom, I., Seiyama, T., 1991. "Chemical and biochemical sensors: Part I", Sensors, A Comprehensive Survey, Vol. 2, Wiley-VCH, Weinheim.

Josse, F., Shana, Z. A., Radtke, D. E., Haworth, D.T., 1990. IEEE Transactions UFFC 37(5), 359-365.

Kanazawa, K.K., Gordon, J.G., 1985. Anal. Chim. Acta 175, 99-105.

Kanazawa, K.K., 1997. Faraday Discuss. 107, 77-90.

Karpovich, D.S., Blanchard, G.J., 1994. Langmuir 10, 3315-3322.

Kaspar, M., Stadler, H., Weiss, T., Ziegler, C., 2000. J. Anal. Chem. 366, 602-610.

Khaled, A., Vafai, K., 2004. J. Micromech. Microeng. 14, 1220–1229.

Kim, D.H., Noh, J., Hara, M., Lee, H., 2001. Bull. Korean Chem. Soc. 3 (22), 276-280.

Kim, G., Rand, A., Letcher, S., 2003. Biosens. Bioelectron. 18 (6), 91-99.

Kortt, A., Gruen, L., Oddie, G., 1997. J. Mol. Recog. 10, 148-158.

Kosinski, J.A., Pastore, R.A., 2001. IEEE Trans. Ultrason. Ferroelectr. Freq. Control 48, 1426–1437.

Kyte, J., Doolittle, R.F., 1982. J. Mol. Biol. 157, 105-132.

Lec, R.M., Lewin, P.A., 1998. IEEE Eng. Med. Biol. Soc. 6, 2779-2784.

Lec, R.M., 2001. IEEE International Frequency Control Symposium, 419-429.

Liao, S., Shnidman, Y., Ulman, A., 2000. J. Am. Chem. Soc. 122, 3688-3694.

Lin, Z., Ward, M.D., 1995. Anal. Chem. 57, 1770-1771.

Liss, M., Petersen, B., Wolf, H., Prohaska, 2002. Anal. Chem. 74, 4488-4495.

Liu, Y. Zhang, W., Yu, X., Zhang, H., Zhao, R., Shangguan, D., Li, Y., Shen, B., Liu, G., 2004. Sens. Actuators B 99, 416-426.

Lucklum, R., Behling, C., Cernosek, R.W., Martin, S.J., 1997. J. Phys. D: Appl. Phys. 30, 346-356.

Lucklum, R., Hauptmann, P., 2000. Sens. Actuators B 70, 30-36.

Lucklum, R., Hauptmann, P., 2003. Meas. Sci. Technol. 14, 1854-1864.

Martin, B.A., Hager, H.E., 1989. J. Appl. Phys. 65, 2630-2635.

Martin, S.J., Frye, G.C., Ricco, A.J., 1993. Anal. Chem. 65, 2910-2922.

Martin, S.J., Granstaff, V.E., Frye, G.C., 1991. Anal. Chem. 63, 2272-2281.

Mirmohseni, A., Alipour, A., 2002. Sens. Actuators B 84, 245-251

Modin, C., Stranne, A-L., Foss, M., Duch, M., Justesen, J., Chevallier, J., Andersen, L.K.,

Hemmersam, A.G., Pedersen, F.S., Besenbacher, F., 2006. Biomaterials 27, 1346-1354.

Muzykantov, V. R., Atochina, E. N., Gavriljuk, V., Danilov, S. M., Fisher, A. B., 1994. J. Nucl. Med. 35, 1358–1365.

Myszka, D., 1999. J. Mol. Recognit. 12, 279-284.

Myszka, D., Morton, T., Doyle, M., Chaiken, I., 1997. Biophys. Chem. 64, 127-137.

Nesbitt, W., Doyle, R., Taylor, K., Staat, R., Arnold, R., 1982. Infect. Immun. 35 (1), 157-165.

Nomura, T., Okuhara, M., 1982. Anal. Chim. Acta 142, 281-284.

Pan, W., Durning , C.J., Turro , N.J., 1996. Langmuir 12**,** 4469-4473.

Pearson, J. E., Gill, A., Vadgama, P., 2000. Ann. Clin. Biochem. 37, 119-145

Piehler, J., Brecht, A., Gauglitz, G., 1996. Anal. Chem. 68, 139-143.

Pierce, G.W., 1923. Proc. Amer. Acad. Sci. 59, 81-82.

Pribyl, J., Hepel, M., Halamek, J., Skladal, P., 2003. Sens. Actuators B 91, 333-341.

Qureshi, M., Yeung, J., Wu, S., Wong, S., 2001. J. Biol. Chem. 276 (49), 46422–46428.

Raschke, G., Kowarik, S., Franzl, T., Sönnichsen, C., Klar, T. A., Feldmann, J., Nichtl, A., Kurzinger, K., 2003. Nano Letters. 3 (7), 935-938.

Ricco, A. J., Martin, S. J., 1987. Appl. Phys. Lett. 50, 1474-1476.

Rodahl, M., Höök, F., Kasemo, B., 1996. Anal. Chem. 68**,** 2219-2227.

Rosebrough, S.F., Hashmi, M., 1996. J. Pharmacol. Exp. Theor. 276, 770–775.

Sabot, A., Krause, S., 2002. Anal. Chem. 74, 3304-3311.

Sakai, G., Saiki, T., Uda, T., Miura, N., Yamazoe, N., 1995. Sens. Actuators B 24-25, 134-137.

Sauerbrey, G.Z.,1959. Z. Phys. 155, 2333-2336.

Schechter, B., Chen, L., Arnon, R., Wilchek, M., 1999. J. Drug Target 6, 337–348.

Schmitt, N., Tessier, L., Watier, H., Patat, F., 1997. Sens. Actuators B 43, 217-223.

Schneider, T.W., Martin, S.J., 1995. Anal. Chem. 67, 3324-3335.

Schwartz, D., 2001. Annu. Rev. Phys. Chem. 52, 107-137.

Shana, Z.A., Josse, F., 1994. Anal. Chem. 66, 1955-1964.

Shen, H., Mark, J., Seliskar, C., Mark, H., Heineman, W., 1997. J. Solid State Electrochem. 1, 148-154.

Shen, Z., Stryker, G., Mernaugh, R., Yu, L., Yan, H., Zeng, X., 2005. Anal. Chem. 77, 797-805.

Sherrit, S., Wiederick, H.D. , Mukherjee, B.K., Sayer, M., 1997. J. Phys. D: Appl. Phys. 30, 2354-2363.

Silva, F., Santa-Marta, M., Freitas-Vieira, A., Mascarenhas, P., Barahona, I., Moniz-Pereira, J., Gabuzda, D., Goncalves, J., 2004. J. Mol. Biology 340, 525-542.

Skládal, P., 2003. J. Braz. Chem. Soc. 14 (4), 491-502.

Soares, D.M., Tenan, M.A., Wasle, S., 1998. Electrochim. Acta 44, 263-268.

Su, X., Low, S., Kwang, J., Chew, V., Li, S., 2001. Sens. Actuators B 75, 29-35.

Su, X-L., Li, Y., 2005. Biosens. Bioelectron. 21(6), 840-848.

Sullivan, C. K., Guilbault, G. G., 1999. Biosens. Bioelectron. 14, 663-670.

Tenan, M.A., Soares, D.M., 1998. Brazilian Journal of Physics 28(4), 405-412.

Urizar, E., Lucia Montanelli, L., Loy, T., Bonomi. M., Swillens, S., Gales, C., Bouvier, M., Smits, G., Vassart, G., Costagliola, S., 2005. The EMBO Journal 24, 1954-1964.

Varela, H., M. Malte, and R.M. Torresi, 2000. Química Nova, 23(5), 664-679.

Willner, I., Wilner, B. , 2001. Trends Biotechnol. 19, 222-230.

Xie, Q., Zhang, V., Xiang, C., Tang, J., Li, Y., Zhao, Q., Yao, S., 2001. Analytical Sciences 17, 613-620.

Yang, X., Gonçalvez, J., Gabuzda, D., 1996. J. Biol. Chem. 271, 10121-10129.

Yao, Z., Zhang, M., Kobayashi, H., Sakahara, H., Nakada, H., Yamashina, I., Konishi, J., 1995. J. Nucl. Med. 36, 837–841.

Zhou[a], A., Zhang, J., Xie, Q., Yao, S., 2000. Sens. Actuators B 67, 68-75.

Zhou[b], X.C., O'Shea, S.J., Li, S.F.Y., 2000 Chem. Comm. 11, 953-954.

Appendix

The appendix has the published articles based on the work described in this thesis:

i. João M. Encarnação, Peter Stallinga, Guilherme N.M. Ferreira. *Influence of electrolytes in the QCM response: Discrimination and quantification of the interference to correct microgravimetric data.* Biosensors and Bioelectronics 22 (2007) 1351–1358.

ii. Guilherme N.M. Ferreira, João M. Encarnaçao, Luis Rosa , Rogério Rodrigues, Roberta Breyner, Sara Barrento, Luisa Pedro, Frederico Aires da Silva, João Gonçalves. *Recombinant single-chain variable fragment and single domain antibody piezoimmunosensors for detection of HIV1 virion infectivity factor*. Biosensors and Bioelectronics 23 (2007) 384–392.

iii. João M. Encarnação, Luis Rosa, Rogério Rodrigues, Luisa Pedro, Frederico Aires da Silva, João Gonçalves, Guilherme N.M. Ferreira. *Piezoelectric biosensors for biorecognition analysis: Application to the kinetic study of HIV-1 Vif protein binding to recombinant antibodies*. Journal of Biotechnology 132 (2007) 142–148.

Available online at www.sciencedirect.com
ScienceDirect
Biosensors and Bioelectronics 22 (2007) 1351–1358
BIOSENSORS & BIOELECTRONICS
www.elsevier.com/locate/bios

Influence of electrolytes in the QCM response: Discrimination and quantification of the interference to correct microgravimetric data

João M. Encarnação [a], Peter Stallinga [b], Guilherme N.M. Ferreira [a,*]

[a] *Centre for Molecular and Structural Biomedicine, University of Algarve, 8000 Faro, Portugal*
[b] *Centre of Electronics, Optoelectronics and Telecommunications, University of Algarve, 8000 Faro, Portugal*

Received 19 January 2006; received in revised form 3 May 2006; accepted 6 June 2006
Available online 1 August 2006

Abstract

In this work we demonstrate that the presence of electrolytes in solution generates desorption-like transients when the resonance frequency is measured. Using impedance spectroscopy analysis and Butterworth–Van Dyke (BVD) equivalent electrical circuit modeling we demonstrate that non-Kanazawa responses are obtained in the presence of electrolytes mainly due to the formation of a diffuse electric double layer (DDL) at the sensor surface, which also causes a capacitor like signal. We extend the BVD equivalent circuit by including additional parallel capacitances in order to account for such capacitor like signal. Interfering signals from electrolytes and DDL perturbations were this way discriminated. We further quantified as $8.0 \pm 0.5\,\mathrm{Hz\,pF^{-1}}$ the influence of electrolytes to the sensor resonance frequency and we used this factor to correct the data obtained by frequency counting measurements. The applicability of this approach is demonstrated by the detection of oligonucleotide sequences. After applying the corrective factor to the frequency counting data, the mass contribution to the sensor signal yields identical values when estimated by impedance analysis and frequency counting.

Keywords: Quartz crystal microbalance; Piezoelectric sensor; Impedance analysis; Equivalent electrical circuit; Butterworth–Van Dyke model; Biosensor

1. Introduction

The integration of electronics and biology to produce biosensors has emerged in very recent years as an area of enormous potential (Willner and Wilner, 2001). The field of (bio)molecular sensors is now beginning to materialize as an aid to understand the underlying biophysical principles of molecular recognition as well as to detect the presence of specific analytes. Generally speaking, to reliably detect an event, and eventually to quantify the kinetics and affinity of molecule interaction, transduction into a measurable sensitive as well as selective signal is needed. Traditionally, transduction is achieved indirectly by gathering a signal generated by specific reporter groups, usually fluorescent or electrochemically active molecules, used to label the targeted analytes. These approaches require labelling the samples with the reporter groups prior to the sensing reaction. Sample labelling constitutes a possible source of error, irreproducibility, and contamination and is detrimental to the sensitivity of the overall (bio)recognition analysis. The development of rapid, simple, selective and label-free methodologies for the detection of (bio)molecular recognition have thus been a long-standing goal. Piezoelectric transduction enables label-free detection of biorecognition events and has been used in microgravimetric devices, generally known as quartz crystal microbalance (QCM), for different applications (Pan et al., 1996; Yang et al., 1998; Etchenique and Brudny, 2000; Liu et al., 2004; Fabreguette et al., 2005; Su and Li, 2005; Wu et al., 2005; Modin et al., 2006).

The operation of a QCM relies on the piezoelectric effect, in which a quartz crystal is driven to mechanically resonate by application of a periodic electric field across its plane. The quartz crystal is the frequency determining element of an electric oscillator and the resonance frequency (f) and/or the frequency change (Δf) are measured. The data is often interpreted based on the Sauerbrey equation (Eq. (1)) which states that the measured frequency change (Δf) is linearly proportional to the mass load at the crystal exposed surface:

$$\Delta f_{\mathrm{m}} = -\frac{2nf_0^2}{\sqrt{\rho_{\mathrm{q}}\mu_{\mathrm{q}}}}\frac{\Delta m}{A} = -C_{\mathrm{f}}\frac{\Delta m}{A} \quad (1)$$

* Corresponding author. Tel.: +351 289800985; fax: +351 289818419.
E-mail address: gferrei@ualg.pt (G.N.M. Ferreira).

0956-5663/$ – see front matter © 2006 Elsevier B.V. All rights reserved.
doi:10.1016/j.bios.2006.06.011

where f_0 is the resonant frequency of the fundamental mode, Δf_m the frequency change due to mass loading, n the harmonic number ($n=1$ for the fundamental mode), ρ_q and μ_q, respectively, the density and the shear mode of the quartz material, Δm the mass change at the crystal surface, and A is the crystal sensitive area. The sensitivity factor (C_f) is a constant that only depends on physical parameters of the crystal sensor.

The Sauerbrey equation (Eq. (1)) makes the assumption that the mass deposited or the film formed at the surface of the crystal follows the vibration of the crystal and therefore the loaded crystal simply behaves as if it was thicker. Thus, this equation is only valid for thin, rigid, and uniform films. If the surface film is not entirely rigid, the quartz response depends not only on the mass load but also on the viscoelastic properties of the attached layer (Etchenique and Weisz, 1999; Lucklum and Hauptmann, 2000). Kanazawa and Gordon (1985) derived a relationship to account for the resonance frequency change of crystals in contact with liquids:

$$\Delta f_L = -f_0^{3/2}\sqrt{\frac{\rho_L \eta_L}{\pi \rho_q \mu_q}} \quad (2)$$

where Δf_L is the frequency change due to liquid loading, ρ_L and η_L are the density and viscosity of the liquid in contact with the sensor surface, respectively. Therefore when detecting analytes in liquid environments both mass and liquid loading contribute to the total frequency change. Martin et al. (1991) have derived a model for the total frequency change accounting for the simultaneous contribution of mass and liquid loading to the sensor signal:

$$\Delta f = \Delta f_m + \Delta f_L = -\frac{2f_0^2}{n(C_{66}\rho_q)^{1/2}}\left[\frac{\Delta m}{A} + \left(\frac{\rho_L \eta_L}{4\pi f_0}\right)^{1/2}\right] \quad (3)$$

where $C_{66} = 2.957 \times 10^{10}\ \mathrm{nm}^{-2}$ is the stiffness of quartz (Martin et al., 1991).

Due to the additive nature of the mass and liquid loading (Eq. (3)) the mass effect cannot be differentiated when the frequency change is tracked, and, therefore, one has to be extremely careful when evaluating and interpreting the measured data. In spite of this apparent disadvantage, QCM sensors are still employed in a variety of applications using standard oscillator techniques and frequency counting, mainly due to its low cost and to the simplicity of the operation.

Impedance spectroscopy methods can provide more detailed information about the surface changes on QCM (Martin et al., 1991; Auge et al., 1995; Bouche-Pillon et al., 1995; Etchenique and Weisz, 1999; Lucklum and Hauptmann, 2000; Zhou et al., 2000a,b). A QCM sensor can be represented by a Butterworth–Van Dyke (BVD) model which consists of an equivalent electrical circuit representation of the system (Fig. 1) that is composed of a static capacitance (C_0) in parallel with a motional branch containing a inductance (L_m), a capacitance (C_m), and a resistance (R_m) in series—Area I in Fig. 1. The parameters of the equivalent electrical circuit are related to the ratio of energy stored in the oscillation and energy dissipation to the mounting structure of the crystal and contacting

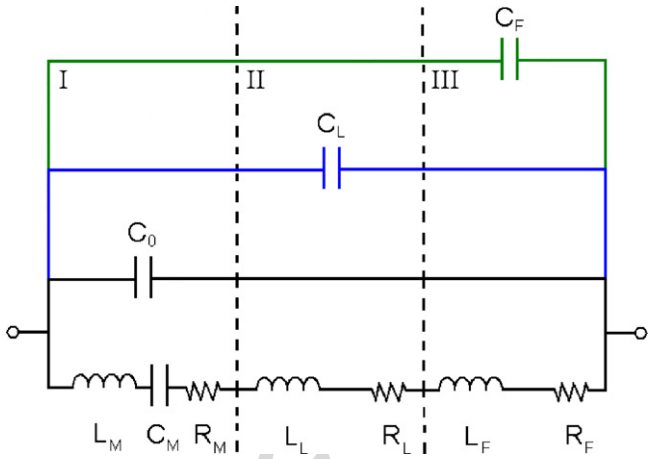

Fig. 1. Butterworth–Van Dyke equivalent circuit model (black circuit) and modified Butterworth–Van Dyke equivalent circuits to account for charged variation upon liquid (blue) and mass (green) loading. Area I, unloaded resonator; Area II, elements added due to liquid exposure; Area III, elements added due to the adsorption of mass on the surface of the sensor. (For interpretation of the references to colour in this figure legend, the reader is referred to the web version of the article.)

medium, i.e. viscous solutions and viscoelastic films (R_m); inertia to oscillation related to mass dislocation (L_m); oscillation energy storage related to the elasticity of the crystal (C_m); parasitic capacitance due to electrodes, holding structure, cables, and connectors (C_0). An advanced measurement system using a network or impedance analyzer enables the quantification of the different contributions R_m, L_m, C_m and C_0, by fitting the impedance/admittance spectrum around the crystal resonance frequency ($f = (4\pi^2 \times L_m C_m)^{-1/2}$) to the BVD model. The contribution of the different stages of the (bio)molecular recognition analysis can be evaluated by adding components to the BVD circuit—Areas II and III in Fig. 1 for liquid and mass loading, respectively—and by calculating the respective parameters.

Even though the quantification of the BVD model parameters enables the discrimination of the different contributions to the sensor signal at the different analysis stages, thus, significantly improving the sensor sensitivity by enabling the elimination of parasitic signals, impedance analysis and equivalent circuit modeling fails in discriminating, and thus in eliminating, the interference of charged molecules (Etchenique and Buhse, 2000, 2002). The presence of charged molecules in solution is known to introduce significant errors in the analytical quantification of adsorbed entities using QCM, even when using advanced impedance analysis (Etchenique and Buhse, 2000). In this work, we demonstrate that the presence of small electrolytes, as well as poly-ion molecules (using oligonucleotides as model) in QCM measurements generate strong interfering signals that cannot be eliminated by standard BVD equivalent circuit modeling. We propose a modification of the BVD model to account for such interferences (Fig. 1) and an example is given in which the modified model is used to the study of DNA hybridization and to correct frequency data, thus enabling the accurate quantification of the adsorbed mass.

2. Experimental

2.1. Reagents

All chemicals and reagents were ultra-pure, pro-analysis, or equivalent grade. Milli-Q water was used. Sodium dihydrogen phosphate, disodium hydrogen phosphate, sodium, potassium, calcium and magnesium chloride, absolute ethanol, and hydrogen peroxide were purchased from Merck. 11-Hydroxy-1-undecanothiol was purchased from Dojindo Molecular Technologies and 10 nm gold nanoparticles were purchased from Sigma.

Oligonucleotides were designed on the basis of human CTLA4 gene, purchased from Thermo Corporation at http://www.interactiva.de and used HPLC pure as received. 5′-Thiol modified oligonucleotide HS-Pr1 (GCT GAA CCT GGC TAC CAG GAC CTG GCC) was used to functionalize the sensor surface in order to detect the target complementary oligonucleotides Tgt1 (GGC CAG GTC CTG GTA GCC AGG TTC AGC) and HS-Tgt1. Tg1 and HS-Tg1 are identical and fully complementary to HS-Pr1 except that HS-Tgt1 is thiol modified to enable labeling with gold nanoparticles (see below).

An oligonucleotide sequence with null complementarity with both the probe and target sequences was used as control—Ctr1 (TAG GAG GTC ATC TCG AGC TAT GGC TCT GTT ATT AGC).

2.2. Oligonucleotide labeling with gold nanoparticles

Oligonucleotides were labeled with gold nanoparticles following a previously published protocol (Csáki et al., 2003). Briefly, 35 μl of a 100 μm solution of HS-Tgt1 were diluted in 5 ml of a 8.7 nm colloidal aqueous solution of 10 nm gold nanoparticles and incubated at room temperature for 16 h. After diluting the reaction mixture with 5 ml of PBS buffer (100 mm phosphate containing 100 mm NaCl, pH 7.0) and incubating at room temperature for 30 h, 11-hydroxy-1-undecanothiol was added to a final concentration of 50 μM and the mixture was incubated at room temperature for additional 12 h. Modified nanoparticles were recovered by centrifugation for 30 min at 12 000 rpm, washed twice with 5 ml PBS, and dispersed in a PBS buffer.

Control gold nanoparticles (Au-SAM nanoparticles) were prepared similarly using Milli-Q water instead of the HS-Tgt1 solution.

2.3. Quartz crystal sensors

One inch diameter 5 MHz AT-cut quartz crystals, coated with optically flat polished gold electrodes on both sides, were purchased from Stanford Research Systems (SRS, Stanford, USA). The active area and sensitivity factor of the crystal are $A = 0.4\,\text{cm}^2$ and $C_f = 56.6\,\text{Hz}\,\text{cm}^2\,\mu\text{g}^{-1}$, respectively.

The crystals were cleaned before use by rinsing with absolute ethanol and Milli-Q water before immersion in Piranha solution (30%(v/v), H_2O_2:H_2SO_4 = 1:3) for 15 min, to obtain a clean gold surface. Cleaned crystals were then rinsed with water and dried in a nitrogen stream.

2.3.1. Quartz crystal sensor functionalization

To functionalize the surface of the crystal sensors, 50 μl of a 5 μm solution of probe HS-Pr1, freshly prepared in PBS buffer, were carefully pipetted onto the surface of a cleaned crystal sensor, and incubated at room temperature for 5 h in a humidified chamber. Unbounded probe was removed by washing the functionalized crystal sensors sequentially with PBS buffer and Milli-Q water. After drying under a nitrogen flow, the functionalized crystal sensors were incubated overnight, at room temperature in an humidified chamber, with 100 μl of a 50 μm 11-hydroxy-1-undecanothiol 10% (v/v) ethanolic solution in order to completely cover exposed surface areas, to remove unspecificaly adsorbed HS-Pr1 probe, and to better organize the monolayer (Herne and Tarlov, 1997).

Control sensors were prepared similarly with the sole difference that clean crystals were incubated with 50 μl PBS buffer instead of HS-Pr1 probe.

2.4. Experimental set-up

Cleaned or functionalized sensors were mounted on a Kynar crystal holder (SRS) with a home-made acrylic cover to form a 300 μl flow cell exposing just one face of the sensor to the solution. Viton O-rings were placed underneath the sensor, sealing the flow cell to avoid wetting or flooding the electrical contacts located on the bottom of the crystal holder. A closed-cycle fluidic circuit was mounted using Tygon tubing to connect the flow cell to an agitated container where all the samples are added. The total volume of the systems is 2 ml and the solutions were recirculated in the system at a flow rate of 500 $\mu\text{l}\,\text{min}^{-1}$ controlled by a Watson–Marlow peristaltic pump. Both the flow cell and the container were installed in a home-made 1l jacketed beaker to control the temperature of the system at 25 ± 0.1 °C by means of a Thermo Haake temperature controller.

The resonance frequency and impedance spectra were recorded alternatingly using a QCM100 Controller and a QCM25 Oscillator (SRS) connected to a Pendulum CNT-66 frequency counter or using a RF HP8712C Network Analyzer, respectively. The network analyzer and the QCM25 Oscillator were electrically connected to the crystal holder through an electronic switch used to select the desired measurement mode. The instruments were interfaced to a computer through IEEE boards and custom made acquisition programs.

2.5. Impedance analysis

Impedance spectra were obtained using a 10 kHz frequency span centred near the crystal's resonant frequency with 16 spectra averaging at 1 Hz resolution.

The BVD equivalent circuit parameters were obtained from the experimental data by calculating the conductance function ($|Y| = |Z|^{-1}$; $|Z|$ being the recorded impedance magnitude) and fitting, using a fitting routine written in Matlab, to the following

equations:

$$|Y| = \sqrt{\left(\frac{R_m}{R_m^2 + U^2}\right)^2 + \left(\omega C_0 - \frac{U}{R_m^2 + U^2}\right)^2} \quad (4)$$

$$U = \omega L_m - \frac{1}{\omega C_m} \quad (5)$$

where $\omega = 2\pi f$ is the angular frequency.

The analysis is initialized by estimating the four BVD parameters (R_m, L_m, C_m and C_0) for the crystal sensor exposed to air. Typical parameters for air exposed crystal sensors in the experimental set-up used are $R_m = 12.925\ \Omega$, $L_m = 33.725$ mH, $C_m = 29.925$ fF, and $C_0 = 184.575$ pF, respectively. Since C_m is related only to the sensor physical material, it is constant within the experiments. The successive contributions of solvents and adsorbed mass are thus obtained by a three parameter fitting (R_m, L_m, C_0) of the respective conductance functions. This procedure is repeated for each stage of the experiment and the BVD parameters of the particular experimental stage, thus of the individual contributions, are calculated by subtracting the global parameters, obtained by fitting, from the respective parameter calculated for the previous stage of the experiment. To facilitate data analysis it is usual to represent a parameter *XL* which is the sensor inductance in resistive units (Ω) obtained by multiplying the calculated inductance value by the angular frequency $\omega = 2\pi f$.

3. Results and discussion

3.1. Effect of small increments of electrolytes

Considering the use of QCM devices in (bio)molecular sensing and recognition, where in the majority of the situations the analytes are present in buffered solutions containing small amounts of electrolytes, a set of experiments was undertaken to study and characterize the influence of such electrolytes in the sensor signal. Milli-Q water was circulated in the sensor flow chamber and, after establishing a stable resonance frequency signal, small volume amounts of concentrated solutions of NaCl, KCl, $MgCl_2$ or $CaCl_2$ were successively added in the sample container in order to achieve the desired ionic strength in the system. As shown in Fig. 2, the QCM sensor responds strongly to small variations on the solution electrolyte concentration when the resonance frequency is directly measured by frequency counting. To evaluate if this response is related to eventual variations of the hydrostatic pressure, owing to the small volume increments, control experiments were performed where similar volume amounts of Milli-Q water were added instead of electrolyte solutions. No frequency variations were observed for these control experiments which indicate that the frequency variations observed (Fig. 2) are related to nothing more than the presence of the electrolytes. Fig. 2 also shows that monovalent and divalent cations affect the frequency variation (Δf) differently. Even though the general tendency is the same, with frequency decreasing for the initial variations and increasing after reaching a minimum, the frequency increase rate is higher for monovalent cations (Na^+ and K^+) when compared to divalent cations (Mg^{2+} and Ca^{2+}).

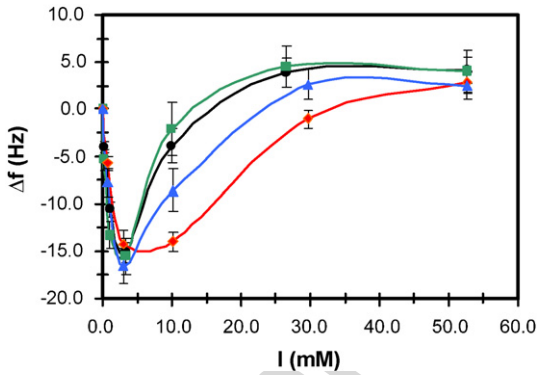

Fig. 2. Average ($n = 6$) resonance frequency variation (Δf) with increasing ionic strength for (●) NaCl, (■) KCl, (♦) $CaCl_2$ and (▲) $MgCl_2$.

If one adopts the mathematical models usually used to interpret frequency variation data (Eqs. (1)–(3)), the increase in the frequency observed (Fig. 2) should be related either to a decrease of the mass over the crystal surface or to a decrease in the solution viscosity and/or density. Considering that: (i) the bulk solution viscosity and density are unchanged during the experiments; (ii) no mass is deposited over the crystal; (iii) the addition of such small quantities of salt has negligible or no effect on the overall system hydrostatic pressure, we propose, in accordance with previously published work (Etchenique and Buhse, 2000), that the anomalous frequency response observed is correlated to the increment of the charge density in the solution due to the addition of electrolytes.

The admittance data associated with the experiments described above were recorded, in order to investigate in more detail the origins of the frequency variation, to differentiate the effect of the different interferences, and to calculate the values of the parameters of the BVD equivalent electrical circuit. Fig. 3 shows the variation of each parameter with the small increments of the solution ionic strength. In accordance with previously published data (Etchenique and Buhse, 2000; Ghafouri and Thompson, 2001), the calculated inductance and resistance increase with increasing ionic strength. This increase occurs up to reaching a certain ionic strength, after which the inductance stabilizes while resistance decreases considerably (Fig. 3A and B). On the basis of the BVD parameters it is possible to predict the resonance frequency variation ($f = (4\pi^2 \times L_m C_m)^{-1/2}$). Fig. 3C shows that the predicted frequency variation with the solution ionic strength is not consistent with the measured values. Even though sharing a similar tendency for the low ionic strengths, with resonance frequency decreasing with increasing ionic strengths, for the higher ionic strengths the predicted resonance frequency variation stabilizes close to its minimum value while the measured resonance frequency variation considerably increases before stabilizing. Furthermore, contrary to the measured data, impedance analysis predicts different sensor responses to mono and divalent cations (Fig. 3C). These results suggest that QCM frequency counting data is affected by interfering signals which can be avoided or eliminated by using full impedance analysis.

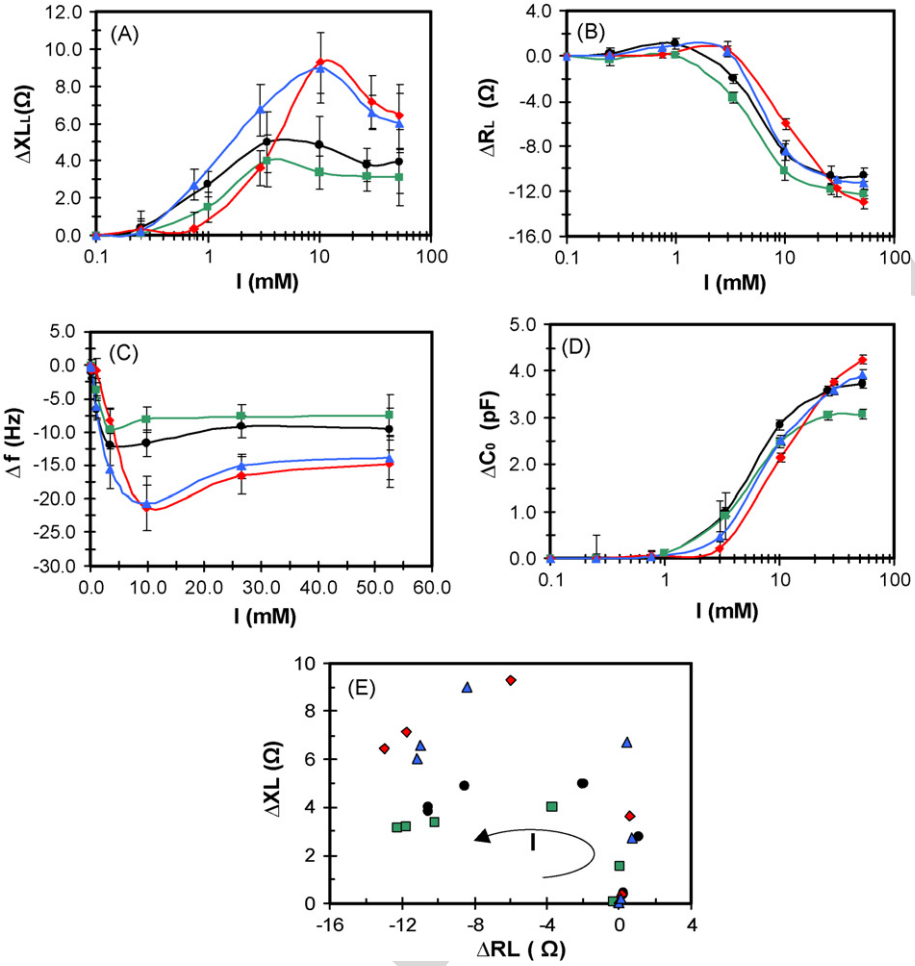

Fig. 3. Variation of the Butterworth–Van Dyke model parameters with the ionic strength for (●) NaCl, (■) KCl, (♦) $CaCl_2$ and (▲) $MgCl_2$: (A) inductance; (B) resistance; (C) calculated resonance frequency variation; (D) parallel capacitance; (E) parametric polar impedance plot. The figures correspond to the average of impedance analysis data resulting from three independent experiments for each data point.

Owing to the assumption that the parallel capacitance (C_0) is related to the physical properties of the system components, such as electrodes, cables, connectors, and holders, this capacitance was expected to be constant within the experiments. Contrary to these expectations, C_0 also increases with increasing the ionic strength (Fig. 3D). This result suggests that variations in the electrolyte composition of the solution results in a capacitive response characterized by a specific addition to C_0. To account for such sensor response, in accordance with previously published experimental work (Xie et al., 2001), we extended the generally used BVD model to include additional capacitances in parallel for each stage of the experiment (Fig. 1). We expect that these additional capacitances will enable the differentiation of the influence of charged species added or removed in each stage, thus the correction of calculated parameters upon rendering the parasitic capacitance (C_0) constant. According to this modification, the parallel capacitance calculated corresponds to the total parallel capacitance of the system ($C_T = C_0 + C_L + C_F$) and includes the contributions from the static capacitance (C_0), and the additional capacitances due to charge variation upon liquid loading (C_L) and/or mass loading (C_F). The influence of the charge variation at a given stage is this way discriminated after subtracting the capacitance values calculated for the previous stages.

Further interpretation of the calculated parameters reveals no variation of the resistance (R) or the capacitance (C_0) with the cation valence (Fig. 3B and D). On the other hand, the simultaneous determined inductance values (Fig. 3A) reveal a strong influence by the cation valence, a result that is consistent with the data gathered by frequency counting (Fig. 2). As shown in Fig. 3A, the resonator inductance increases to a further extent, both considering the amplitude and the ionic strength, when divalent cations are present. Since the resonance frequency is affected by the motional inductance and capacitance ($f = (4\pi^2 \times L_m C_m)^{-1/2}$) these results show that, for the same ionic strength, divalent cations generate higher frequency drops and slower responses to ionic strength variations which are driven just by the inductive contribution of the resonator.

3.2. *Piezoelectric resonators sense and respond to modifications of the diffusive electrical double layer*

Considering the physical meaning of the BVD parameters, in particular the fact that *XL* is related to vibrating mass, hence

reflecting mass displacement, and that R is related to acoustic energy loss owing to medium damping (viscous losses), a more detailed analysis of the experimental data reveals that the recorded profiles, both by frequency counting and impedance measurements, can be divided into two distinct regions. In the low ionic strength region ($I < 1$ mM) the resonant frequency drops while both the calculated inductance and resistance rise. This is compatible to an increase of the density and/or of the viscosity near the crystal's surface. On the other hand, for higher ionic strengths ($I > 1$ mM) the resonant frequency increases and the resonator impedance is characterized by $XL \gg R$ which indicates the formation of a rigid enough layer that moves in phase with the resonant surface.

It seems thus that a layer is formed at the crystal surface whose viscosity/rigidity depends on the solution electrolyte nature and composition. The viscoelastic behavior of this layer can be characterized by the parametric polar impedance plots, which are graphical representations of the variation of the calculated inductance with the variation of the calculated resistance (Fig. 3E). In general, parametric polar impedance plots of Newtonian or viscoelastic fluids are characterized by linear relationship between of XL and R whose slope equals 1 for Newtonian fluids (Etchenique and Buhse, 2002). On the other hand, fluids or layers of variable viscosity or elasticity are characterized by a curvature in the XL versus R plots (Etchenique and Buhse, 2002). As such, the circular shape of the XL versus R plots of Fig. 3E leads to the conclusion that a thin film with variable viscosity/elasticity is formed between the crystal surface and the solution bulk.

Considering that the solutions in contact with the crystal surface consist of water and electrolytes, the only possible layer being formed or "deposited" on the crystal surface is a diffuse electrical double layer (DDL). The thickness of the DDL, the Debye length, is known to be influenced by the concentration and by the valence of electrolytes (Atkins, 1990). By increasing the solution ionic strength, or by using ions with higher valences, the Debye length decreases, resulting in a reduced distance between charged particles, as well as the entire double layer drawing nearer the surface, resulting therefore in the accumulation of charges at the electrode's surface. Thus, more rigid films and higher charge accumulation are expected to be formed close to the sensor surface for higher ionic strengths and valences, detected by higher inductance values (Fig. 3A). Moreover, higher capacitances (Fig. 3D) are measured as a consequence of the additional parallel capacitances.

3.3. Use of modified BVD data as corrective tool to evaluate and quantify DNA hybridization

To further demonstrate the applicability of the proposed modification to the BVD model we evaluated the sensor response as a DNA detector. DNA fragments, and oligonucleotides, are polyelectrolytes in neutral aqueous solution and a strong interfering signal resulting from DDL perturbation can be expected. Crystal sensors were functionalized with oligonucleotides, mounted in the experimental set-up, and used to detect complementary oligonucleotides (Fig. 4). As shown in Fig. 4A, the signals measured by frequency counting for unlabeled oligonucleotides and for the controls are similar. Such a result leads to the conclusion that either the sensor is not fully operational or no complementary sequences are present. The lack of signal variation in frequency counting measurements when using unlabeled oligonucleotide or DNA fragments has been reported by other authors that used gold nanoparticles as labels for mass amplification in order to force a signal resulting from DNA hybridization at the sensor surface (Zhou et al., 2000a,b; Su and Li, 2005). Even though resonance frequency variations are measured when using gold labeled targets (Fig. 4A), target labeling withdraws from piezoelectric sensors the advantages of direct transduction of unlabeled targets. Moreover, the total frequency variation obtained for the gold labeled oligonucleotides measured by frequency counting is $\Delta f = 19$ Hz (Fig. 4A) which only accounts for 63% of the frequency change predicted from impedance analysis data (Fig. 4B). This discrepancy indicates that quantitative calculations based on frequency counting (e.g. mass determination) can be underestimated due to the interfering signal resulting from the effect of the charges on the sensor surface and adjacent layers.

In order to account for the effects of charges we propose the calculation of the respective interfering capacitances C_L and C_F (Fig. 1). The total frequency variation (Δf_T) due to mass

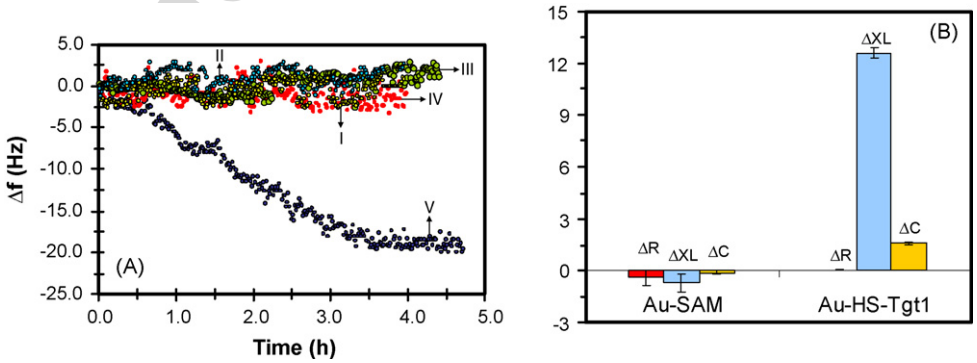

Fig. 4. Crystal sensor response to DNA hybridization. All crystal sensors used were functionalized with HS-Pr1 probe and blocked with 11-hydroxy-1-undecanothiol: (A) resonance frequency recorded for crystal sensors incubated with (I) PBS buffer, (II) 1 μM of Ctr1, (III) 1 μM of Tgt1, (IV) 1.7 nM of Au-SAM nanoparticles, (V) 1.7 nM of Au–HS-Tgt1 nanoparticles; (B) impedance data acquired for crystal sensors incubated with gold nanoparticles modified with 11-hydroxy-1-undecanothiol (Au-SAM) and gold nanoparticles functionalized with complementary target HS-Tgt1 (Au–HS-Tgt1).

loading (Δf_M), viscoelasticity of the adsorbed/deposited mass (Δf_V), liquid (Δf_L) and charge interference (Δf_C) should be thus obtained by:

$$\Delta f_T = \Delta f_M + \Delta f_V + \Delta f_L + \Delta f_C \quad (6)$$

When operating the QCM in the oscillator/frequency counting mode in liquid phase (Δf_M), (Δf_V), (Δf_C) can not be differentiated, and the measured frequency variations is given by $\Delta f_T - \Delta f_L$. In analogy to the case of the generally accepted correction for the liquid loading effects, where the contribution of the buffer viscosity/elasticity and density to the total frequency change (Δf_L) is estimated from a linear relationship established between Δf and ΔR (Martin et al., 1991; Zhou et al., 2000a,b), we seek for a parameter that could be used to correct the underestimation of frequency counting quantification. Considering, once again, that the frequency variations shown in Figs. 2 and 3, results only from charge interferences ($\Delta f_M = \Delta f_L = \Delta f_V = 0$), we used the data from these figures to estimate the values of such a parameter. A plot of the measured frequency variation against the calculated interfering capacitance (Fig. 5) shows that these parameters are linearly correlated within the range investigated, leading to the conclusion that the frequency variation is linearly dependent on the calculated capacitance variation (demonstrated by the close to one correlation coefficients and by the p-values (Fig. 5). Moreover, the similarity of the slopes may indicate that the observed frequency variations are due to the capacitive effect and could be independent on the charged species involved. Thus, calculating the average of the slopes we find a frequency variation of $8.0 \pm 0.5\,\text{Hz pF}^{-1}$ resulting from charge interference. To test the applicability of this hypothesis we apply this corrective factor to the data gathered for the gold labeled oligonucleotide detection (Fig. 4). For this case, the charge interference was quantified as $C_F = 1.60 \pm 0.02$ pF (Fig. 4B) which results in an estimated contribution to the frequency variation of $\Delta f_C = 12.8 \pm 0.8$ Hz. Since the immobilized mass has a negligible viscous effect ($\Delta R \approx 0$, Fig. 4B), the use of Eq. (6) estimates the frequency variation due to mass load as $\Delta f_M = \Delta f_T - \Delta f_L + \Delta f_C = 31.8$ Hz. The similarity between this value and the 30 Hz estimated from the impedance data demonstrates that charge interferences can reliably be corrected by using the parameter obtained from Δf versus ΔC correlations.

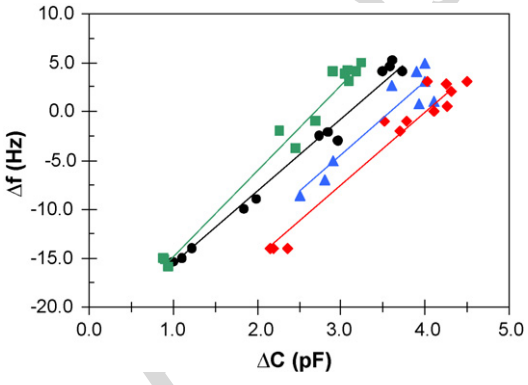

Fig. 5. Relationship between measured resonance frequency variation and calculated parallel capacitance in the range of 1 mM ≤ I ≤ 50 mM. Triplicate independent experiments for (●) NaCl (12 experimental points), (■) KCl (12 experimental points), (♦) $CaCl_2$ (12 experimental points), and (▲) $MgCl_2$ (9 experimental points) were performed; linear regression of experimental data yielded the correlations $\Delta f = (7.8 \pm 0.4) \times \Delta C + (-24 \pm 1)$, $r = 0.9862$, $p < 0.0001$, for NaCl, $\Delta f = (8.7 \pm 0.3) \times \Delta C + (-23.6 \pm 0.8)$, $r = 0.9935$, $p < 0.0001$, for KCl; $\Delta f = (7.8 \pm 0.5) \times \Delta C + (-31 \pm 2)$, $r = 0.9790$; $p < 0.0001$, for $CaCl_2$; $\Delta f = (7.7 \pm 0.9) \times \Delta C + (-28 \pm 4)$, $r = 0.9372$, $p = 0.0002$ for $MgCl_2$.

4. Conclusions

In this work, we demonstrated that the response of QCM is affected by the presence of electrolytes in solution. This interference leads to transients mimicking desorption, with frequency variations (Δf) decreasing with increasing densities of charges in solution, and can thus have a considerable impact in biosensor applications, up to the point of leading to less accurate conclusions. The influence of electrolytes results in non-Kanasawa response, which, for the low ionic strengths, is characterized by a frequency drop and by an increase of the sensor inductance and resistance owing to the increase of the density and viscosity near the sensor surface as a diffuse electric double layer develops. For high ionic strengths, charge effects predominate, leading to increasing resonance frequencies, while the resistance drops and the parallel capacitance increases. We propose a modification to the Butterworth–Van Dyke model to include additional parallel capacitances in order to account for the influence of charges to the sensors response. Such influence is linearly correlated with the measured resonance frequency variation in the range of 1 mM ≤ I ≤ 50 mM and is characterized by a desorption-like signal of $8.0 \pm 0.5\,\text{Hz pF}^{-1}$. The use of this factor allows for the correction of the mass-frequency variation, which otherwise is close to 40% underestimated, resulting in a convergence of the values measured by frequency counting and impedance analysis. Estimating the influence of electrolytes and its contribution to the measured frequency variation thus enables the acquisition of more accurate data and this represents a step forward in the use of piezoelectric sensors for quantitative direct transduction of molecular recognition events.

Acknowledgments

This work was supported by the Portuguese Science Foundation an organization of the Portuguese Ministry of Science and Higher Education. Contract numbers POCTI/CTM/37719/2000 and POCI/BIO/61912/2004 are acknowledged. PhD grant no. SFHR/BD/12772/2003 to J.M. Encarnação is also acknowledged.

References

Auge, J., Hauptmann, P., Hartmann, J., Rösler, S., Lucklum, R., 1995. Sens. Actuators B 24, 43–48.
Atkins, P.W., 1990. Physical Chemistry, 4th ed. Oxford University Press, UK.
Bouche-Pillon, D., Gabrielli, C., Perrot, H., 1995. Sens. Actuators B 25, 257–259.
Csáki, A., Kaplanek, P., Möller, R., Fritzche, W., 2003. Nanotechnology 14, 1262–1268.
Etchenique, R., Weisz, A.D., 1999. J. Appl. Phys. 86 (4), 1994–2000.

Etchenique, R., Brudny, V.L., 2000. Langmuir 16, 5064–5071.
Etchenique, R., Buhse, T., 2000. Analyst 125, 785–787.
Etchenique, R., Buhse, T., 2002. Analyst 127, 1347–1352.
Fabreguette, F.H., Sechrist, Z.A., Elam, J.W., George, S.M., 2005. Thin Solid Films 488 (1/2), 103–110.
Ghafouri, S., Thompson, M., 2001. Analyst 126, 2159–2167.
Herne, T.M., Tarlov, M.J., 1997. J. Am. Chem. Soc. 119, 8916–8920.
Kanazawa, K.K., Gordon, J.G., 1985. Anal. Chim. Acta 175, 99–105.
Liu, Y., Zhang, W., Yu, X., Zhang, H., Zhao, R., Shangguan, D., Li, Y., Shen, B., Liu, G., 2004. Sens. Actuators B 99, 416–426.
Lucklum, R., Hauptmann, P., 2000. Sens. Actuators B 70, 30–36.
Martin, S.J., Granstaff, V.E., Frye, G.C., 1991. Anal. Chem. 63, 2272–2281.
Modin, C., Stranne, A.-L., Foss, M., Duch, M., Justesen, J., Chevallier, J., Andersen, L.K., Hemmersam, A.G., Pedersen, F.S., Besenbacher, F., 2006. Biomaterials 27, 1346–1354.
Pan, W., Durning, C.J., Turro, N.J., 1996. Langmuir 12, 4469–4473.
Su, X.-L., Li, Y., 2005. Biosens. Bioelectron. 21 (6), 840–848.
Willner, I., Wilner, B., 2001. Trends Biotechnol. 19, 222–230.
Wu, T.-Z., Su, C.-C., Chen, L.-K., Yang, H.-H., Tai, D.-F., Peng, K.-C., 2005. Biosens. Bioelectron. 21 (5), 689–695.
Xie, Q., Zhang, V., Xiang, C., Tang, J., Li, Y., Zhao, Q., Yao, S., 2001. Anal. Sci. 17, 613–620.
Yang, M., Yau, H.C.M., Chan, H.L., 1998. Langmuir 14, 6121–6129.
Zhou, X.C., O'Shea, S.J., Li, S.F.Y., 2000a. Chem. Commun. 11, 953–954.
Zhou, A., Zhang, J., Xie, Q., Yao, S., 2000b. Sens. Actuators B 67, 68–75.

Available online at www.sciencedirect.com
ScienceDirect
Biosensors and Bioelectronics 23 (2007) 384–392
BIOSENSORS & BIOELECTRONICS
www.elsevier.com/locate/bios

Recombinant single-chain variable fragment and single domain antibody piezoimmunosensors for detection of HIV1 virion infectivity factor

Guilherme N.M. Ferreira [a,*], João M. Encarnação [a], Luis Rosa [a], Rogério Rodrigues [a], Roberta Breyner [b], Sara Barrento [a], Luisa Pedro [a], Frederico Aires da Silva [c], João Gonçalves [c]

[a] *IBB-Institute for Biotechnology and Bioengineering, Centro de Biomedicina Molecular e Estrutural, Universidade do Algarve, 8000 Faro, Portugal*
[b] *ITODYS, Université Paris7, France*
[c] *URIA-Centro de Patógenese Molecular, Faculdade de Farmácia, Universidade de Lisboa, Portugal*

Received 31 January 2007; received in revised form 27 April 2007; accepted 27 April 2007
Available online 6 May 2007

Abstract

In this paper recombinant single-chain fragments (scFv-4BL), and single domain antibodies (4BL-V_H) and (4BL-V_HD) generated against HIV1 virion infectivity factor (Vif) are used to develop piezoimmunosensors for HIV1 recognition. Mixed self assembled monolayers were generated at the surface of gold coated crystal sensors to which scFv-4BL, 4BL-V_H, or 4BL-V_HD were immobilized. Impedance analysis was used to discriminate interfering signals from frequency variation data and to increase the sensor sensitivity. The elimination of interfering signals enabled the quantification of the amount of immobilized protein and gave some indication on the viscoelasticity of immobilized biofilms. All the modified sensors were able to specifically recognize HIV1 Vif in liquid samples. The results indicate that lower sensitivities are obtained with 4BL-V_H single domain antibodies, possibly due to its higher hydrophobic character. The sensitivity obtained when using scFv-4BL was reestablished when using the more hydrophilic 4BL-V_HD single domain. 4BL-V_HD piezoimunosensors were effective in recognizing HIV1 Vif from protein mixtures and from cell extracts of human embryonic kidney cells expressing HIV1 Vif. The results presented in this paper demonstrate the potential applicability of the developed piezoimmunosensors to monitor HIV1 infection evolution.

Keywords: Immunosensors; QCM; Piezoelectric; Biosensors; Recombinant antibody; single-chain antibody; Single domain antibody; Affinity binding

1. Introduction

The development of biosensor systems for the rapid, selective and label-free detection of target analytes has been a long-standing goal in biorecognition for medical, safety and environment applications. Piezoelectric transduction enables label free detection of biorecognition events and has been used in microgravimetric devices, generally known as quartz-crystal microbalance (QCM) (Pan et al., 1996; Yang et al., 1998; Liu et al., 2004; Etchenique and Brudny, 2000; Su and Li, 2005; Wu et al., 2005; Modin et al., 2006).

Binding of target analytes onto biomolecule layers immobilized at the sensor surface in QCM devices is directly transduced into a resonance frequency variation signal (Δf_m). The mass change occurring at the QCM surface upon analyte binding is usually estimated using the Sauerbrey equation, $\Delta f_m = [-2nf_0\,2/(\rho_q\mu_q)1/2] \times [\Delta m/A]$, where Δf_m is the frequency change due to mass loading, f_0 is the resonant frequency of the fundamental mode, n is the harmonic or overtone number, ρ_q and μ_q are, respectively, the density and the shear mode of the crystal, Δm is the mass change, and A is the sensor active area. The Sauerbrey equation is only valid for thin, rigid and uniform films. Several studies have demonstrated that the QCM signal also depends on the viscoelastic properties of the buffers (Etchenique and Weisz, 1999; Lucklum and Hauptmann, 2000) and attached layers (Ogi et al., 2006) and on the presence of electrolytes and surface charge variations (Etchenique and Buhse, 2000; Ghafouri and Thompson, 2001; Encarnação et al., 2007). Therefore when detecting analytes in liquid environments both mass and liquid loading contribute to the total frequency change. The contributions of mass, liquid loading, and charge variations are additive and can not be distinguished by frequency counting

* Corresponding author. Tel.: +351 289 800 985; fax: +351 289 818 419.
E-mail address: gferrei@ualg.pt (G.N.M. Ferreira).

0956-5663/$ – see front matter © 2007 Elsevier B.V. All rights reserved.
doi:10.1016/j.bios.2007.04.022

measurements (Encarnação et al., 2007; Kanazawa and Gordon, 1985; Martin et al., 1991). Impedance spectroscopy methods are generally used to obtain more detailed information on the changes occurring at the QCM sensor surface (Etchenique and Weisz, 1999; Lucklum and Hauptmann, 2000; Encarnação et al., 2007; Kanazawa and Gordon, 1985; Martin et al., 1991; Auge et al., 1995; Bouche-Pillon et al., 1995; Zhou et al., 2000). As such, QCM sensors are commonly represented as equivalent electrical circuits, also known as Butterworth–Van Dyke (BVD) model (Fig. S-1). The model parameters—resistance (R_m), inductance (L_m), capacitance (C_m), and static capacitance (C_0)—are related to: the energy stored in the oscillation and energy dissipation to the crystals' mounting structure and contacting medium (i.e. viscous solutions and viscoelastic films); to the inertial forces related to mass dislocation; to the oscillation energy storage related to the crystal's elasticity; and to the parasitic capacitance due to electrodes, holding structure, cables, and electrical connections, respectively. The quantification of the BVD model parameters by impedance analysis enables thus the discrimination of the different contributions to the sensor signal (liquid loading, viscoeleasticity of films, mass, and charges) at the different analysis stages, therefore enabling the elimination of interfering signals (Encarnação et al., 2007).

In this work impedance analysis is used to identify and to eliminate QCM sensor interfering signals to develop piezoimmunosensors based on recombinant single-chain variable fragments (scFv) and recombinant single domain fragment antibodies. Single-chain variable fragments (scFv) are molecular assemblies of the two functional heavy-chain (V_H) and light-chain (V_L) variable domains of an antibody. These are the domains responsible for the recognition of the antigenic epitope and are usually covalently linked by a poly-peptide linker. scFvs have been recently used to develop piezoelectric immunosensors since they can be immobilized at high surface densities while maintaining the binding specificity and selectivity of monoclonal and polyclonal antibodies with reduced nonspecific contaminant trapping (Shen et al., 2005; O'Brien et al., 2000).

The target analyte used in this work is the HIV1 virion infectivity factor (Vif). HIV1 Vif is a ~23 kDa phosphorilated protein localized in the cytoplasm of HIV1 infected cells which is essential for viral replication and viral spread in peripheral blood lymphocytes, primary macrophages, as well as in T cell lines (Silva et al., 2004). HIV1 Vif enhances infectivity of virus particles through inhibition of intracellular antiviral defenses (Gonçalves and Santa-Marta, 2004) and was identified as potential target in antiviral therapy (Silva et al., 2004). A functional scFv (scFv-4BL), composed by heavy-chain 4BL-V_H and light-chain 4BL-V_L domains covalently linked through an 18 amino acid peptide, was previously generated towards HIV1 Vif to be used as an intrabody in antiviral therapy strategies (Goncalves et al., 2002).

Even though scFvs are the minimal construction derived from human antibodies necessary for antigen binding, antibodies from Camelids (camels, dromedaries, and llamas) are composed by two heavy-chains with no light-chain (Muyldermans et al., 2001). Single V_H domains derived from camelids are more soluble, more stable and have similar selectivities and affinities as compared to scFvs (Muyldermans et al., 2001). Therefore modified V_H chains of scFvs, mimicking camelids single domain fragments, have been investigated as minimal antigen binders (Muyldermans et al., 2001). In particular single anti-HIV1 Vif (4BL-V_H) and (4BL-V_HD) single domains were generated (Silva et al., 2004). The last was derived from 4BL-V_H by protein engineering to increase the single domain its hydrophilicity (Silva et al., 2004).

In this work we evaluate the usefulness of scFv-4BL, 4BL-V_H and 4BL-V_HD single domain antibodies to detect HIV1-Vif in order to generate anti HIV1 piezoimmunosensors. HIV1 virion incorporates 7–20 Vif molecules (Camaur and Trono, 1996) and thus Vif detection and monitoring of its variation in infected cells may be used to follow-up HIV1 infection.

2. Experimental section

2.1. Reagents

All chemicals and reagents were ultra-pure, pro-analysis, analytical, electrophoretic or equivalent high purity grade. All solutions were prepared using ultra-pure and low conductivity Milli-Q water.

Hydrochloric acid, Tris(hydroxymethyl)–aminomethan (Tris), sodium chloride, imidazole, oxygen peroxide, di-sodium-hydrogen-phosphate, potassium-di-hydrogen-phosphate and absolute ethanol were purchased from Merck-VWR. Acrylamide/Bis-acrylamide solution and Bio-Rad protein assay were purchased from BioRad. Dithio-bis-succinimidyl-undecanoate (DSU) and 11-hydroxy-1-undecanethiol (HUT) were purchased from Dojindo Laboratories. Anti-HA high affinity monoclonal antibody conjugated with peroxidase (HRP/anti-HA) were acquired from Roche. ECL detection kit was purchased from GE Healthcare.

2.2. Production of HIV1 Vif and anti-HIV1 Vif scFv-4Bl, 4Bl-V_H, and 4BL-V_HD

All expressed proteins contained hemagglutinin (HA) epitope and were tagged with His6. The HA-tag is recognized by horseradish peroxidase (HRP)/anti-HA monoclonal antibody conjugate, thus enabling protein detection by immunoassays, while His-tag enables protein purification by metal chelate affinity chromatography.

HIV1 virion infectivity factor (Vif) was cloned into pD10 bacterial expression vector and expressed in *E. coli* Top10F′ as described (Yang et al., 1996). The His6-Vif protein was recovered and purified from inclusion bodies by metal chelate affinity chromatography as previously published (Silva et al., 2004).

Anti-Vif single-chain variable fragment (scFv-4BL) and single domains 4BL-V_H and 4BL-V_HD were cloned and expressed in *E. coli* Top10F′ by induced expression of the pComb3X-4BL, pComb3X-VH and pComb3X-VHD plasmids as described earlier (Silva et al., 2004; Goncalves et al., 2002). The proteins were obtained from bacterial periplasmatic extracts as previously

published (Goncalves et al., 2002) as well as from the culture medium. The culture medium was clarified by centrifugation ($4000 \times g$, 30 min, 4 °C), and dialfiltrated against 20×10^{-3} M Tris buffer pH 8 containing 0.5 M NaCl in a 10 kDa cut-off Millipore Pellicon XL ultrafiltration membrane to a final 10-fold protein concentration factor. The concentrated proteins were further purified in Ni(II) chelating sepharose fast flow XK16 column (GE healthcare), packed to 2.5 cm bed height. After elution with 0.1 M imidazole, scFv-4BL, 4BL-V_H, and 4BL-V_HD were concentrated with 10 kDa cut-off centricons (Millipore) and desalted in a HyTrap Desalting column (GE healthcare).

Protein concentration was assessed using the Bio-Rad BCA protein assay kit, and protein purity was assessed by SDS-PAGE and Western blot analysis. Western blots using HRP/anti-HA monoclonal antibody conjugates were autoradiographed with the chemiluminescent ECL-Plus kit (GE healthcare) according to the manufacturer instructions.

2.3. Expression of HIV1-Vif in HEK 293 T cells and preparation of cell extracts

HIV1-Vif was cloned in the pAmCyan1-N1 expression vector (Clontech). Briefly HIV1-Vif gene was amplified from the ector pD10Vif using the primers:

- Forward: TCAGATCTCGAGCTGAAAACAGATGGCAGGTGATG
- Reverse: TCTAGTGGATCCGTGTCCATTCGTTGTATGGCT.

Amplified DNA fragments were purified from agarose gels, digested with the restriction enzymes BamHI/XbaI, and further cloned by compatible ends into the vector pAmCyan1-N1 (previously digested with the same restriction enzymes). The expression vector pAmCyan1-N1/Vif was hence obtained were HIV1 Vif is linked to the N-terminal of the *Anemonia majano* cyan fluorescent protein, expressed as a fusion protein under the control of the CMV promoter.

Human embryonic kidney cells (293T) were grown in Dulbecco's Modified Eagle's Medium supplemented with 2 mM L-glutamine, 10% fetal calf serum, 100 μg/ml of penicillin and streptomycin, and 0.25 μg/ml of fungizone. When a 7.5×10^5 cells/well cell density was achieved, the cells were transfected with 1 μg of pAmCyan1-N1/Vif expression vector using Fugene six reagent (Roche) according to the manufacturer's instruction. The transfected cells were kept in culture for additional 48 h at 37 °C in a 5% CO_2 atmosphere with 95% relative humidity. The cells were then washed with PBS, detached from the culture T-flasks using PBS flux, and recovered by centrifugation at $1000 \times g$ and 4 °C.

Cell extracts were prepared by freeze-thaw (freezing at −80 °C, incubation at 25 °C and vortexing) and clarified by centrifugation at $16{,}000 \times g$ at room temperature.

Protein expression was visualized during cell culture by monitoring the emission of the cyan fluorescent protein in a Leica DM IL inverted microscope.

2.4. Quartz crystal sensors activation and functionalization

One inch diameter 5 MHz AT-cut quartz crystals, coated with optically polished gold electrodes on both sides, and with a 0.4 cm^2 active area were purchased from Standford Research Systems (SRS, Standford, USA). The crystals were cleaned by rinsing with absolute ethanol and Milli-Q water and immersed in Piranha solution (30% (v/v), H_2O_2:H_2SO_4 (1:3)) for 15 min, to obtain a clean Au surface. Cleaned crystals were then rinsed with water, dried under nitrogen flow, and activated with 30 μl of a 100 μM Dimethilformamide (DMF) solution of dithiobis-succinimidyl undecanoate (DSU) (2 h incubation at room temperature in a saturated atmosphere). Unbounded DSU was removed by washing the activated crystal sensors sequentially with DMF and Milli-Q water. Activated sensors were dried under nitrogen flow and incubated for additional 2 h at room temperature with 50 μL of a 50 μM 11-hidroxy-1-undecanothiol (HUT) ethanolic solution in a saturated atmosphere, washed sequentially with absolute ethanol and Milli-Q water, and dried under nitrogen flow. Purified scFv-4BL, 4BL-V_H, or 4BL-V_HD were then attached to the surface of activated sensor surfaces. Thirty microliters of purified protein solution at 200 μg/ml in phosphate buffer saline (PBS-0.1 M phosphate buffer pH 7.4 containing 0.1 M NaCl) were pipetted over the activated sensor surface and left to react for 2 h at room temperature in a saturated atmosphere. Unbounded proteins were removed by washing sequentially with PBS buffer and Milli-Q water, and the remaining unreacted binding sites at the sensor surface were further blocked with ethanolamine.

2.5. Piezoimmunosenor experimental set-up

Crystal sensors were assembled on a Kynar crystal holder (SRS) with a home made acrylic cover to generate a 300 μl flow cell just exposing one face of the sensor to the solution. Viton O-rings were placed underneath the sensor to seal the flow cell to avoid wetting or flooding the electrical contacts located on the bottom of the crystal holder. A closed fluidic circuit was mounted using Tygon tubing to connect the flow cell to an agitated container where all the samples were applied. The total volume of the system was 2 ml and the solutions were re-circulated in the system at a flow rate of 1.5 ml min^{-1} controlled by a Watson–Marlow peristaltic pump. Both the flow cell and the container were installed in a home made 1 l jacketed beaker maintained at 30.0 ± 0.1 °C by means of a Thermo Haake temperature controller.

The resonance frequency and impedance spectra were recorded alternatively with a QCM100 Controller and a QCM25 Oscillator (SRS) connected to a Pendulum CNT- 66 frequency counter and a RF HP8712C Network/Spectrum/Impedance Analyzer, respectively. Both the Network/Spectrum/Impedance Analyzer and the QCM25 Oscillator were electrically connected to the crystal holder through a switch used to select the desired measurement mode (shielded coaxial cables were used in all electrical connections to minimize signal instability arising from electrical interference). The instruments were interfaced with a computer through IEEE boards, and a Pascal program was

written to control the operation and to acquire experimental data.

Impedance spectra were obtained using a 10 kHz frequency span centred near the crystal's resonant frequency with 16 spectra averaging at 1 Hz resolution. The BVD equivalent circuit parameters—inductance (XL), resistance (R), and capacitance (C_0)—were obtained from the experimental data by fitting the conductance function with the help of Matlab, as described (Encarnação et al., 2007)—see supporting information for further details.

2.6. Electrochemical characterization

Cyclic voltammetry (CV) was performed using a PalmSense potentiostat, biased to gold electrode of the quartz crystal sensor. A normal three-electrode configuration consisting of a modified quartz crystal (working electrode), a homemade Ag/AgCl reference electrode, and a platinum counter electrode was used. PBS buffer was used as the supporting electrolyte which was deoxygenated using a nitrogen gas purge for 20 min. CV was performed between −0.75 and 0.9 V at a 0.1 V/s scan rate in the presence of 4×10^{-3} M of $K_3[Fe(CN)_6]$.

2.7. Atomic force and scanning electron microscopy surface characterization

Samples were imaged by a Nanoscope III Digital Instrument in the tapping mode using an Si_3N_4 tip cantilever. The cantilever oscillation frequency was set at 300 kHz. Tips of the cantilever were characterised by the radius of their curvature equal to 792 nm. No computer filtering procedure was used to treat the images. Tapping mode imaging was recorded with 256 pixels per line with a scan rate of 1.0 Hz. Surface roughness (Ra) was determined at the same scale (2 μm) for each sample.

Scanning electron microscopy (SEM) micro-analysis was carried out on gold coated samples, using a Cambridge Stereoscan 120 instrument operating at an accelerating voltage of 20 kV.

3. Results and discussion

3.1. Purification of HIV1-Vif and anti-Vif recombinant antibodies

HIV1 Vif and anti-Vif scFv-4BL, and 4BL-V_H and 4BL-V_HD single domains were purified by metal chelate affinity chromatography using a Ni(II) Sepharose column. Purified proteins were analyzed using silver stained SDS-PAGE and Western blot to evaluate their purity and integrity. As shown in Fig. 1, under reducing conditions, scFv-4BL, 4BL-V_H and 4BL-V_HD migrate as single bands with the expected molecular weight as predicted from the proteins primary structure: scFv-4BL∼29,000 Da; 4BL-V_H∼12,729 Da; and 4BL-V_HD∼12,733 Da. Western blot analysis (Fig. 1) reveals no degradation or multimerization of the purified proteins. On the other hand, regarding purified HIV1 Vif, both SDS-PAGE and Western blots show a major band migrating with the expected MW (∼23,000 Da) together with multimeric forms and degradation products originated from possible protein conjugation and degradation processes occurring in the inclusion bodies, or during protein refolding. A densitometry analysis of the lane show that 75% of the proteins detected in the Western blots correspond to monomeric Vif forms. Unfortunately, this was the best purity level achieved due to HIV1 Vif tendency to aggregate. This fraction was thus used as target antigen in the following studies.

3.2. Sensor activation

The formation of self-assembled monolayers (SAM) on gold surfaces offers one of the simplest ways to generate a reproducible, thin and well-ordered layer, which is suitable for further modification with proteins (Mayes, 2002; Schlereth, 2005; Zaugg and Spencer, 1999). Particularly, the generation of mixed SAMs of hydroxyalkanethiols and alkanethiols with specific functional groups (e.g. carboxyl, succinimidyl) is considered the most favorable option since it results in a flexible and uncharged environment, rich in hydroxyl groups, with the required surface modification for protein anchorage (Mayes,

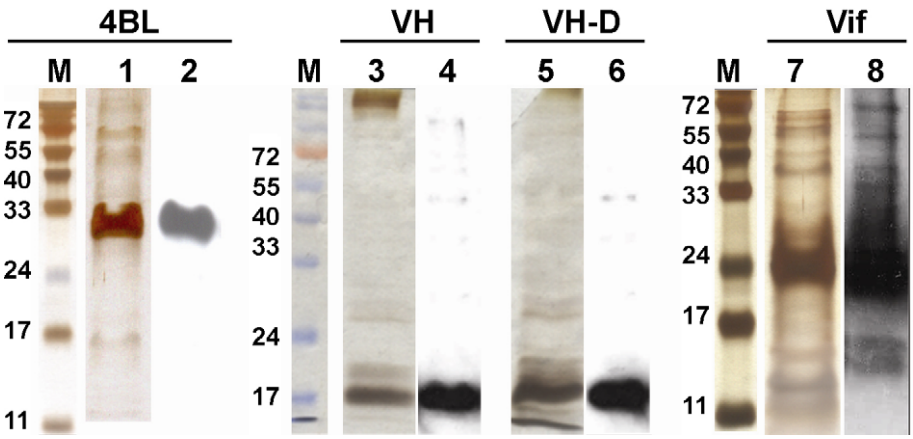

Fig. 1. Silver-stained SDS-PAGE of purified scFv-4BL (lane 1), 4BL-V_H (lane 3), 4BL-V_HD (lane 5) and Vif (lane 7) and respective Western blot autoradiographs (lanes 2, 4, 6, and 8); M—molecular weight markers.

2002; Schlereth, 2005). Additionally, such mixed SAMs result in highly hydrated and unionized surface at physiological conditions, thus minimizing the possibility of nonspecific protein binding through hydrophobic or electrostatic interactions, as well as reducing the degree of protein unfolding and denaturation (Mayes, 2002). Hence, similarly to previous published works (Zaugg and Spencer, 1999), our option was to activate the quartz crystal sensors with a mixed SAM of DSU and HUT. DSU was initially deposited and self assembled onto clean sensor surfaces, generating an oriented monolayer with exposed succinimidyl groups. HUT was then deposited in order to fully cover the gold surface by filling eventual monolayer defects (e.g. gaps) resulting from steric hindrance effects during DSU deposition.

The formation of a mixed SAM was verified by atomic force microscopy (AFM), scanning electron microscopy (SEM) and by cyclic voltammetry (CV)—Fig. 2. Compared to unmodified sensor gold surfaces, which revealed a grainy topography of ~20 nm size (panel (i)-Fig. 2a), AFM imaging of DSU modified gold surfaces resulted in similar micrographs (Fig. 2a). Nevertheless, the presence of the adsorbed monolayer was identified by the variation of the image sharpness (panel (ii), Fig. 2a), resulting from the interferences caused by adsorbed organic molecules in the contact tip. The formation of DSU SAM was ultimately confirmed by SEM micrographs (Fig. 2b) showing a typical dendrimer structure of adsorbed alkanethiols derivatives (Kang et al., 2005).

The integrity of the SAM assembled at the sensors surface was further probed by cyclic voltammetry in the presence of electrochemically active $[Fe(CN)_6]^{3+}$. Considering that electron tunneling in monolayers of alkanethiols with similar lengths as the ones used, results in negligible current intensities (Wang et al., 2003), electron transfer between electrochemically active species and the electrode may only occur through holes or defects in the monolayer. Therefore, although a considerable attenuation of the faradic current is observed for DSU SAM (Fig. 2c), as compared with unmodified sensors, $[Fe(CN)_6]^{4+}/[Fe(CN)_6]^{3+}$ redox peaks are still observed which indicate the existence of exposed electrode areas corresponding to SAM defects. Fig. 2c also shows that full electrode passivation and insulation is achieved with the subsequent deposition of HUT. These cyclic voltammetry experiments demonstrate that uniform SAMs (e.g without holes) are generated with a combination of DSU and HUT which presents a barrier to electrochemically active species.

3.3. Immobilization of scFv-4BL, 4BL-V_H, and 4BL-V_HD

Quartz crystal sensors activated with the mixed DSU/HUT SAMs were assembled onto the sensor flow cell and the experimental setup was used to follow the immobilization of scFv-4BL, 4BL-V_H, and 4BL-V_HD. PBS solutions with increasing concentrations (50×10^{-6} to 200×10^{-6} g/ml) of scFv-4BL, 4BL-V_H, or 4BL-V_HD were recirculated over the

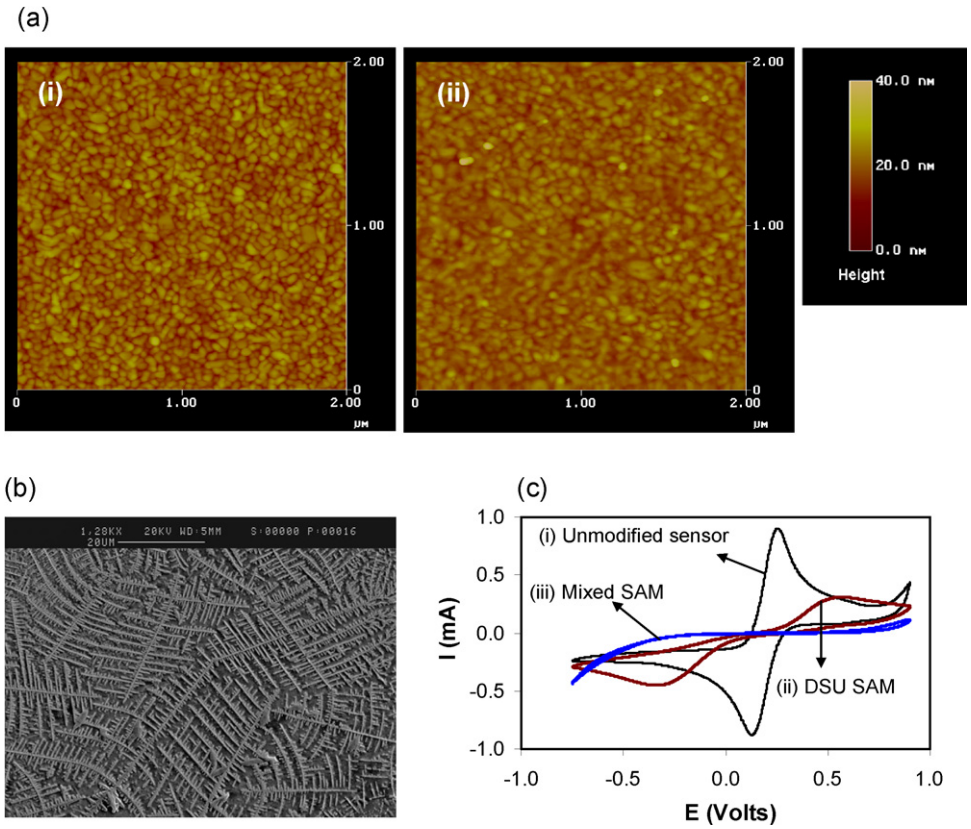

Fig. 2. Characterization of activated sensors. (a) Atomic force microscopy at 1 Hz scan rate of unmodified – panel (i) – and DSU activated – panel (ii) – gold-coated QCM crystals. (b) SEM micrograph of DSU-Gold dendrites formed on the sensor surface after adsorption of DSU. (c) Cyclic voltammograms (scan rate 100 mV/s) of (i) unmodified sensors, (ii) sensors activated with DSU, and (iii) sensors with a mixed DSU and HUT SAM.

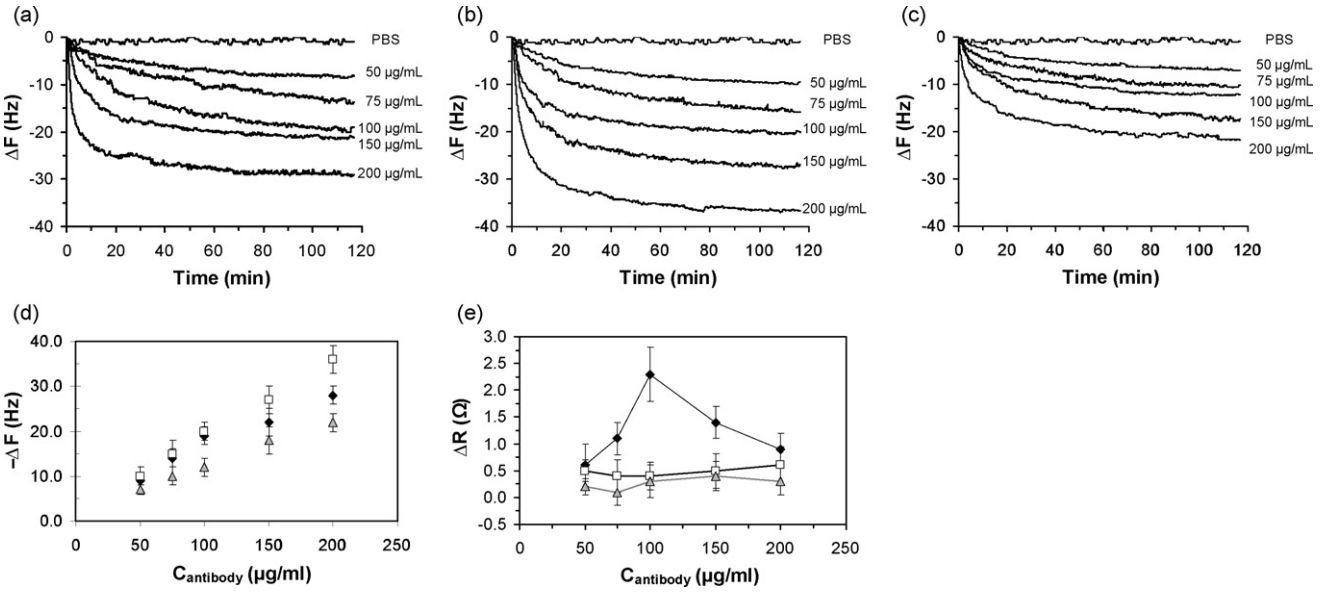

Fig. 3. Immobilization of the recombinant proteins on the surface of activated sensors. Measured resonance frequency variation during antibody immobilization using solutions of increasing concentration of (a) anti-Vif scFv-4BL, (b) anti-Vif 4BL-V_H single domain, and (c) anti-Vif 4BL-V_HD single domain; (d) immobilization isotherms of scFv-4BL, 4BL-V_H, and 4BL-V_HD; and (e) total variation of the resonator resistance obtained after at the equilibrium for immobilization of (♦) scFv-4BL, (□) 4BL-V_H and (▲) 4BL-V_HD.

activated sensors and the resonance frequency variation over time was monitored (Fig. 3a–c). As shown, no saturation of the sensor was achieved within the concentrations evaluated, and the immobilization of the proteins followed a linear isotherm (Fig. 3d).

The amount of immobilized protein in each experiment can be estimated from the total frequency variation provided that the Sauerbrey relationship is valid. However, as mentioned earlier, measurements of resonance frequency variation in quartz crystal resonators are known to be affected by viscoelastic effects, both from solution and adsorbed films (Etchenique and Weisz, 1999; Lucklum and Hauptmann, 2000; Kanazawa and Gordon, 1985; Martin et al., 1991), as well as by the presence of electrolytes and local charge variations (Etchenique and Buhse, 2000; Ghafouri and Thompson, 2001; Encarnação et al., 2007). These interferences limit the use of quartz crystal sensors for analytical detection and quantification of biological material mass in liquid phase. Acoustic impedance analysis of the resonator enables the isolation and quantification of such interfering signals. As was shown recently (Encarnação et al., 2007), the measured frequency variation (Δf_T) is the total of the contributions of mass loading (Δf_M), viscoelasticity (Δf_V), and charge interference (Δf_C): $\Delta f_T = \Delta f_M + \Delta f_V + \Delta f_C$. The use of experimental correlations to quantify Δf_V (Martin et al., 1991) and Δf_C (Encarnação et al., 2007), translated to $\Delta f_V = 2.4 \times \Delta R$ and $\Delta f_C = 8 \times 10^{12} \Delta C_0$ for the sensors used in this study, respectively, allowed the elimination of interfering signals from experimental data and the quantification of the adsorbed mass through the application of the Sauerbrey relationship.

Acoustic impedance analysis and equivalent electrical circuit modeling were used to determine simultaneously the acoustic impedance parameters of the resonators (R, XL, and C_0) – Fig. 3e and Fig. S-2 in the supporting information. As expected, the resonator inductance (XL) increased upon protein immobilization as an indication of mass deposition at the sensor surface (Fig. S-2). Viscoelastic (Martin et al., 1991) and charge interferences (Encarnação et al., 2007) were identified by variations of the resonator resistance (R) and capacitance (C_0), respectively. No capacitance variation was measured during the immobilization of all proteins within the concentration range investigated (Fig. S-2), which indicates that charge interferences are negligible. On the other hand, the resonator resistive component was found unchanged only for 4BL-V_H and 4BL-V_HD single domains for all tested concentrations (Fig. 3e). This indicates that immobilized 4BL-V_H and 4BL-V_HD behave as a rigid film and thus the amount of immobilized protein can be analytically quantified from frequency variation data through the Sauerbrey relationship. A different conclusion is taken for the immobilization of scFv-4BL. As shown in Fig. 3e the resonator is characterized by variations of the resistive component with a protein concentration dependency. Viscoelastic interference cannot be neglected and its contribution to the total frequency variation has to be accounted if the quantification of immobilized protein is aimed. Since scFv-4BL contain two domains attached by a linker, we hypothesize that immobilized scFv-4BL has some flexibility which results in acoustic energy losses and hence in viscoelastic interferences (as indicated by the increasing resistance variation) – Fig. 3e. As the surface density of immobilized scFv-4BL increases, higher packaging is achieved resulting in a stereochemical induced rigidity, hence, to the decrease of the resonator resistance variation observed (Fig. 3e).

Considering the linear immobilization isotherm (Fig. 3d), it was decided to use a 200 µg/ml concentration of scFv-4BL, 4BL-V_H and 4BL-V_HD to functionalize the sensors. Higher immobilized surface densities are achieved for this

concentration which after eliminating the interfering signals, are calculated as 462 ± 40, 615 ± 50, and 377 ± 40 ng cm^{-2}, for scFv-4BL, 4BL-V_H and 4BL-V_HD modified sensors, respectively.

3.4. Selective detection of HIV1 Vif

The performance of the sensors functionalized with scFv-4BL, 4BL-V_H, and 4BL-V_HD to detect the target antigen (Vif) was evaluated. PBS buffer was recirculated over the surface of scFV-4BL, 4BL-V_H, or 4BL-V_HD modified sensors. Upon stabilization of the measured frequency signal, increasing concentrations of Vif were applied and the sensor resonance frequency was monitored over time until the equilibrium was reached (Fig. 4). To evaluate the selectivity for the target antigen, the modified sensors were challenged with protein solutions without Vif. As shown in Fig. 4 no frequency variation is observed when 100 μg/ml cytochrome C, BSA, or ribonuclease A are applied. Unspecific binding of Vif to the mixed SAM monolayer was also evaluated using activated sensors with no immobilized proteins, in which case no frequency variations were monitored (not shown). Taken together, these controls demonstrate the selectivity of immobilized biofilms of scFv-4BL, 4BL-V_H and 4BL-V_HD to detect Vif.

Fig. 4 also reveals that scFv-4BL, 4BL-V_H and 4BL-V_HD modified sensors detect the target antigen differently. While similar frequency variations are obtained for scFv-4BL (Fig. 4a) and 4BL-V_HD (Fig. 4c) biofilms, approximately half the signal is achieved with single domain 4BL-V_H biofilms (Fig. 4b) in similar conditions. The apparent contradiction with the calculated immobilized antibody surface density can be explained considering the more hydrophobic character of this protein. The grand average of hydropathicity (GRAVY) is a factor used to measure the tendency of proteins to seek an aqueous or a hydrophobic environment, with greater GRAVYs corresponding to higher hydrophocic character of the proteins (Kyte and Doolittle, 1982). A bioinformatic analysis of the recombinant antibodies sequences (ProtParam at http://www.expasy.org) calculate GRAVYs as −0.113, −0.247, and −0.214, for 4BL-V_H, 4BL-V_HD and scFv-4BL, respectively. We therefore hypothesize that the higher hydrophobicity of 4BL-V_H molecules results in a surface orientation were the molecule antigen recognition regions are oriented in such a way that they become closer to the hydrophobic aliphatic chains of the SAMs. As such 4BL-V_H antigen binding sites are hindered and less antigen binds to the biofilm. On the other hand, when using 4BL-V_HD single domains, which are derived from 4BL-V_H single domains by protein engineering (Silva et al., 2004) resulting in a ~2.2-fold increase of the hydrophilicity, as indicated by the GRAVY factor, higher frequency variation signals were measured. In addition to the surface density data, this indicates that more antigen binding sites are exposed.

The data obtained for the selective detection of HIV1 Vif is consistent with qualitative ELISA analysis (Silva et al., 2004). As shown (Fig. 4d), the measured signal for QCM sensors modified with 4BL-V_H single domains is considerably lower (<3-fold) then the one measured with anti-Vif scFv-4BL modified sensors. Furthermore, the signal obtained with single domain antibodies is considerably improved when using the more hydrophilic 4BL-V_HD single domain, in which case signals of similar order of magnitude as scFv-4BL were measured. The minimum amount of Vif detected with scFv-4BL, 4BL-V_H, and 4BL-V_{HD} was calculated from the sensors' analytical sensitivity as 0.3, 1.1, and 0.47 μM, respectively.

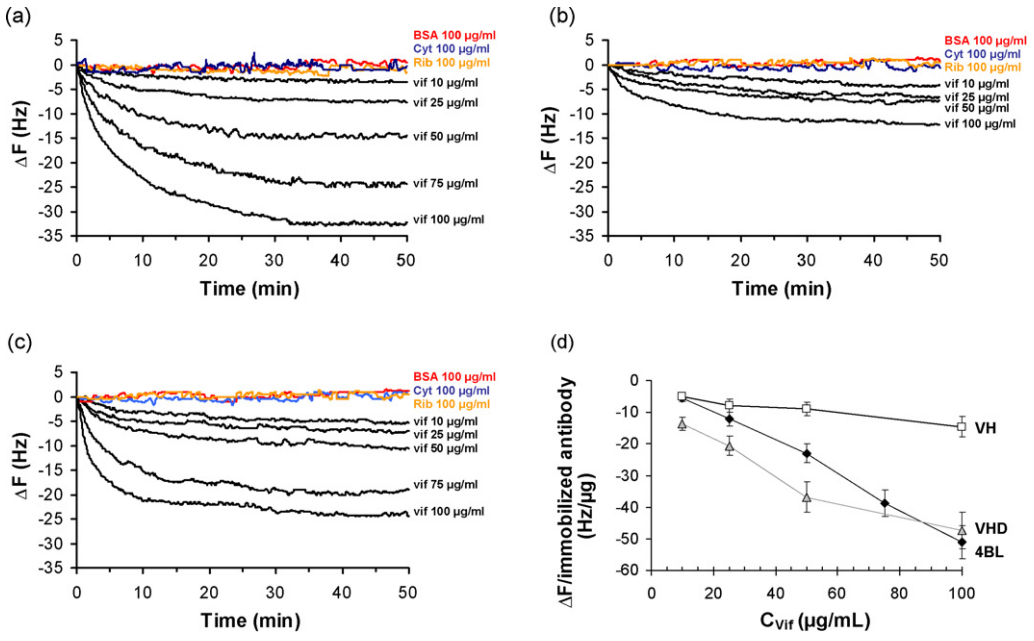

Fig. 4. Binding of HIV1 Vif preparations of increasing concentrations to sensors modified with (a) anti-Vif scFV-4BL, (b) anti-Vif single domain antibody 4BL-V_H and (c) anti-Vif single domain antibody 4BL-V_HD. The data presented correspond to average transients from $n = 6$ independent measurements for each Vif concentration. Indicated concentrations refer to total protein quantification in purified HIV1 Vif preparations and not to HIV1 Vif monomeric isoforms. Cytochrom C, BSA, and Ribonuclease A, all at a concentration of 100 μg/ml, were used as controls.

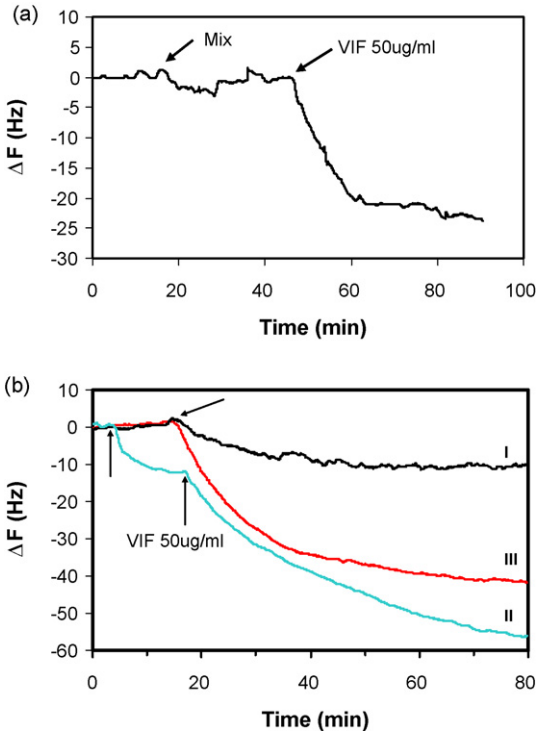

Fig. 5. Detection of HIV1 Vif in complex mixtures with V_HD camelized single domain antibody piezoimmunosensors. Arrows indicate the moment of sample application to the sensor. (a) A mixture of 100 μg/ml BSA, Cytochrome C, and Ribonuclease A was added to the crystal and the frequency was monitored for a period of time before spiking with 50 μg/ml HIV1 Vif preparation; (b) sensor response obtained for cell extracts: HEK293T cell extracts from the control cell cultures (cells only expressing CFP) were applied to the sensor (curve I) and spiked with 50 μg/ml HIV1 Vif preparation (curve II). Curve III shows the sensor response obtained for cell extracts of HEK293T expressing Vif.

3.5. Detection of HIV1 Vif in complex mixtures

The data presented show that piezoelectric sensors modified with scFv-4BL, 4BL-V_H and 4BL-V_HD are able to selectively recognize HIV1 Vif in solution. The detection of target analyte in complex mixtures constitutes a step further towards the eventual applicability of HIV1 Vif immunosensors to real-life situations such as in the follow-up of HIV1 clearance during antiretroviral therapy. We selected the 4BL-V_HD modified sensor and challenged it with a mixture of pure proteins and with cellular extracts obtained from HIV1 Vif producing animal cell cultures (Fig. 5). A 50 ug/ml HIV1-Vif preparation spike to a mixture of BSA, cytochrome C and ribonuclease results in a frequency variation of ∼23 Hz (Fig. 5a), which constitutes a further evidence of the sensor selectivity. Going further in increasing the analyte complexity, a ∼10 Hz frequency variation was measured when the sensor was challenged with cell extracts obtained from control cell cultures – Fig. 5b and Fig. S-3 in the supplementary information. Although this might reveal eventual unspecific binding of components from such complex mixture, impedance analysis showed a major signal contribution (up to 7 Hz) from viscoelastic interferences. A spike of HIV1 Vif preparation (Fig. 5b), as before, results in a ∼5-fold increase of the measured frequency variation as the protein is specifically recognized and binds to the 4BL-V_HD single domain immunosensor. Fig. 5b also shows that the anti-HIV1 Vif immunosensor developed in this work detects the presence of HIV Vif in cell extracts from cell cultures expressing this protein intracellularly (see also Fig. S-3). Considering that cells expressing HIV1 Vif intracellularly were used to mimic HIV1 infected cells, the ∼4-fold increase in the measured frequency variation, as compared with the control cell extracts, is an additional evidence of the immunosensor selectivity and of its ability to recognize HIV1 Vif in complex cellular mixtures.

4. Conclusions

In this work piezoelectric immunosensors based on scFvs and single domain recombinant antibodies were developed to recognize HIV1 virion infectivity factor (Vif). All modified sensors were able to selectively recognize HIV1 Vif. The sensors were stable and antigen specific even when using complex protein mixtures.

Quantitative analysis was possible by measuring simultaneously both the sensors resonant frequency variation and the acoustic impedance. Interfering signals from viscoelastic forces and electroacoustic coupling effects were identified and quantified. Frequency variation data was corrected accordingly in order to enable the use of the Sauerbrey relationship for the analytical quantification of the mass adsorbed at the sensor surface. An additional advantage of acoustic impedance analysis is that, to some extent, structural aspects of the immobilized antibodies can be derived. In particular insights were taken regarding the molecule-to-surface orientation. Furthermore, the methodology described in this paper, as shown for the 4BL-V_HD single domain modified sensor, was effective in the detection of HIV1 Vif in human cell extracts.

Unfortunately it was not possible to obtain HIV1 Vif preparations with higher purity owing to the protein tendency to aggregate. This results in uncertainties in the quantification of HIV1 Vif monomers which disables any attempt to quantify the amount of protein from the measured frequency variation data. As a consequence, eventhough kinetic models could be applied and fitted to the experimental data set presented in this paper, accurate binding constants could not be estimated. Nevertheless, we have shown that HIV1 Vif protein can be detected specifically by piezoelectric sensors modified with single-chain fragments and single domain antibodies. Although being semi-quantitative, the results demonstrate the potential use of anti-HIV1 Vif 4BL-V_HD to recognize specifically this viral protein in complex cellular extracts. Finally we have demonstrated the potential use of the piezoelectric immunosensors developed in this paper as a HIV1 biosensor.

5. Supplementary material available

A description of the impedance analysis methodology, including the sensor BVD circuit model and the variation of the BVD parameters measured during antibody immobilization is available as 5 pages Supporting Information. SI also includes a brief description of the rationale involved in the expression

of HIV1 Vif in HEK293 cell cultures, indication of the controls, and photomicrographs of cell cultrures. Current ordering information is found on any masthead page.

Acknowledgments

This work was supported by the Portuguese Science Foundation an organism of the Portuguese Ministry of Science and Higher Education. Contract number POCI/BIO/61912/2004 is acknowledged. PhD grant number SFHR/BD/12772/2003 to J.M. Encarnação is also acknowledged.

Appendix A. Supplementary data

Supplementary data associated with this article can be found, in the online version, at doi:10.1016/j.bios.2007.04.022.

References

Auge, J., Hauptmann, P., Hartmann, J., Rösler, S., Lucklum, R., 1995. Sens. Actuator B 24, 43–48.
Bouche-Pillon, D., Gabrielli, C., Perrot, H., 1995. Sens. Actuator B 25, 257–259.
Camaur, D., Trono, D., 1996. J. Virol. 70, 6106–6111.
Encarnação, J., Stallinga, P., Ferreira, G.N.M., 2007. Biosens. Bioelectron. 22, 1351–1358.
Etchenique, R., Brudny, V.L., 2000. Langmuir 16, 5064–5071.
Etchenique, R., Buhse, T., 2000. Analyst 125, 785–787.
Etchenique, R., Weisz, A.D., 1999. J. Appl. Phys. 86, 1994–2000.
Ghafouri, S., Thompson, M., 2001. Analyst 126, 2159–2167.
Gonçalves, J., Santa-Marta, M., 2004. Rectrovirology 1, 28.
Goncalves, J., Silva, F., Freitas-Vieira, A., Santa-Marta, M., Malhó, R., Yang, X., Gabuzda, D., Barbas, C., 2002. J. Biol. Chem. 277, 32036–32045.
Kanazawa, K.K., Gordon, J.G., 1985. Anal. Chim. Acta 175, 99–105.
Kang, Z., Wang, E., Lian, S., Mao, B., Chen, L., Xu, L., 2005. Mater. Lett. 59, 2289–2291.
Kyte, J., Doolittle, R.F., 1982. J. Mol. Biol. 157, 105–132.
Liu, Y., Zhang, W., Yu, X., Zhang, H., Zhao, R., Shangguan, D., Li, Y., Shen, B., Liu, G., 2004. Sens. Actuator 99, 416–426.
Lucklum, R., Hauptmann, P., 2000. Sens. Actuator B 70, 30–36.
Martin, S.J., Granstaff, V.E., Frye, G.C., 1991. Anal. Chem. 63, 2272–2281.
Mayes, A.G., 2002. In: Gizeli, E., Lowe, C.R. (Eds.), Biomolecular Sensors. Taylor and Francies, London.
Modin, C., Stranne, A.-L., Foss, M., Duch, M., Justesen, J., Chevallier, J., Andersen, L.K., Hemmersam, A.G., Pedersen, F.S., Besenbacher, F., 2006. Biomaterials 27, 1346–1354.
Muyldermans, S., Cambillau, C., Wyns, L., 2001. Trends Biochem. Sci. 25, 230–235.
O'Brien, J.C., Jomes, V.W., Porter, M.D., 2000. Anal. Chem. 72, 703–710.
Ogi, H., Motoshisa, K., Takashi, M., HataNavak, K., Hirao, M., 2006. Anal. Chem. 78, 6903–6909.
Pan, W., Durning, C.J., Turro, N.J., 1996. Langmuir 12, 4469–4473.
Schlereth, D.D., 2005. In: Gorton, L. (Ed.), Biosensors and Modern Analytical Techniques. Elsevier, Amsterdam.
Shen, Z., Stryker, G.A., Mernaugh, R.L., Yu, L., Yan, H., Zeng, X., 2005. Anal. Chem. 77, 797–805.
Silva, F., Santa-Marta, M., Freitas-Vieira, A., Mascarenhas, P., Barahona, I., Moniz-Pereira, J., Gabuzda, D., Goncalves, J., 2004. J. Mol. Biol. 340, 525–542.
Su, X.-L., Li, Y., 2005. Biosens. Bioelectron. 21, 840–848.
Wang, W., Lee, T., Reed, M.A., 2003. Phys. Rev. B 68, 354161–354167.
Wu, T.-Z., Su, C.-C., Chen, L.-K., Yang, H.-H., Tai, D.-F., Peng, K.-C., 2005. Biosens. Bioelectron. 21, 689–695.
Yang, M., Yau, H.C.M., Chan, H.L., 1998. Langmuir 14, 6121–6129.
Yang, X., Gonçalvez, J., Gabuzda, D., 1996. J. Biol. Chem. 271, 10121–10129.
Zaugg, F.G., Spencer, N.D., 1999. J. Mat. Sci. 10, 255–263.
Zhou, A., Zhang, J., Xie, Q., Yao, S., 2000. Sens. Actuator B 67, 68–75.

Available online at www.sciencedirect.com
ScienceDirect
Journal of Biotechnology 132 (2007) 142–148
Journal of BIOTECHNOLOGY
www.elsevier.com/locate/jbiotec

Piezoelectric biosensors for biorecognition analysis: Application to the kinetic study of HIV-1 Vif protein binding to recombinant antibodies

João M. Encarnação [a], Luis Rosa [a], Rogério Rodrigues [a], Luisa Pedro [a], Frederico Aires da Silva [b], João Gonçalves [b], Guilherme N.M. Ferreira [a,*]

[a] *Institute for Biotechnology and Bioengineering (IBB), Centro de Biomedicina Molecular e Estrutural, Universidade do Algarve, 8000 Faro, Portugal*
[b] *URIA-Centro de Patógenese Molecular, Faculdade de Farmácia, Universidade de Lisboa, Portugal*

Received 29 December 2006; received in revised form 4 April 2007; accepted 19 April 2007

Abstract

In this work three piezoelectric sensors modified with anti-HIV-1 Vif (virion infectivity factor) single fragment antibodies (4BL scFV), single domains (VH) and camelized single domains (VHD) were constructed and used to detect HIV1 Vif in liquid samples. Dithio-bis-succinimidyl-undecanoate (DSU) and 11-hydroxy-1-undecanethiol (HUT) mixed self assembled monolayers (SAM) were generated at the sensors surface onto which the antibodies were immobilized. All sensors detected specifically the target HIV1-Vif antigen in solution and no unspecific binding was monitored. Impedance analysis was performed to quantify electroacoustic and viscoelastic interferences during antibody immobilization and antigen recognition. The elimination of such interferences enabled the quantitative use of the piezoelectric immunosensors to estimate the antibody surface density as well as antigen binding and equilibrium constants. In spite of the possible limitation regarding mass transport and other related molecular phenomena, which were not considered in the binding model used, this work demonstrates the usefulness of piezoelectric biosensors in biorecognition analysis and evidences the advantages on using simultaneous impedance analysis to bring analytical significance to measured data, and thus to improve piezoelectric sensors sensitivity and applicability.

Keywords: Biosensors; Piezoelectric; Impedance analysis; Self assembled monolayer; Recombinant antibodies; Rate constants

1. Introduction

Biosensors are analytical devices in which biomolecules (e.g. antibodies, DNA, receptors, enzymes) are interfaced to signal transducers to measure binding events. Biosensors have important medical, environment, public safety, and defence applications. The ideal biosensor would be sensitive, rapid, reliable, robust, and inexpensive. The use of biosensors for biomolecule detection often employ absorbance, fluorescence, amperometric, or radiochemical transduction mechanisms. Such approaches require labeling the samples with appropriate reporter groups to detect indirectly the analytes. The use of labeled targets, however, generally results in additional preparative steps and higher overall costs, and constitutes a possible source of error, irreproducibility, and contamination, being thus detrimental to the sensitivity of the overall (bio)recognition analysis. Several techniques have been developed aiming the direct detection of analytes in immunoassays. Piezoelectric transduction enables label free detection of biorecognition events and has been used in microgravimetric devices, generally known as quartz crystal microbalance (QCM), for different applications (Pan et al., 1996; Yang et al., 1998; Etchenique and Brudny, 2000; Ewalt et al., 2001; Liss et al., 2002; Liu et al., 2004; Fabreguette et al., 2005; Su and Li, 2005; Modin et al., 2006). Piezoimmunosensors are biosensors which use antibodies and a quartz crystal microbalance to detect mass changes as antigens bind to antibodies immobilized on the QCM surface.

The basis for piezoelectric transduction in QCM biosensors is the variation of the quartz resonance frequency occurring upon mass deposition onto the crystal surface. For rigid and uniform films strongly coupled to the resonator surface the piezoelectric transduction gives a direct response signal that characterizes binding events. In such cases, the mass change occurring at the surface of the sensors is estimated using the Sauerbrey

* Corresponding author. Fax: +351 289818419.
E-mail address: gferrei@ualg.pt (G.N.M. Ferreira).

0168-1656/$ – see front matter © 2007 Elsevier B.V. All rights reserved.
doi:10.1016/j.jbiotec.2007.04.010

equation, $\Delta f_m = [-2nf_0^2/(\rho_q\mu_q)^{1/2}] \times [\Delta m/A]$, where Δf_m is the frequency change due to mass loading, f_0 is the resonant frequency of the fundamental mode, n is the harmonic or overtone number, ρ_q and μ_q are, respectively, the density and the shear mode of the crystal (Sauerbrey, 1959). Although their potential is theoretically quite high, in practice, the usefulness of piezoelectric sensors and thus their applicability as biosensors have been limited due to the complexity of the physical properties of aqueous environments which renders difficult the establishment of such an explicit relationship between the added mass and a change in the resonant frequency. QCM is known to respond to the viscoelasticity properties both of adsorbed films and aqueous environment (Martin et al., 1991; Etchenique and Weisz, 1999; Lucklum and Hauptmann, 2000) as well as to variations of charges near the sensor surface (Etchenique and Buhse, 2002; Etchenique and Buhse, 2000; Ghafouri and Thompson, 2001; Encarnação et al., 2007). These interferences result in non-mass effects in the measured frequency variation signals and have to be accounted in order to interpret and use measured frequency variation data for analytical quantification of analytes and for kinetic analysis. Using impedance analysis in complement with resonant frequency variation measuring it is possible to get more detailed information on the changes occurring at, or near the, sensor surface (Martin et al., 1991; Auge et al., 1995; Bouche-Pillon et al., 1995; Etchenique and Weisz, 1999; Lucklum and Hauptmann, 2000; Zhou et al., 2000; Sabot and Krause, 2002; Encarnação et al., 2007). Interfering signals can be identified and eliminated and the frequency signal generated by the binding event can be isolated and related to variation of the mass attached at the sensor surface (Encarnação et al., 2007).

In this work we use impedance analysis in complement to frequency variation measurements to study the interaction of recombinant antibodies against a rectroviral protein in QCM biosensors. Recombinant antibodies generated against the HIV1 virion infectivity factor protein (Goncalves et al., 2002) were immobilized at the surface of quartz crystal sensors to generate immunosensors to detect the target HIV1 virion infectivity factor protein (vif) in a buffer flow. HIV1 vif is a phosphorylated 23 kDa protein mainly found in the cytoplasm of HIV-1 infected cells (Camaur and Trono, 1996) and has been pointed out has a strong candidate target for HIV-1 treatment. In the process of better understanding its role in the viral replication cycle, the recombinant antibodies used in this work – 4BL scFv, VH single domain, and VHD camelized single domain – were originally generated as tools to inactivate this protein during viral replication (Goncalves et al., 2002; Silva et al., 2004). Owing to their small size and homogeneity, recombinant antibodies can be coupled at high density and order onto the sensor surface, therefore reducing the possibility of unspecific adsorption and trapping of contaminant molecules and thus enhancing the capacity of the sensor to recognize the target molecule (Shen et al., 2005).

Using HIV1 vif recognition by these recombinant antibodies we demonstrate the applicability of our approached to complement QCM resonant frequency variation measurements with impedance analysis in order to enable its accurate use in the quantitative detection of specific targets and in the determination of binding constants.

2. Materials and methods

2.1. Reagents

All products used were ultra-pure, pro-analysed, or equivalent grade. All solutions were prepared using ultra-pure and low conductivity Milli-Q water. Absolute ethanol and DMF were purchased from Riedel-de-Häen. Ethanolamine, hydrochloric acid, tris(hydroxymethyl)-aminomethan (Tris), sodium chloride, imidazole, oxygen peroxide, di-sodium-hydrogen-phosphate, potassium-di-hydrogen-phosphate and absolute ethanol were purchased from Merck-VWR. Dithio-bis-succinimidyl-undecanoate (DSU) and 11-hydroxy-1-undecanethiol (HUT) were purchased from Dojindo Laboratories. Anti-HA high affinity monoclonal antibody conjugated with peroxidase (HP/anti-HA) and precipitating BM Blue peroxidase substrate were acquired from Roche. Acrylamide/bis-acrylamide solution and Bio-Rad protein assay were purchased from Bio Rad.

2.2. Production of recombinant antibodies and HIV1 virion infectivity factor

All proteins used in this work were expressed with a hemagglutinin (HA) epitope, to enable detection with HP/anti-HA in immunoassays, and a 6× His tags to enable the protein purification by metal chelate affinity chromatography.

The *E. coli* expression vectors were a gift from Prof. João Goçalves group (*URIA-Centro de Patógenese Molecular*, *Faculdade de Farmácia*, *Universidade de Lisboa*) and details for their construction can be found elsewhere (Yang et al., 1996; Goncalves et al., 2002; Silva et al., 2004). The proteins were expressed and purified from inclusion bodies (HIV1 vif) or from periplasmatic extracts (recombinant antibodies) as previously published (Yang et al., 1996; Goncalves et al., 2002; Silva et al., 2004). Recombinant antibodies were also recovered and purified from the exhaust culture medium. Exhaust culture medium was clarified by centrifugation (4000 × *g*, 30 min, 4 °C), and dialfiltrated against 20×10^{-3} M Tris buffer pH 8 containing 0.5 M NaCl in a 10 kDa cut-off Millipore Pellicon XL ultrafiltration membrane to a final 10-fold protein concentration factor. The antibodies were further purified in Ni(II) chelating sepharose fast flow XK16 column (GE healthcare), packed to 2.5 cm bed height. After elution with 0.1 M imidazole, the antibodies were concentrated with 10 kDa cut-off centricons (Millipore) and desalted in a Hytrap Desalting column (GE healthcare).

The Bio-Rad BCA protein assay kit was used to determine protein concentration and the purity was assessed by SDS-PAGE and Western blot analysis. Western blots using HP/anti-HA monoclonal antibody conjugates were autoradiographed with the chemiluminescent ECL-Plus kit (GE healthcare) according to the manufacturer instructions.

2.3. Piezoelectric immunosensor

2.3.1. Quartz crystals

5 MHz quartz crystals were purchased from Standford Research Systems (SRS, Standford, USA). Each sensor has 1 in.

in diameter quartz crystals and is covered on both sides with optically polished gold electrodes. Before use, the crystals were first cleaned with absolute ethanol and Milli-Q water and then subjected to a 15 min exposure to Piranha solution (30% (v/v), H_2O_2:H_2SO_4 = 1:3). Cleaned crystals were finally rinsed with water and dried under a nitrogen stream.

2.3.2. Quartz crystal sensor functionalization

The cleaned crystals were activated with 30 μl of a 100 μM DMF solution of DSU and incubated at room temperature for 2 h. The crystals were then sequentially washed with DMF and Milli-Q to remove unbounded DSU molecules.

Activated crystal sensors were dried under a nitrogen flow, and exposed to 50 μl of an ethanolic solution of 50 μM of HUT for 2 h, at room temperature and in a humidified chamber. After washing with absolute ethanol, Milli-Q water and drying under a nitrogen flow, activated crystals were functionalized with purified recombinant antibodies by incubating for 2 h at room temperature with 30 μl of a 200 μg/ml PBS solution of antibody. After washing sequentially with PBS buffer and Milli-Q water, the functionalized crystal sensors were incubated with 50 μl of ethanolamine solution (2 h at room temperature) to block unreacted binding sites.

2.3.3. Experimental set-up

A Kynar crystal holder (SRS) with a homemade acrylic cover to create a 300 μl flow cell was used to install the sensors and thus enable exposing just the functionalized face of the sensor to the solution. To avoid wetting or flooding the electrical contacts located on the bottom of the crystal holder, viton O-rings were placed underneath the sensor, sealing the flow cell. The flow cell was connected to an agitated container where all the samples are applied, using Tygon tubing thus forming a closed fluidic circuit with a total volume of 2 ml. The solutions were re-circulated in the system using a Watson-Marlow peristaltic pump at a flow rate of 1.5 ml min^{-1}. Both the flow cell and the container were installed in a 1 L jacketed beaker to control and maintain the temperature of the system at 30.0 ± 0.1 °C using of a Thermo Haake temperature controller.

2.3.4. Resonance frequency and impedance analysis

The resonant frequency was recorded using a QCM100 Controller and a QCM25 Oscillator (SRS) connected to a Pendulum CNT-66 frequency counter. Impedance spectra were recorded using a RF HP8712C Network Analyzer. The network analyzer and the QCM25 Oscillator were electrically connected to the crystal holder through a switch used to select the desired measurement mode. Shielded coaxial cables were used in all electrical connections to minimize signal instability arising from electrical interference. The instruments were interfaced to a computer through IEEE boards and a homemade Pascal program was used to extract experimental data.

Impedance spectra were obtained using a 10 kHz frequency span centered near the crystal's resonant frequency, with 16 spectra averaging at 1 Hz resolution. Impedance data was interpreted on the basis of a Butterworth–Van Dyke (BVD) model. BVD is an equivalent electrical circuit representation of the QCM (Fig. 1) composed by a static capacitance (C_0 parasitic capacitance due to electrodes, holding structure, cables and charged species) in parallel with a motional branch containing a motional inductance (L_m – inertia to oscillation related to mass dislocation), a motional capacitance (C_m – oscillation energy storage related to the crystal's elasticity), and a motional resistance (R_m – energy dissipation to the mounting structure of the crystal and contacting medium) in series. The quantification of the BVD model parameters by impedance analysis enables the discrimination of the different contributions to the sensor signal (liquid loading, viscoelasticity of films, mass, and charges). The BVD equivalent circuit parameters were obtained from the experimental data by fitting the conductance function (Eq. (1)) using a Matlab routine:

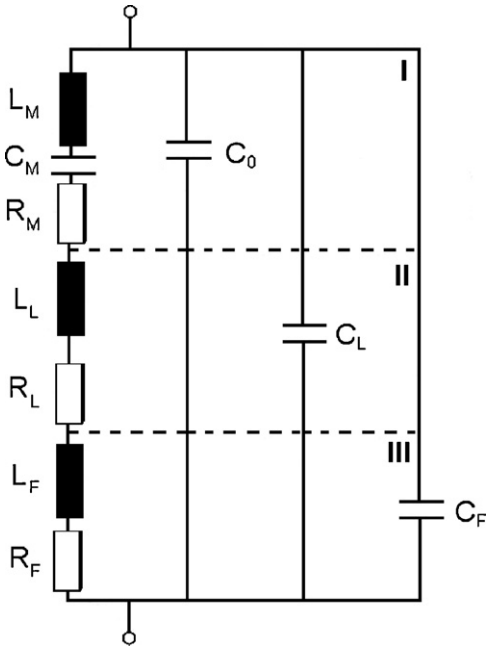

Fig. 1. Butterworth van Dyke equivalent circuit model of QCM sensors (I) unloaded resonator, (II) elements added due to liquid medium exposure, and (III) elements added due to the adsorption of mass on the surface of the sensor.

$$|Y| = \sqrt{\left(\frac{R_m}{R_m^2 + U^2}\right)^2 + \left(\omega C_0 - \frac{U}{R_m^2 + U^2}\right)^2} \quad (1)$$

where $\omega = 2\pi f$ is the angular frequency and $U = \omega L_m - 1/\omega C_m$.

The analysis is initialized by estimating the four BVD parameters (R_m, L_m, C_m and C_0) for the crystal sensor exposed to air. Typical parameters for air exposed crystal sensors in the experimental set-up used are R_m = 12.925 Ω, L_m = 33.725 mH, C_m = 29.925 fF, and C_0 = 184.575 pF, respectively. Since C_m is related only to physical properties of the sensor, it is constant within the experiments. The successive contributions of solvents and adsorbed mass are thus obtained by a three parameter fitting (R_m, L_m, C_0) of the respective conductance functions. This procedure is repeated for each stage of the experiment and the BVD parameters of the particular experimental stage, thus of the individual contributions, are calculated by subtracting the global parameters, obtained by fitting, from the respective parameter

Table 1
Frequency and impedance characterization of the immobilization of recombinant antibodies (antibody bulk concentration: 200 μg/ml)

Antibody	ΔF (Hz)	ΔXL_F (Ω)	ΔR_F (Ω)	ΔC_F (pF)
4BL	28 ± 2	12 ± 1	0.9 ± 0.3	−0.02 ± 0.01
VH	36 ± 3	15 ± 2	0.6 ± 0.4	−0.04 ± 0.02
VHD	22 ± 2	9 ± 1	0.3 ± 0.2	0.03 ± 0.01

calculated for the previous stage of the experiment. To facilitate data analysis it is usual to represent a parameter *XL* which is the sensor inductance in resistive units (Ω) obtained by multiplying the calculated inductance value by the angular frequency $\omega = 2\pi f$.

3. Results and discussion

3.1. Antibody immobilization

Purified recombinant antibodies (Ferreira et al., 2007) were immobilized on functionalized sensors with a mixed dithio-bis-succinimidyl-undecanate and 11-hydroxy-1-undecanothiol self assembled monolayer (SAM) (Fig. 2). The surface of quartz crystal sensors, cleaned with piranha solution, was initially exposed to 100 μM DSU to generate an oriented monolayer with exposed succinimidyl groups to the liquid interface and then exposed to 50 μM HTU in order to fully passivate the sensor surface and to enhance the SAM surface organization (Ferreira et al., 2007; Schwartz, 2001). SAM functionalized sensors were then activated by incubation with 200 μg/ml solutions of each anti-HIV1 Vif recombinant antibody—4BL, VH, and VHD. Recombinant antibodies are immobilized through the formation of amine bounds formed upon nucleophilic attack of secondary amines resulting in the release of the succinimidyl group (Fig. 2).

Table 1 summarizes the total frequency variation and electroacoustic impedance data measured for the immobilization of each recombinant antibody. The total frequency variation is known to result from mass (Δf_m), liquid and film viscoelasticity (Δf_v), and charge variations (Δf_c) contributions (Encarnação et al., 2007) – $\Delta f_T = \Delta f_m + \Delta f_v + \Delta f_c$. Thus, in order to quantify the amount of antibody immobilized using the Sauerbrey equation to correlate Δf_m, the different contributions to frequency variation must be identified. Impedance analysis enables the identification and quantification of such contributions. While the mass dislocated during the resonator vibration, therefore the mass deposited or adsorbed at the sensor surface, is identified by the impedance inductance (XL_F), liquid loading effects and film viscoelasticity are identified by changes in the measured series resistance (R_F), resulting in a total frequency variation of $\Delta f_v = 4\pi L_m(\Delta R_F)^{-1}$ (Martin et al., 1991; Zhou et al., 2000), L_m being the inductance value of the sensor for the quartz crystal exposed to air. Additionally, the presence of electrolytes and charged molecules in solution is identified by a variation of the sensor parallel capacitance (C_F) which results in a frequency variation of $\Delta f_c = 8 \times 10^{12} \Delta C_F$ (Encarnação et al., 2007).

The variation of the inductance values (Table 1) is in accordance to the expected, as the overall mass increases upon antibody immobilization. On the other hand, no significant variations of the resistive and capacitive values were found, which indicates that the frequency contribution from viscoelasticity and charge variations, respectively, can be neglected. Viscoelastic and charge interferences were quantified in the frequency ranges 0.7–2.1 Hz and (−0.3) −0.2 Hz, respectively, which are within the uncertainty associated with the measured frequency variation (Table 1).

These data thus indicate that the effect of viscoelastic and electroacoustic charge interferences is neglected, therefore the resonance frequency variations measured for antibodies immobilization are directly associated with the mass of immobilized antibody. The Sauerbrey equation was thus used to calculate the sensor surface antibody densities 0.64 ± 0.05 μg/cm^2 for anti-HIV1 Vif VH, 0.49 ± 0.04 μg/cm^2 for anti-HIV1 Vif 4BL, and 0.39 ± 0.04 μg/cm^2 for anti-HIV1 Vif VHD.

3.2. Analysis of antigen recognition

The piezoelectric immunosensors developed were evaluated for HIV1-Vif recognition in liquid samples. As shown in Fig. 3, all sensors selectively respond to HIV-1 Vif as no frequency variations were monitored for control experiments with PBS, cytochrome *c*, and BSA. Furthermore, no Vif binding was observed when using non functionalized sensors (bare gold surface), sensors functionalized only with

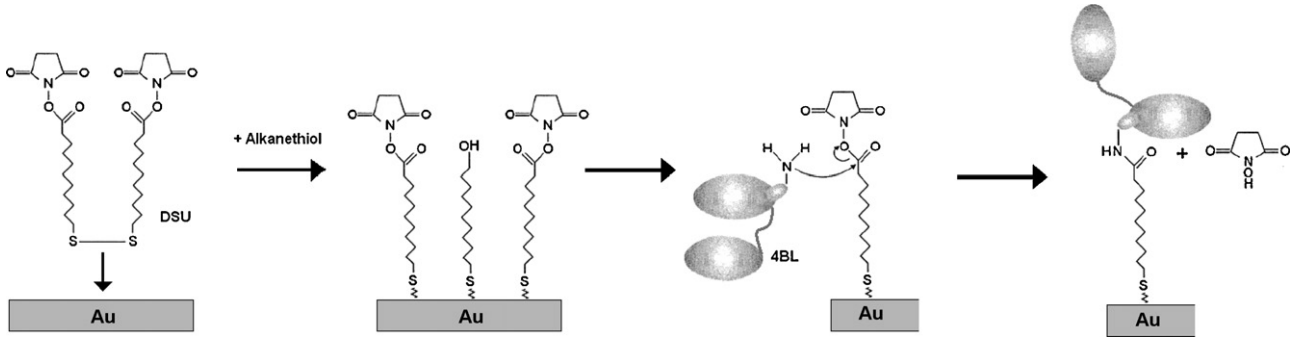

Fig. 2. Scheme of the main steps taken for the functionalization of the piezoelectric sensors, starting with the formation of the mixed SAM and followed by the immobilization of the recombinant antibodies.

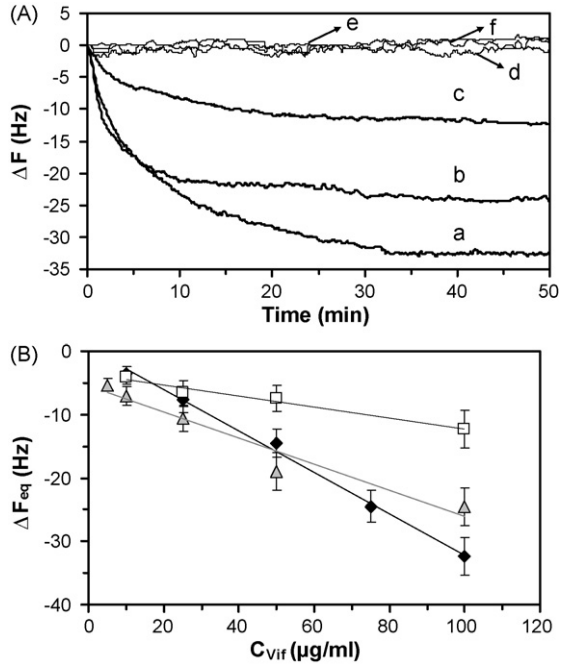

Fig. 3. (A) Transients obtained with 4BL (a), VHD (b) and VH (c) immunosensors for a Vif concentration of 100 μg/ml, compared to control assays where the antigen injection was substituted by PBS (d), cytochrome *c* (100 μg/ml) (e) and BSA (100 μg/ml) (f). (B) Relationship between the total resonant frequency shift at the end of each transient and the bulk concentration of Vif, for each of the immunosensors: (♦) 4BL, (□) VH and (▲) VHD (lines are an aid to the eye). Each presented data is the average result of six independent experiments.

11-hydroxy-1-undecanothiol SAM, sensors activated with BSA, and functionalized sensors with the mixed DSU/HUT SAM and fully blocked with low-fat milk and with ethanolamine, used as controls to evaluate antigen unspecific binding (not shown).

HIV1-Vif binding to 4BL, VH and VHD modified sensors was found to be linear within the concentration range evaluated (Fig. 3B). It is also evident that VH modified sensors respond differently than 4BL and VHD modified sensors, resulting approximately in half the signal in similar experimental conditions. This result apparently goes contrary to the expectation considering antibody surface density. However, as demonstrated elsewhere (Ferreira et al., 2007), the higher hydrophobicity and packaging of VH biofilms may explain such response differences. Due to the hydrophobic character of the VH molecule, when in contact with an aqueous solutions, the antibody molecules adopt a surface conformation unfavorable to bind Vif, being closer to the hydrophobic aliphatic chains of the SAMs and thus with the binding residues hindered (Ferreira et al., 2007). The higher VH surface density may also lead to conformational issues related with immobilized antibody molecule interactions resulting in possible stereochemical effects that inhibit antigen recognition (Myszka, 1999). Our data is consistent with previously published qualitative Elisa analysis (Silva et al., 2004), where the signal obtained with VH single domain antibodies is considerably lower than the one obtained for 4BL scFvs, and considerably improved when using the camelized VHD single domain (Silva et al., 2004; Ferreira et al., 2007).

Table 2
Rate and equilibrium constants for the binding of Vif to immobilized recombinant antibodies

Antibody	k_1 ($M^{-1}\,s^{-1}$)	k_{-1} (s^{-1}) × 10^3	K_D (M) × 10^6
4BL	305 ± 47	1.1 ± 0.1	3.6 ± 0.8
VH	587 ± 47	0.41 ± 0.09	0.7 ± 0.2
VHD	845 ± 70	1.2 ± 0.2	1.5 ± 0.4

A 1:1 binding model (Eq. (2)) was used to estimate the binding rates of HIV1-Vif to the modified immunosensors.

$$\frac{d\theta}{dt} = k_1(1-\theta)C - k_{-1}\theta, \tag{2}$$

where θ is the relative amount of antibody–Vif complex (i.e. surface coverage), C is the initial Vif concentration, and k_1 and k_{-1} are the association and dissociation rate constants, respectively.

Upon integration of the rate equation (Eq. (2)) an expression is obtained to describe the time dependency of the sensor surface coverage (Eq. (3)):

$$\theta = \frac{C}{C + k_{-1}/k_1}\theta_\infty \left[1 - \exp(-t/\tau)\right] \tag{3}$$

where θ_∞ is the total available binding sites at the sensor surface and $\tau = [k_1 \times C + k_{-1}]^{-1}$ is the relaxation time of binding.

The rate constants k_1 and k_{-1} can be calculated from the sensor data whenever θ is proportional to the measured frequency variation. As mentioned earlier, the Sauerbrey relationship provides such proportionality provided that the validity of the assumptions of the Sauerbrey relationship is guarantied. As before, it is necessary to eliminate interfering signals derived from the viscoelasticity of adsorbed films, from the properties of the aqueous environment, and from local charge density variation.

Impedance analysis was performed, as before, in order to identify and eliminate interfering signals. As shown in Fig. 4, the change of damping resistance owing to viscoelastic effects is negligible ($\Delta R \sim 0$) in all cases. Together with the increase of the inductive component (ΔXL), these results demonstrate that Vif is recognized and binds to the modified sensors resulting in biofilms exhibiting a rigid behavior. Electroacoustic interferences were also found negligible for the majority of the cases. However, for the highest Vif concentrations evaluated for the 4BL and VH modified sensors, as much as 16% of the measured frequency variation signal corresponds to electroacoustic interferences (Fig. 4C).

The impedance analysis data was used to correct the measured frequency data variation in order to eliminate interfering signals. Corrected frequency variation is related to the sensor surface coverage (θ) and thus the relaxation time of binding (τ) can be estimated for each Vif concentration by non-linear fitting of Eq. (3) to frequency variation transients. According to the proposed binding model, the binding rate constants, k_1 and k_{-1}, are obtained, respectively, from the slope and intercept of the linear relationship of the reciprocal of the relaxation time (τ^{-1}) versus Vif concentration (Fig. 5). The values of the rate constants are summarized in Table 2 together with the dissociation

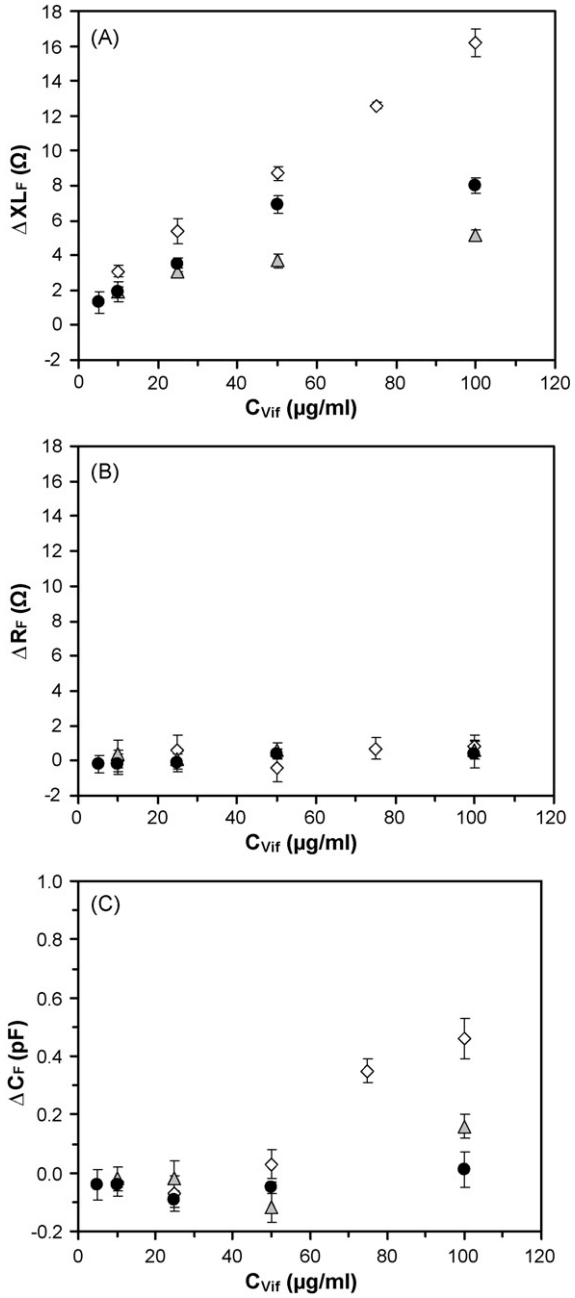

Fig. 4. (A) (ΔXL), (B) (ΔR), and (C) (ΔC) present the variation of the Butterworth van Dyke model parameters, relatively to the response of the three immunosensors (◊) 4BL, (△) VH and (●) VHD to different concentrations of Vif. Each presented data is the average result of six independent experiments.

equilibrium constant ($K_D = k_{-1}/k_1$). The calculated dissociation rate constants are in the same order of magnitude of other affinity interactions with scFvs and single domains, even though the association rate constants being ~3 orders of magnitude lower (Hengerer et al., 1999; Pribyl et al., 2003). In conjunction with the low equilibrium constant (K_d), in the micro-molar range as compared with the nano-molar range described with other affinity pairs using recombinant antibodies (Hengerer et al., 1999), our results suggest that anti-Vif 4BL scFv, VH and VHD single domains, although selective, are not strong binders to Vif. We also hypothesize that other factors, which are intrinsic

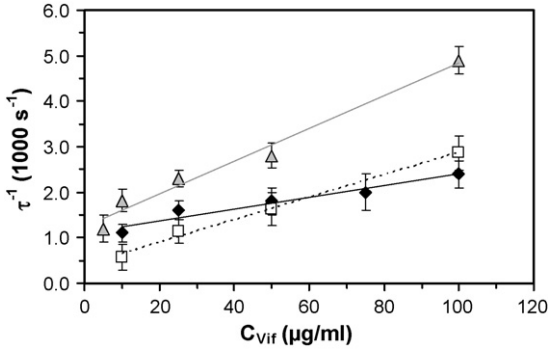

Fig. 5. Linear dependence of the 1:1 molecular model calculated constant τ^{-1}, to the bulk Vif concentrations used for each immunosensor: (♦) 4BL, (□) VH and (▲) VHD. Linear regression of experimental data yielded the correlations: $\tau^{-1} = (1.3 \pm 0.2) \times 10^{-5} \times C + (1.1 \pm 0.1) \times 10^{-3}$; $r = 0.9697$; $p = 0.0063$, for 4BL; $\tau^{-1} = (2.5 \pm 0.2) \times 10^{-5} \times C + (0.4 \pm 0.09) \times 10^{-3}$; $r = 0.9963$; $p = 0.0037$, for VH; $\tau^{-1} = (3.6 \pm 0.3) \times 10^{-5} \times C + (1.2 \pm 0.2) \times 10^{-3}$; $r = 0.9885$; $p = 0.0015$, for VHD. Each presented data is the average result of six independent experiments.

to the system used such as steric hindrance and mass transfer effects, may also contribute to the low calculated kinetic and equilibrium constants. Unfortunately there is a lack of published quantitative affinity data for the antibodies used in this study and, therefore, no definitive conclusion regarding the origins of the low kinetic constants obtained can be taken at this moment.

4. Conclusions

In this work piezoelectric immunosensors based on scFvs and single domain recombinant antibodies were developed to recognize HIV1 viral infective factor (Vif). All modified sensors were able to selectively recognize HIV1 Vif. The sensors were stable and antigen specific even when using complex protein mixtures.

Impedance analysis was performed simultaneously with resonant frequency measurements in order to identify and eliminate interfering signals from electroacoustic and viscoelastic effects. This approach increased the usefulness of piezoimmunosenors rendering possible its use for quantitative analysis and detection of target antigens, kinetic parameters, and equilibrium constants.

This study shows that HIV1 Vif recognition by modified sensors with anti-Vif 4BL scFv, VH single domain, and VHD camelized single domain, can be modeled by a 1:1 binding model from which kinetic and equilibrium constants were calculated. Even though the low calculated kinetic constants suggest that the antibodies studied are poor binders to HIV1 Vif, no final and definitive conclusion can be taken yet. Other phenomena such as mass transfer, steric hindrance and sensor sensitivity may also contribute to such low constants. Nevertheless, the study presented in this paper provides a valuable insight into Vif molecular recognition by anti-Vif ScFv 4BL, VH and VHD single domains with impact in ongoing research focused on the use of these recombinant antibodies as intrabodies for the functional neutralization of the Vif protein as a strategy to strongly neutralize HIV1 infectivity. Furthermore, this paper demonstrates the

applicability of piezoelectric sensors in biorecognition analysis and evidences its potential as a quantitative biosensor.

Acknowledgments

This work was supported by the Portuguese Science Foundation, an organisation of the Portuguese Ministry of Science and Higher Education. Contract number POCI/BIO/61912/2004 and the Ph.D. grant number SFHR/BD/12772/2003 to J.M. Encarnação are acknowledged.

References

Auge, J., Hauptmann, P., Hartmann, J., Rösler, S., Lucklum, R., 1995. New design for QCM sensors in liquids. Sens. Actuators B 24, 43–48.

Bouche-Pillon, D., Gabrielli, C., Perrot, H., 1995. Validation of the quartz-crystal microbalance response in liquid for sensor applications. Sens. Actuators B 25, 257–259.

Camaur, D., Trono, D., 1996. Characterization of human immunodeficiency virus type 1 Vif particle incorporation. J. Virol. 70, 6106–6111.

Encarnação, J.M., Stallinga, P., Ferreira, G.M.N., 2007. Influence of electrolytes in the QCM response: discrimination and quantification of the interference to correct microgravimetric data. Biosens. Bioelectron. 22, 1351–1358.

Etchenique, R., Brudny, V.L., 2000. Characterization of porous thin films using quartz crystal shear resonators. Langmuir 16, 5064–5071.

Etchenique, R., Buhse, T., 2000. Anomalous behavior of the quartz crystal microbalance in the presence of electrolytes. The Analyst 125, 785–787.

Etchenique, R., Buhse, T., 2002. Viscoelasticity in the diffuse electric double layer. Analyst 127, 1347–1352.

Etchenique, R., Weisz, A.D., 1999. Simultaneous determination of the mechanical moduli and mass of thin layers using nonadditive quartz crystal acoustic impedance analysis. J. Appl. Phys. 4 (86), 1994–2000.

Ewalt, K.L., Haigis, R.W., Rooney, R., Ackley, D., Krihak, M., 2001. Detection of biological toxins on an active electronic microchip. Anal. Biochem. 289, 162–172.

Fabreguette, F.H., Sechrist, Z.A., Elam, J.W., George, S.M., 2005. Quartz crystal microbalance study of tungsten atomic layer deposition using WF_6 and Si_2H_6. Thin Solid Films 488 (1–2), 103–110.

Ferreira, G.N.M., Encarnação, J.M., Rosa, L., Rodrigues, R., Breyner, R., Barrento, S., Pedro, L., Aires da Silva, F., Gonçalves, J., 2007. Recombinant single-chain and single domain antibody piezoimmunosensors for detection of HIV1 virion infectivity factor. Biosens. Bioelectron. 23, 384–392.

Ghafouri, S., Thompson, M., 2001. Electrode modification and the response of the acoustic shear wave device operating in liquids. Analyst 126, 2159–2167.

Goncalves, J., Silva, F., Freitas-Vieira, A., Santa-Marta, M., Malhó, R., Yang, X., Gabuzda, D., Barbas, C., 2002. Functional neutralization of HIV-1 Vif protein by intracellular immunization inhibits reverse transcription and viral replication. J. Biol. Chem. 277, 32036–32045.

Hengerer, A., Kößlinger, C., Decker, J., Hauck, S., Queitsch, I., Wolf, H., Dübel, S., 1999. Determination of phage antibody affinities to antigen by a microbalance sensor system (QCM). BioTechniques 26, 956–964.

Liss, M., Petersen, B., Wolf, H., Prohaska, E., 2002. An aptamer-based quartz crystal protein biosensor. Anal. Chem. 74, 4488–4495.

Liu, Y., Zhang, W., Yu, X., Zhang, H., Zhao, R., Shangguan, D., Li, Y., Shen, B., Liu, G., 2004. Quartz crystal biosensor for real-time kinetic analysis of interaction between human TNF-α and monoclonal antibodies. Sens. Actuators B 99, 416–424.

Lucklum, R., Hauptmann, P., 2000. The quartz crystal microbalance: mass sensitivity, viscoelasticity and acoustic amplification. Sens. Actuators B 70, 30–36.

Martin, S., Granstaff, V., Frye, G., 1991. Characterization of a quartz crystal microbalance with simultaneous mass and liquid loading. Anal. Chem. 63, 2272–2281.

Modin, C., Stranne, A.-L., Foss, M., Duch, M., Justesen, J., Chevallier, J., Andersen, L.K., Hemmersam, A.G., Pedersen, F.S., Besenbacher, F., 2006. QCM-D studies of attachment and differential spreading of pre-osteoblastic cells on Ta and Cr surfaces. Biomaterials 27, 1346–1354.

Myszka, D., 1999. Improving biosensors analysis. J. Mol. Recognit. 12, 279–284.

Pan, W., Durning, C.J., Turro, N.J., 1996. Kinetics of alkanethiol adsorption on gold. Langmuir 12, 4469–4473.

Pribyl, J., Hepel, M., Halamek, J., Skladal, P., 2003. Development of piezoelectric immunosensors for competitive and direct determination of atrazine. Sens. Actuators B 91, 333–341.

Sabot, A., Krause, S., 2002. Simultaneous quartz crystal microbalance impedance and electrochemical impedance measurements. Investigation into the Degradation of thin polymer films. Anal. Chem., A–H.

Sauerbrey, G., 1959. Use of quartz vibrator for weighing thin films on a microbalance. Z. Phys., 206–222.

Schwartz, D., 2001. Mechanisms and kinetics of self-assembled monolayer formation. Annu. Rev. Phys. Chem. 52, 107–137.

Shen, Z., Stryker, G., Mernaugh, R., Yu, L., Yan, H., Zeng, X., 2005. Engineered recombinant single-chain fragment varible antibody for immunosensors. Anal. Chem. 77, 797–805.

Silva, F., Santa-Marta, M., Freitas-Vieira, A., Mascarenhas, P., Barahona, I., Moniz-Pereira, J., Gabuzda, D., Goncalves, J., 2004. Camelized rabbit-derived VH single-domain intrabodies against Vif strongly neutralize HIV-1 infectivity. J. Mol. Biol. 340, 525–542.

Su, X.-L., Li, Y., 2005. A QCM immunosensor for Salmonella detection with simultaneous measurements of resonant frequency and motional resistance. Biosens. Bioelectron. 21, 840–848.

Yang, X., Gonçalvez, J., Gabuzda, D.J., 1996. Phosphorylation of Vif and its role in HIV-1 replication. Biol. Chem. 271, 10121–10129.

Yang, M., Yau, H.C.M., Chan, H.L., 1998. Adsorption kinetics and ligand-binding properties of thiol-modified double-stranded on a gold surface. Langmuir 14, 6121–6129.

Zhou, A., Zhang, J., Xie, Q., Yao, S., 2000. Impedance analysis for the investigation of the behaviors of piezoelectric quartz crystal in the liquid at harmonic resonance. Sens. Actuators B 67, 68–75.